



HAL
open science

On the biomechanics of the tactile perception of friction

Laurence Willemet

► **To cite this version:**

Laurence Willemet. On the biomechanics of the tactile perception of friction. Biomechanics [physics.med-ph]. Aix-Marseille-Université (AMU), 2021. English. NNT: . tel-03583769

HAL Id: tel-03583769

<https://theses.hal.science/tel-03583769>

Submitted on 22 Feb 2022

HAL is a multi-disciplinary open access archive for the deposit and dissemination of scientific research documents, whether they are published or not. The documents may come from teaching and research institutions in France or abroad, or from public or private research centers.

L'archive ouverte pluridisciplinaire **HAL**, est destinée au dépôt et à la diffusion de documents scientifiques de niveau recherche, publiés ou non, émanant des établissements d'enseignement et de recherche français ou étrangers, des laboratoires publics ou privés.

AIX-MARSEILLE UNIVERSITÉ

Doctoral School: Sciences du Mouvement Humain

INSTITUT DES SCIENCES DU MOUVEMENT (UMR 7287)

A thesis submitted in fulfillment of the requirements for the degree of Doctor at
Aix-Marseille Université

On the biomechanics of the tactile perception of friction

Laurence Willemet

Defended on 6th of December 2021 before committee:

Philippe Lefèvre	Université Catholique de Louvain, Belgium	Reviewer
Ilana Nisky	Ben-Gurion University of the Negev, Israel	Reviewer
Frédéric Danion	Université de Poitiers, France	Examiner
Véronique Perdereau	Sorbonne Université, France	Examiner
Bruno Cochelin	Laboratoire de Mécanique et d'Acoustique, France	co-Director
Michaël Wiertelowski	TU Delft, The Netherlands	Director

Declaration of Authorship

I, Laurence Willemet, declare that this thesis titled, “On the biomechanics of the tactile perception of friction” and the work presented in it are my own. I confirm that:

- This work was done wholly or mainly while in candidature for a research degree at this University.
- Where any part of this thesis has previously been submitted for a degree or any other qualification at this University or any other institution, this has been clearly stated.
- Where I have consulted the published work of others, this is always clearly attributed.
- Where I have quoted from the work of others, the source is always given. With the exception of such quotations, this thesis is entirely my own work.
- I have acknowledged all main sources of help.
- Where the thesis is based on work done by myself jointly with others, I have made clear exactly what was done by others and what I have contributed myself.

Signed:

Date:

“J’ai vu plus loin que les autres parce que je me suis juché sur les épaules des géants.”

Isaac Newton

AIX-MARSEILLE UNIVERSITÉ

Abstract

Doctoral School: Sciences du Mouvement Humain

On the biomechanics of the tactile perception of friction

by Laurence Willemet

When manipulating objects, humans rely on their sense of touch to perceive subtle movements and micro slippages. This synergy between sensations and motion permits them to manipulate an impressive range of objects of different sizes, shapes, and surface properties. This incredible dexterity relies on fast and unconscious adjustments of the grip force by placing a 20% safety margin before slip that holds an object strong enough to avoid a catastrophic fall yet gentle enough not to damage it. In addition to being accurate, this regulation is swift: only a hundred milliseconds after first making contact, grip forces are already adjusted by taking into account the actual frictional strength of the contact. This astonishing performance is owed to the sense of touch, which informs on the physical properties of the surrounding world and contact state. Within the fingertip, thousands of mechanoreceptors convert the complex mechanical interaction into action potentials. However, how the brain copes with large amounts of data to infer the state of the contact is still debated.

This thesis covers how the cutaneous tactile afferent made it possible for a swift and precise regulation of the grip. Firstly, I show that humans can assess friction without slippage, suggesting that the radial stretch of the skin can provide enough information to regulate grip at the contact initialization. Secondly, I show that the perceptual system uses a compact code to estimate the safety margin from the skin deformation during an incipient slip, suggesting a mechanism to explain the rapid reactions. Finally, I expose a new model based on contact mechanics to quantify the sensitivity of the mechanoreceptors to the patterns of skin deformation highlighted in the first two chapters. This model also correlates the spatial and temporal detection threshold to detect a moving stimulus, suggesting a persistence of touch that bridges discrete sensations into a continuous stimulus.

Taken together, these results reveal how the perception of friction is encoded in the spatio-temporal deformation of the skin. The findings are useful for designing bio-inspired tactile sensors for robotics or prosthetics and for improving haptic human-machine interactions.

Résumé

Lorsque nous manipulons des objets, nous nous fions à notre sens du toucher pour percevoir les mouvements subtils et les micro glissements. Cette synergie entre sensations et mouvement nous permet de manipuler une grande variété d'objets de différentes tailles, formes ou matériaux. Cette remarquable dextérité repose sur une régulation rapide et inconsciente de notre force de préhension, en maintenant une marge de sécurité avant glissement de 20% nous permettant ainsi de serrer l'objet suffisamment fort pour éviter une perte d'adhérence mais suffisamment délicatement pour ne pas l'endommager. En plus d'être précise, cette régulation est très rapide : après seulement une centaine de millisecondes après l'initialisation du contact, la force de préhension est déjà ajustée en fonction du frottement disponible à l'interface. Nous devons cette performance hors-du-commun au sens du toucher qui nous informe sur les propriétés physiques du monde qui nous entoure ainsi que de l'état de contact. Le doigt humain est équipé de milliers de mécanorécepteurs qui convertissent l'interaction mécanique complexe en potentiels d'actions. Cependant, comment le cerveau reconstruit l'état de contact à partir de ce volume considérable de données, continue à faire débat.

Cette thèse explore comment les afférents tactiles cutanés rendent possible une régulation rapide et précise de la force de préhension. Tout d'abord, une expérience psychophysique a permis de montrer que les humains étaient capables d'apprécier le frottement à l'interface sans glissement, indiquant qu'une expansion radiale de la peau peut apporter suffisamment d'informations pour réguler la force de préhension à l'initialisation du contact. Dans un second temps, je propose un encodage compact qui pourrait être utilisé par le système perceptuel pour estimer la safety margin à partir de la déformation de la peau lors d'un glissement partiel, suggérant un mécanisme pour expliquer nos prompts réactions. Enfin, j'expose un nouveau modèle basé sur la mécanique du contact pour quantifier la sensibilité des mécanorécepteurs aux motifs de déformation mis en évidence dans les deux premières parties. Ce modèle corrobore également avec les seuils de détection spatial et temporel, évoquant la présence d'une persistance tactile comblant un signal discret en stimulus continu.

Dans leur ensemble, ces travaux révèlent l'encodage de la perception du frottement dans la déformation spatio-temporelle de la peau. Ces résultats pourront être utiles pour le design de capteurs tactiles bio-inspirés pour la robotique ou les prothèses. Ils ont également vocation à améliorer les interactions haptiques homme-machine.

List of publications

Willemet, L., Kanzari, K., Monnoyer, J., Birznieks, I. & Wiertlewski, M. (2021). Initial contact shapes the tactile perception of friction. *Proceedings of the National Academy of Sciences*

Willemet, L.(2019) Workshop: The Neuroscience of Touch: From finger skin deformation to perception. *WorldHaptics 2019*, Tokyo, Japan.

Willemet, L., Cochelin, B. & Wiertlewski, M. (2019). Mind the spatiotemporal gap: Skin deformation limits our perception of discontinuous motion. *WorldHaptics 2019*, Tokyo, Japan.

Huloux, N., **Willemet, L.**, & Wiertlewski, M. (2021). How to measure the area of real contact of skin on glass. *IEEE Transactions on Haptics*, Best paper award of WorldHaptics Conference 2021.

Lin, X., **Willemet, L.**, Bailleul, A., & Wiertlewski, M. (2020). Curvature sensing with a spherical tactile sensor using the color-interference of a marker array. *IEEE International Conference on Robotics and Automation (ICRA)* (pp. 603-609)

Acknowledgements

C'est à la fin d'une expérience comme celle-ci que l'on se rend compte qu'elle aurait été impossible sans l'aide de mes collègues, de ma famille et de mes amis.

Tout d'abord, je tiens à remercier mon directeur de thèse, Michaël, pour m'avoir permis de grandir en tant que chercheuse. Sa passion et son enthousiasme pour mon sujet de recherche ont été contagieux et des grands facteurs de motivation pour moi. Je tiens également à le remercier pour sa curiosité au quotidien grâce à laquelle je ne mangerais plus mes pizzas de la même façon. Ma gratitude va également à mon co-directeur de thèse, Bruno, pour sa bienveillance et sa rigueur.

Je tiens également à remercier tous mes collaborateurs qui ont été une grande source d'inspiration dans mon travail de thèse. Ingvars Birznieks, Benoît Delhaye, Khoubeib Kanzari, Jocelyn Monnoyer, et Alessandro Moscatelli, j'ai beaucoup apprécié travaillé à vos côtés ainsi que les passionnantes discussions que l'on a pu échangé. J'aimerais également remercier mon organisme financeur, l'Agence Nationale de la Recherche, pour sa confiance tout au long du projet.

Evidemment, cette expérience n'aurait pas été la même sans mes collègues de l'équipe biorobotique de Marseille: Aimie pour ton oreille attentive, Xi pour me faire relativiser, Corentin pour ton goût de l'aventure, Nicolas pour ton franc parler, Jocelyn pour ta sérénité, Anna pour nos vices partagés, Evandro pour tes cheveux, Jean-Marc pour ta patience, Valentin, Léandres, Ilya, Léo, Christophe et Lucia. Vous avez tous contribué à la bonne ambiance et vous étiez une source de soutien sans faille au quotidien. J'ai également beaucoup apprécié terminé la rédaction de ce manuscrit à TU Delft et partager mes pauses avec Felix, Albe, Yasemin, Becca, Dirk-Jan, Mostafa et Zhaochong.

J'aimerais remercier chaleureusement mes amis qui ont contribué de près ou de loin à la réussite de cette thèse par leur présence et leur soutien: Julien, Noémie, Camille, Maxime, Rebecca, Alvi, et Violette, et une mention spéciale à Sélène pour la relecture de ce manuscrit. Enfin, je voudrais dire un merci tout particulier à mes parents, mes frères et soeur, à ma marraine Claire et à Matthieu pour avoir toujours cru en moi et m'avoir encouragé durant ces longues études. Merci d'avoir toujours été là pour moi et d'avoir partager mes joies comme mes doutes.

Contents

Declaration of Authorship	iii
Abstract	vii
List of publications	ix
Acknowledgements	xi
1 Introduction	1
1.1 Problem statement	1
1.2 Thesis overview	3
2 State of the art	5
2.1 How do humans interact: Bio-tribology of skin	6
2.1.1 Finger anatomy	6
2.1.2 Mechanical properties of skin	8
2.1.3 Frictional properties of the skin	11
2.1.4 Mechanical models of skin tissue	16
2.2 How do humans encode the mechanical deformation: Mechanotransduction	19
2.2.1 Four types of afferents	20
2.2.2 Summary	22
2.3 How do humans perceive	23
2.3.1 Tactile sensitivity	23
2.3.2 Slip detection	29
2.3.3 Friction perception	31
2.4 How do humans manipulate: Human hand's action	31
2.4.1 Action and perception	32
2.4.2 Grip force control	32
2.4.3 Passive vs active sensing	34
2.4.4 Predictive coding	35
2.5 Conclusion	36

3	Mechanical model of skin deformation	37
3.1	Introduction	38
3.2	Finite-difference mechanical model	39
3.2.1	Dynamic equation	40
3.2.2	Sizing of the model	41
3.2.3	Contact modeling	42
3.3	Results of the simulation	43
3.3.1	Static deformation: comparison with the waterbed model	43
3.3.2	Ultrasonic clic caused by rapid changes in friction	44
3.3.3	Stick-slip transition	45
3.3.4	Bump exploration	45
3.4	Discussion	47
3.5	Conclusion	47
4	Mechanics of friction perception	49
4.1	Introduction	50
4.2	Materials and Methods	51
4.2.1	Participants and protocol	51
4.2.2	Setup	52
4.2.3	Data analysis	55
4.3	Results	58
4.3.1	Empirical skin deformation	58
4.3.2	Friction discrimination performance	59
4.3.3	Friction influences skin deformation	60
4.3.4	Skin deformation and friction perception	62
4.3.5	Influence of the kinematics of the exploratory procedure	63
4.3.6	Strain energy and mechanoreceptors thresholds	64
4.3.7	Ideal Observer Analysis	66
4.4	Predictions from the mechanical model	67
4.5	Discussion	69
4.6	Conclusion	71
5	The mechanical basis encoding stick-slip transition	73
5.1	Introduction	74
5.1.1	Encoding of slippage	76
5.1.2	Efficient coding hypothesis	76
5.1.3	Rationale behind dimensionality reduction	77
5.2	Materials and Methods	78
5.2.1	Data collection	78
5.2.2	Dataset of spatio-temporal skin deformation	79
5.3	Results	81
5.3.1	Empirical strain patterns	81
5.3.2	Model validation	82

5.3.3	Dimensionality reduction	82
5.3.4	Tactile encoding efficiency of the safety margin	84
5.4	Discussion	86
5.5	Conclusion	87
6	Space-time fusion of discrete tactile events	89
6.1	Introduction	90
6.2	Viscoelastic model of the skin	91
6.2.1	Spatial stress distribution	91
6.2.2	Temporal attenuation of strain	92
6.3	Mechanical stresses and strains at the depth of the mechanoreceptors	92
6.3.1	Influence of friction on strains during a simple press	92
6.3.2	Evolution of strains during the transition from stick to slip	92
6.4	Tactile persistency	95
6.4.1	Spatio-temporal model	95
6.4.2	Materials and Methods	96
6.4.3	Results	96
6.5	Conclusion	98
7	Conclusion	99
7.1	Summary of the contributions	99
7.2	Applications to robotics	100
7.3	Future directions	100
A	Additional results of the friction perception experiment	107
A.1	Motivations	107
A.2	Strain components	107
A.3	Individual performance	107
B	Appendix B: Skin strains during incipient slippage	111
C	Appendix C: Dimensionality reduction technique	113
	Bibliography	117

List of Figures

2.1	Mechanical representation of the sagittal section of the fingertip	8
2.2	Non-linear stress-strain relation	10
2.3	Finger skin imaging	14
2.4	Skin modeled as a semi-infinite half plane	16
2.5	Structural mechanical models of human skin	18
2.6	Coulomb, Viscous coulomb and Stribeck models of friction	18
2.7	Mechanical equivalent of Dahl and LuGre models	20
2.8	Four types of mechanoreceptors and their action potentials	21
2.9	Spatio-temporal sensitivity of skin mechanoreceptors	23
2.10	Tactile spatial sensitivity	25
2.11	Tactile temporal sensitivity	26
2.12	Tactile illusions of motion	27
2.13	Incipient slippage visualization on a contact mechanics point of view	30
2.14	Forces coordination when lifting objects	33
2.15	Exploratory procedures of for active tactile perception	35
2.16	From object contact to human hand action	36
3.1	Mechanical model of finger skin	40
3.2	Sizing of the mechanical model	42
3.3	Surface deflection profile under a line load	43
3.4	Simulated skin displacement during a rapid friction change	44
3.5	Simulated strains during the transition from stick to slip for 3 friction coefficients	45
3.6	Physical and Virtual bump exploration	46
4.1	Setup for friction perception experiment	52
4.2	Ultrasonic friction reduction	54
4.3	Fingertip image processing	56
4.4	Empirical skin deformation when pressed against high- and low-friction surface	58

4.5	Experimental protocol and psychophysical results of friction perception experiment	60
4.6	Link between friction and skin deformation	60
4.7	Influence of friction on displacement field components	61
4.8	Influence of the kinematics of the exploratory procedure	63
4.9	Strains, strain rates and strain energy for each vibration amplitude	65
4.10	Ideal Observer Analysis	66
4.11	Predictions from the mechanical model	68
5.1	Evolution of forces and contact area during an incipient slip	75
5.2	Steps of perceptual computation from a friction-dependent strain field to a friction-invariant estimate of the safety margin.	76
5.3	Experimental setup for generating finger slippage	78
5.4	Typical trial of skin strain and safety margin during an incipient slippage for 3 friction condition	80
5.5	Experimental and simulated strain patterns during an incipient slippage	81
5.6	Singular Value Decomposition of the strains	83
5.7	Estimation of the safety margin from the skin deformation	84
6.1	Infinite half-plane model of the skin	91
6.2	Influence of friction on in-depth strains during a simple press	93
6.3	Influence of friction on in-depth strains during sliding	94
6.4	Spatiotemporal filtering of the strains applied on the surface	95
6.5	Setup and protocol for the experiment of persistency	97
6.6	Results of the psychophysical experiment of persistency	97
7.1	Curvature estimation with a tactile sensor	101
7.2	Manipulandum equipped with friction reduction glass plate	102
7.3	Hierarchical predictive coding	104
A.1	Strains and strain rates computation and their evolution for each vibration amplitudes	108
A.2	Strain energy densities and total strain energy variable according to friction condition	109
A.3	Individual performance in friction discrimination	110
B.1	Strains for all subjects (S1 to S12) when the relative displacements between the finger and the plate is 6 mm.	112
B.2	Median compressive strains (A) and tensile strains (B) as a function of the vibration amplitude when the relative displacement is 6 mm.	112
C.1	Overview of the dimensionality reduction methods.	113
C.2	Comparison between dimensionality reduction methods.	114

List of Tables

2.1	Thickness and Young's moduli of the four skin layers	11
2.2	Mechanoreceptors properties	23

List of Abbreviations

2-AFC	2-Alternative Forced Choice
CNS	Central nervous system
CFL	Courant-Friedrich-Lewy
EP	Exploratory procedure
FA	Fast Adapting
FDTD	Finite Difference Time Domain
FTIR	Frustrated Total internal reflection
ISOI	Inter-Stimulus Onset Interval
MoBS	Modified Binary Search
PC	Pacinian Corpuscle
SA	Slowly Adapting
SR	Stick Ratio
SVD	Singular Value Decomposition
SVM	Support vector machine

*A mon grand-père, à ma grand-mère
A ma maman qui se bat chaque jour pour voir les couleurs de
l'arc-en-ciel*

Chapter 1

Introduction

Contents

1.1 Problem statement	1
1.2 Thesis overview	3

1.1 Problem statement

THE sense of touch is so familiar we cannot imagine living without it. Right now you have my thesis manuscript in your hand, you are probably holding it without thinking about how much grip force you have to apply to keep it from slipping, even with your eyes closed. On the other hand, you have probably already experienced, on a snowy winter night, going back home and dreaming about getting warm by the fire, only to meet the difficult task of putting the key in the lock of your door with numb fingers. Indeed, when your finger is exposed to low temperature, cutaneous feedback is impaired and despite a perfectly functioning motor system, precision manipulation can become challenging. Both of these examples from our daily life show how valuable your sense of touch is. Holding and manipulating are instinctive mechanisms, much simpler than playing chess, however, there are barely understood in humans and almost never embedded in robotic grippers without involving a huge amount of data. Where the robots are now capable of defeating human in chess play, they still cannot play chess because of manipulation complexity.

Robots today rely mostly on vision systems to perform tasks. Developing robots that safely interact with humans is becoming a necessity in the field of rehabilitation, assistive robotics, industrial fine manipulation, and to study human behavior. To meet this tremendous challenge, future robots cannot rely only on vision, they have to be equipped with other modalities such as touch to perceive their surrounding environment. Objects possess plenty of global and local properties such as weight, texture, and slipperiness that can only be perceived through touch and are hardly accessible by vision.

Biology can serve as an inspiration for the development of these robotics systems. Even if research on the human touch is lagging that of the visual sense, studying the fantastic dexterity of the human hand can serve as inspiration for robotic systems in the years to come. The mechanical interaction with our environment is captured by our brain to produce the proper motor commands for a good force coordination. Now, imagine that you are not holding my thesis manuscript but an egg (I hope you will manipulate it with the same care). At the very moment you enter in contact with the egg surface, the mechanical deformation of your skin and the resistance opposed to your limb inform the central nervous system about the contact attributes, such as its texture, its curvature and its slipperiness. If you feel the surface as slippery, you will increase your grip force to avoid it from slipping out of your hand. Conversely, if the surface provides more grip, you will relax the squeezing force to avoid potential damages. This delicate balance relies on tactile cues and comes as a result of a reliable transduction of friction [238, 8].

But amongst all the surface attributes that the human sensorimotor has to factor in to decide the grasping force, friction is arguably the most important. So much so that in our daily lives, we sometimes purposefully increase friction to successfully perform these tasks. For example, to turn the page of this thesis, it would be easier if you moistened your finger before, water increasing considerably the friction at the interface. Friction is often defined in the case where two solids are sliding in contact, as the resistance opposed to relative sliding between them. However, friction also exists in static since the opposite resulting forces can be caused by adhesion, surface roughness, and deformation and depend both on the biomechanics and on the materials. Successful evaluation of the frictional information at the interface between our skin and an object is responsible for human performance in stable grasp.

The perception of friction is a central aspect of human and robotic grasping, yet the cutaneous deformation that leads to an estimation of the frictional property of a surface remains largely unknown. This thesis addresses two fundamental questions about our innate sense of friction:

- **How do frictional properties of a surface influence skin deformation?** A short mechanical interaction between our finger and an object allows us to extract contact information. When the finger is sliding relatively to the object, particular strain patterns of the skin are involved to decode the frictional properties of the object in order to adjust the grip force. This force adjustment occurs before the object starts to be lifted [107], which means that this strain patterns appear well before a net tangential force develops.
- **How do mechanoreceptors embedded deeper in the skin capture these rapid interactions?** Skin mechanoreceptors are located deep in the skin tissue. The skin, being a soft viscoelastic material, acts as a mechanical filter that is both spatial and temporal. This filter limits our perception of

mechanical events and causes many tactile illusions. In particular, typical strains pattern of skin surface induced by frictional changes can be altered at the depth of the mechanoreceptors.

Solving these two questions would help understanding the main contribution of skin mechanics to detect friction and incipient slippage, ensuring a stable grasp. It could help, in a near future, to mimic human performance in robotic grippers.

1.2 Thesis overview

This thesis is organized as follows:

Chapter 2 provides a literature review of human touch, from their interaction with objects to the action of their hand. First, I present the mechanical structures and properties of skin tissue and how they can be modeled. Then, I detail the principles of mechanotransduction to understand which kind of signals are transmitted to the Central Nervous System (CNS). In the following section, I review how these signals are shaped to produce actual percepts in terms of sensibility to pressure, localization, and temporality. Finally, I present the control loop which allows us to adjust the grip force for a proper manipulation.

Chapter 3 describes a computationally efficient mechanical model able to capture large deformation of the skin, its viscoelastic behavior using Kelvin-Voigt material and the local elastoplastic frictional interaction at the interface. The model is purposefully made as parsimonious as possible, while balancing the accurate representation of the influence of friction on the skin deformation. It is constructed with a bottom-up approach, using as few parameters as possible to match the observed static and dynamic behavior during exploration.

Chapter 4 elucidates the effects of the frictional properties of objects during initial contact before slippage occurs. This chapter highlights a correlation between participants' conscious perception of frictional properties and stereotypical patterns of skin deformation, validated by the model explained in the previous chapter. This correlation provides insights into the tactile cues made available by contact mechanics to the sensorimotor regulation of grip, as well as to the conscious perception of the frictional properties of an object.

Chapter 5 pictures how the skin deforms when the finger slips on surfaces with varying friction coefficient. In this chapter, we show a compact lexicon of skin deformation modes able to encode the information of safety margin along the slippage with 85% of accuracy.

Chapter 6 predicts the strains the mechanoreceptors (buried inside the skin layers) are subjected to when the finger is pressing or sliding on a surface. The skin is a viscoelastic medium which acts as a mechanical filter for the stress applied on the surface. This filtering process can be responsible for the tactile persistency illusion, already well-known in vision.

Chapter 7 concludes and discusses the main contributions of this thesis. In this chapter, I also identify future research questions arising from the contributions and their limitations.

Chapter 2

State of the art

Contents

2.1	How do humans interact: Bio-tribology of skin	6
2.1.1	Finger anatomy	6
2.1.2	Mechanical properties of skin	8
2.1.3	Frictional properties of the skin	11
2.1.4	Mechanical models of skin tissue	16
2.2	How do humans encode the mechanical deformation: Mechanotransduction	19
2.2.1	Four types of afferents	20
2.2.2	Summary	22
2.3	How do humans perceive	23
2.3.1	Tactile sensitivity	23
2.3.2	Slip detection	29
2.3.3	Friction perception	31
2.4	How do humans manipulate: Human hand's action	31
2.4.1	Action and perception	32
2.4.2	Grip force control	32
2.4.3	Passive vs active sensing	34
2.4.4	Predictive coding	35
2.5	Conclusion	36

Preface to Chapter 2

HUMAN sense of touch provides a wealth of information about the contact condition and the properties of the object being manipulated, such as its material, curvature and frictional capacity at the interface. An accurate estimation of these properties is crucial for a good object manipulation. This chapter reviews the literature from the very interaction of the finger skin to the active hand motion for a stable grasping. It is divided into four sections:

1. **How do humans interact?** This section describes hand's anatomy, mechanics and skin structure. At the end, a review of the mechanical models of skin tissues are also presented.
2. **How do humans sense?** Tactile sensing system relies on mechano-transduction ensured by thousands of mechanoreceptors. These afferents are converting mechanical touch to processable tactile signals by the central nervous system.
3. **How do humans perceive?** Once a skin deformation is sensed, i.e. sent to the brain via the nerves, the central nervous system is responsible for extracting information about objects or contact from the raw signals.
4. **How do humans manipulate?** This section details the control of grasping and manipulation tasks using the contact information extracted from the tactile signals as feedback.

2.1 How do humans interact: Bio-tribology of skin

Tribology comes from the greek *tribos* and means rubbing. The science of tribology studies friction, wear, lubrication and how surfaces are interacting in relative motion in general. As the human skin is always one of the interacting surfaces when manipulating, this section explores first the anatomical structure of the fingertip and how its biomechanical properties naturally arise from its anatomy.

2.1.1 Finger anatomy

The skin is the largest organ of our body. Its surface approximates 1.5 to 2 m² in adults and its weight can reach 3.5 to 4 kg, which represents 16% of the total body weight of an adult. Skin can be considered as a membrane and its thickness varies between 2 mm and 4 mm according to body locations [239]. The skin is simultaneously impermeable to protect us against the external aggression as light or microbe and permeable to interact with the environment [112].

There are two kinds of human skin: hairy skin characterized by hair follicles and glabrous (hairless) skin found on the palms of the hands and on the soles of the feet.

The glabrous skin is relatively rigid and thicker than the hairy skin, which is thin and soft [112]. Skin structure is a complex superposition of layers, including the epidermis, the dermis and the hypodermis, from surface to depth. The thickness of these layers can range from 100 μm to few millimeters depending on anatomic locations, subjects, gender and age. Each cutaneous layer is composed of different type of cells. The structural differences of these layers make them specialized for different functions.

Epidermis

The epidermis is the uppermost layer of the skin. It is almost totally impermeable for two reasons: keeping water inside the body and acting as a barrier to viruses. The epidermis is not smooth but instead folds into epidermal ridges and valleys forming the fingerprints. The periodicity of these ridges is approximately 400 μm . This layer is 0.1 mm thick on average, even if it varies from 0.04 mm at the eyelids to 1.6 mm at finger palm. Corcuff [43] obtained μm -precision measure via Confocal Microscopy, and the thickness of the epidermis on the human forearm has been measured to 36 μm with this method.

The epidermis is constituted of four layers of cells, called keratinocytes, stacked on top of each other. The cells of the basal layer migrate gradually from towards the surface, uptaking of keratin. Once they arrived at the surface, these cells are eliminated by washing or rubbing clothing.

Stratum corneum

The superficial layer of the epidermis, called stratum corneum, is only 15 to 20 μm thick [178]. It contains mainly water, which is responsible for its flexibility [241, 136]. Dry stratum corneum has an elastic modulus of about 1 GPa, but this value can be reduced by approximately four orders of magnitude when it is saturated with water [64]. The stratum corneum is also very fragile and can lead to infection when it is damaged.

Dermis

Just below the epidermis, the dermis is the thickest layer of the skin. Its thickness can be measured using ultrasound method. Interval between two echos provides information about tissue inhomogeneities and can thus give a measure of the dermal and epidermal thickness with a precision of 0.1 mm. This method results in thickness for the dermis and the epidermis of 0.55 ± 0.88 mm on the forearm, depending on age and sex [69].

The interface between epidermis and dermis shows some micro-waves or papillae. It is made of cells called fibroblasts surrounded by an extra-cell matrix, blood vessels and nerve endings. The fibroblasts produce permanently collagen fibers and elastic fibers (elastin). These fibers are embedded in a fluid extracellular

matrix, called the ground substance, which makes 20% of the dry weight. Collagen fibers are the main constituent of the dermis (70% of the dry weight) and form an irregular network of wavy coiled bundles. Collagen is characterized by high strength (tensile strength of 1.5-3.5 MPa), low extensibility (rupture at strains in the order of 5-6%), and high stiffness (Young's modulus approximately 0.1 GPa to 1 GPa [150]). The width of the bundles is 1-40 μm . Elastin fibers are the second main component of the dermis (4% of the dry weight). They are extremely elastic compared to collagen and show reversible strains of more than 100% [84]. Their diameter ranges between 0.5 and 3 μm . Collagen and elastin enable to take into account the possible impact of stresses or strains while ensuring resistance and elasticity to the skin (see section 2.1.2).

Hypodermis

Also known as subcutaneous tissue, the hypodermis is mainly composed of adipose cells. This layer [60] is 1.1 mm thick on average and constitutes about 10% of the body mass. Its role is to connect bones and muscles with the dermis.

Nail

The finger nail can be used as tools, weapons or for body care [74]. Thus, it has to be hard but flexible and not too brittle. This hardness is controlled by skin moisture [72]. The finger nail, principally composed of keratin, is linked to the distal phalanx via two ligaments [148].

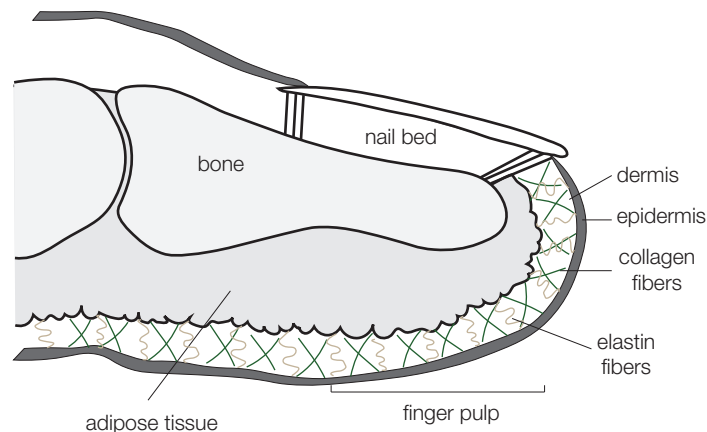


FIGURE 2.1: Mechanical representation of the sagittal section of the fingertip

2.1.2 Mechanical properties of skin

Non-linear elasticity

Human skin *in vivo* is known as a complex mechanical material: non-linear, viscoelastic, non-homogeneous, anisotropic and with hysteresis. The mechanical

properties are intimately associated with its complex structure [173]. The dermis is assumed to be the principal structure contributing to the mechanical properties of the skin [60, 236], because of its significant stiffness and its high content of collagen fibers.

The fingertip can be geometrically approximated to a hemisphere, however, it does not obey the Hertzian theory of contact during indentation. Dynamic loading properties affect the mechanical response of the fingertip [172, 158]. The relation between force indentation and displacement of the finger pulp, called the stress-strain relationship, can be split into 3 stages as represented on the Figure 2.2 [200, 96]. In the first stage, for small strains, the relationship is linear with a Young's modulus of 5 kPa on average. This initial low stiffness can be attributed to the elastin network in the dermis [164] and is responsible for the deformability of the fingertip even at small loads. With a 1 N normal force, the indentation depth already reaches 1 mm [172]. In the second stage, for strain greater than 0.3, the collagen fibers begin to align and straighten in the direction of the applied load. They are involved gradually stretch instead of the elastin fibers, resulting in a non-linear exponential stress relationship. As a result, the skin becomes stiffer and the resulting force increases rapidly with indentation. Finally, in the third stage, for large strains, all collagen fibers are stretched, so further extension of the skin requires extension of the collagen fiber. The stress-strain behavior appears as a straight line again. The slope is steeper, which means that skin becomes more stiff. It has been shown that this high stiffness is similar to that of pure collagen [201].

Even if the structure of the dermis is the principal cause of this non-linearity, some authors also recognize the influence of the stratum corneum [52] and the epidermis. As a matter of fact, skin is on average three times stiffer along the ridges than across them [225]. As a result, fingertip skin can sustain a relative deformation of 100% in stretching or shearing without any damage, while preserving its strength along the ridges. Nonetheless, Delhayé et al. [56] highlighted a realignment of the fingerprints perpendicularly to the tangential loading direction during sliding, suggesting that fingerprints shape how the skin deforms under a tangential traction.

Viscosity

Viscoelastic behavior of skin tissues has been evaluated in few studies [171, 159] and was found to be highly non-linear [225, 124]. Viscoelastic effects are noticeable during stage II and stage III, in which the collagen fibers are carrying part of the load. A removal of the ground substance of the dermis induces a decrease in stress level, stiffness and relaxation [153]. Thus, the ground substance is probably responsible for this viscoelastic behavior. More precisely, the time-dependent behavior of the skin can be attributed to the movement of the collagen network in the ground substance [236]. Fibers exhibit viscous resistance while moving through the ground substance to align in the direction of the load.

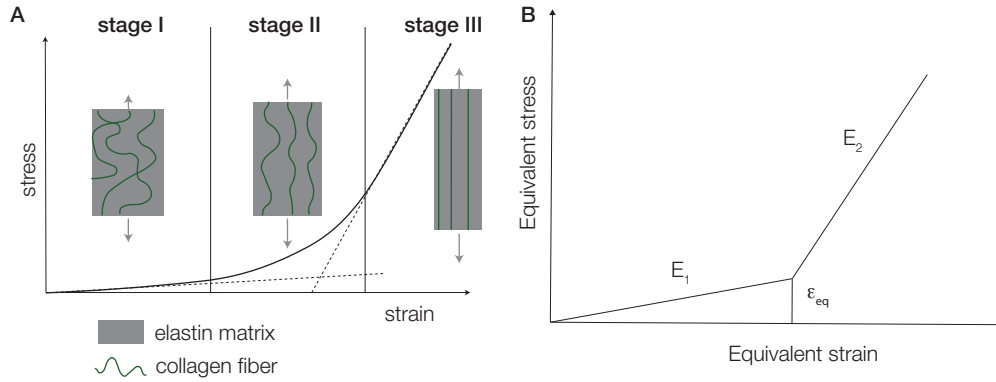


FIGURE 2.2: **A.** Non-linear stress-strain relation for human skin under a tension test. **B.** Equivalent model characterized by three parameters: E_1 , E_2 and ϵ . (from [96])

Skin also exhibits the two main properties of viscoelastic materials: adhesion and hysteresis. Adhesion occurs when skin surface asperities form a bond, creating a sticky contact. Hysteresis is the energy lost within the tissue between loading and unloading. It could be characterized by the delayed responses of a material to the forces acting on it. These mechanisms will cause a relaxation behavior characteristic of viscoelastic materials [114].

Pre-tension

The human skin is normally in a state of tension all along our lives. This tension varies from body region in order to regulate extracellular matrix metabolism through mechanochemical transduction [201]. *In vivo* tension ranges widely from 1.7 N/m to 138 N/m [101, 76, 61]. This value gives us an indication of the stress-free configuration of the soft tissue.

Young's modulus

The non-linear domain of the stress-strain curve occurs at stress levels which are not normally encountered by *in vivo* skin for more than very short time periods [49]. Thus, the elasticity of the skin (Young's modulus) is given by the ratio of stress over strain in the first stage, when the strain experienced by the skin is less than 0.3. The Young's modulus can be measured thanks to a variety of methods: compression or indentation tests, torsion tests, tensile tests and suction tests.

Indentation test determine the skin behavior under compressive loading. This method is mostly used to measure the elastic limit and compressive strength. Young's modulus can then be calculated using Hertz theory of contact (2.1).

$$d = \frac{P(1 - \nu^2)}{2R \cdot E} \quad (2.1)$$

where P is the applied load, d the resulting deformation, ν the Poisson's ratio and R the indenter radius. Bader and Bowker [9] used this method to obtain a Young's modulus of 1.1 ± 1.4 kPa depending on age and sex.

In a torsion test, a torque is applied by a disc attached to the skin. This test can provide global mechanical properties as Young's modulus. With this test, the Young's modulus ranges from 0.02 to 1.32 MPa depending on age [185, 5, 69].

Tensile test determine the skin behavior under axial tensile loading. The skin is loaded parallel to its surface [146]. Across the tibia, a maximum Young's modulus of 4 MPa was measured for strain lower than 0.3 and along the tibia, maximum Young's modulus can reach 20 MPa.

Suction test measure skin deformation caused by the application of a partial vacuum via optical or ultrasound system. In the linear part of the stress-strain relationship, skin elevates of 0.1 to 0.6 mm, which corresponds to a Young's modulus of 0.13-0.26 MPa [10, 60].

The dermis is known as the main contributor but as intimate connections exist between skin layers, it is hard to isolate the contribution of the dermis from that of the epidermis and the subcutaneous tissues. The table 2.1 summarizes the Young's moduli measured *in vitro* for each of the four skin layers.

	Thickness [μm]	Young's modulus [MPa]
Stratum corneum	15-20 [42, 178]	13 – 175 [241]
Epidermis	36 [43]	0.75 ± 2.4 [46, 79]
Dermis	$0.80-0.87 \cdot 10^3$ [60]	0.035-0.075 [136, 165]
Hypodermis	$1.1-1.2 \cdot 10^3$ [60]	0.002-0.008 [136, 165]

TABLE 2.1: Thickness and Young's moduli of the four skin layers. Note that the values gathered in this table are average across a large population of subjects but skin thickness and elasticity vary considerably between individuals.

The measured Young's moduli is presenting a lot of variability coming from many factors: the nature of the experimental techniques, but also skin thickness [54], skin humidity, age, sex and regions of body [5, 136].

Poisson's ratio

The Poisson's ratio has only been measured *in vitro* for a cow teat and varies from 0.5 to 1.3 depending on the direction [132]. However, many studies assume the Poisson's ratio of human skin to be approximately equal to 0.48-0.5 [136].

2.1.3 Frictional properties of the skin

Friction is the resistance opposed to relative sliding between two objects in contact. It is described by the friction coefficient μ , which is the ratio between the tangential (F_t) and the normal component (F_n) of the interacting force according to Amontons'

law:

$$F_t = \mu F_n \quad (2.2)$$

The value varies from 0 for the most slippery material as silk to 1 for the surface with more adherence as sandpaper. Previous studies of friction have shown that static coefficient of friction μ_s is both material and system dependent. It can vary with normal load, sliding velocity, apparent contact area and also some environmental factors [1, 170]. Dynamic coefficient of friction μ_d can be estimated when the finger is sliding on the surface.

As skin presents a viscoelastic behavior as shown in section 2.1.2, it is subjected to the law of adhesion and hysteresis. These two phenomena imply a higher frictional force than require breaking contact. Indeed, the junctions created because of adhesion have to be sheared, and a larger force is required to compensate the energy loss because of hysteresis.

Friction is more important during a distal-proximal exploration while during an exploration in the ulnar and distal direction, the friction would be reduced [38]. This privileged direction is probably imposed by the fingerprints, even if their role is still controversial and minor [228]. On the other hand, fingerprints are believed to reinforce friction and adhesion [188] because the papillary ridges, mirror of the fingerprint ridges, act as a lever that amplifies the mechanical stress [33].

How to measure the frictional strength

The frictional strength is defined as the lateral force at which the finger starts sliding. At a macroscopic scale, the frictional strength of a contact is typically found from the lateral force at which relative motion occurs [14]. But even when no tangential force is exerted, this frictional strength is present, since the intimate contact of skin on the surface holds a potential for adhesion. At the microscopic scale, the contact between the skin and an atomically-flat surface is made by a collection of individual junctions of a micrometer-scale area. The sum of the areas of all junctions constitutes the *real* area of contact [174]. An increase in normal force will create more junctions, each of which will have a larger area. Each of these junctions can carry a certain amount of shear stress τ_0 before local sliding can occur, and therefore the friction force can be found to be linearly related to the real area of contact such that $F = \tau A^R$, where A^R is the *real* area of contact. This linear dependence is observed for a large set of materials, including rubbery and biological materials [12, 234].

τ is the interfacial shear strength of the contact, which arises from the dissipated energy from the rupture of molecular junctions at the sliding interface. Hence, this coefficient depends on the mean contact pressure $\frac{W}{A^R}$ as follows [28]:

$$\tau = \tau_0 + \alpha \frac{W}{A^R} \quad (2.3)$$

W is the contact pressure and τ_0 is estimated when $W = 0$. τ_0 and α vary with contact pressure and skin hydration [170]. When $W = 5 \text{ N}$, τ_0 has been estimated

to 5.6 kPa and $\alpha = 0.8 \pm 0.1$ [7]. Consequently, the frictional force is given by a two-term relation:

$$F = \tau_0 A^R + \alpha W \quad (2.4)$$

Thus, a powerful method to estimate the frictional resistance of a contact, even before the fingertip starts sliding, is to measure an approximation of the real contact area directly. An accurate measurement of the real area of contact can be found by optical means in the case of biological materials such as glabrous skin. As a testament of their efficacy, the real area of contact reported by these methods correlates with friction force, confirming the adhesive theory of friction even in the case of soft materials [234, 183].

The real contact area made by the collection of asperities is only a fraction of the size of the apparent contact area that encompasses the entire contact [27]. Consequently, to measure the real area of contact of the finger on a glass surface, ellipsoid fitting cannot be used, instead we must find a way to count the individual asperities in intimate contact. For randomly rough surfaces, the asperities form a self-similar pattern, where the general structure of the contact is found at different levels of magnification [174]. Because of the fractal nature of this surface, the real contact area made by rough surfaces depends on the magnification level, in the same way that the length of the coast of Britain depends on the size of the measurement quanta [145]. For a given spatial resolution, each pixel essentially aggregates the complex fractal pattern. Therefore, using the optical measurement, a value of the real area can only be found at a given length-scale, which is set by the optical setup.

Simply looking through the glass plate at the contact region does not allow for discriminating the intimate contact to the rest of the picture. Some methods take the advantage of the reflection property of glass and absorption property of skin to achieve high contrast between the regions where the skin asperities are in intimate contact and the regions where the skin is further away from the plate.

The two methods reported in the literature that can achieve a separation of the asperities from the background use the principle of frustrated reflection. When light is incident on the interface of two media, it is partly transmitted into the second medium and partly reflected back to the first one. If the angle of incidence of the light beam exceeds a critical angle, the light beam is totally reflected back in the first medium and does not propagate into the second one, called total internal reflection [90]. However, there must be some light penetrating into the second medium because the electric and magnetic fields cannot be discontinuous at the interface. The amount of light entering this way into the second medium falls off exponentially with penetration depth. Thus, if a third medium is placed at a distance from the first medium in the order of magnitude of the light wavelength, the incident light can then be transmitted to the third medium. This phenomenon is called frustrated internal reflection. This principle allows imaging the asperities of the fingertip interacting with a transparent glass plate, the thin air gap between the

fingertip and the glass plate playing the role of the second medium.

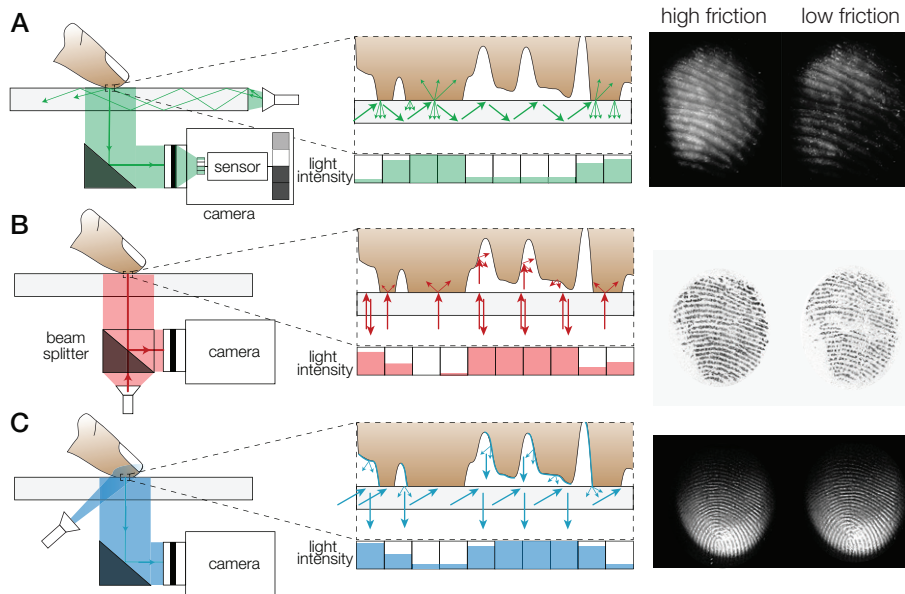


FIGURE 2.3: Finger skin imaging. **A.** Frustrated total internal reflection method. **B.** Coaxial method. **C.** Dark-field light illumination.

The incident light ray can be reflected, either totally in the case of a total internal reflection [7, 234, 24, 63], or partially in the case of an orthogonal reflection [213, 123, 55, 183] at the interface, enabling two different configurations:

- *Frustrated total internal reflection (FTIR)* is based on the evanescent wave phenomenon and is illustrated Figure 2.3A. It can be achieved by capturing the reflected image through a prism [7] or by collecting the scattered image of light trapped inside a plate [234]. When the incident beam is at a shallow angle with the surface, the glass plate is illuminated sideways and acts as a light trap. Asperities of the fingertip close to the glass up to a few hundred nanometers scatter the light out of the glass. This configuration has the advantage of being compact, however, it produces images with fuzzy contour of the contact.
- The *coaxial method* leverages an illumination exactly perpendicular to the surface using a half-mirror (Figure 2.3B). Images have a sharper contour than the FTIR method, but less contrasted because of a lesser amount of light reflected back to the imager.

When the asperities of the skin couple with the transmitted wave field, the reflected light is absorbed and scattered. This scattering creates darker regions in the reflected image and provides a highly contrasted image of the individual asperities in intimate contact. The reflected image highlighting the region where no asperities are in contact and darkening the region of intimate contact can be sampled with a camera. During this process, the number of photons collected on each pixel is inversely correlated to the number of asperities present in the region

imaged by the pixel. If the exposure of the camera is fixed, the brightness field corresponds to an inverse image of the density of junctions resolved at a length scale comparable to the half-wavelength of light. Darker areas represent a higher density of asperities in intimate contact.

To capture this reflected image, the camera sensor discretizes the number of photons collected during the exposure. The darker areas receive fewer photons and lead to a lower value of the pixels. Conversely, the areas that do not face any finger asperities receive the maximum number of photons per unit area. Therefore, the exposure can be set such that this maximum number of photons induces a value of the pixel that reaches the top of the dynamic range.

From the high-contrast image, it is possible to recover a value that is proportional to the area of real contact at half-wavelength of light lengthscale. First, consider the image without a fingertip, which might have a non-uniform illumination. The resulting background image I_0 corresponds to the dynamic range of each pixel. To normalize the illumination on every subsequent image of the contact I_f , a pixel-to-pixel division of the image by the background image can be used. Once this is done, the normalized image must be inverted to find the estimate of the light absorbed by the contact I_a such that:

$$I_a = 1 - I_f/I_0 \quad (2.5)$$

The contact area is therefore found by summing the brightness of every pixel of the absorption image I_a .

The absorbed-light method provides a granular measurement of the fractal real contact area, with a theoretical resolution at the wavelength of the incident light, which is in the order of 300 nm. The resolution is orders of magnitude better than a simple thresholding and pixel-counting procedure, used in [64, 183] for instance. The reason is that thresholding places the effective resolution at the size of a pixel, which is in the order of tens of micrometers. Finally, the optical estimation of the real area of contact A^O is calibrated using a measurement of the apparent area of contact, A^A , expressed in mm, knowing that the real and apparent area are identical in the hypothetical case that the contact is total.

Both previous methods allow a visualization of the intimate contact but when friction is reduced, the center of the contact experienced ultrasonic levitation, creating those white regions where asperities were not in intimate contact (Figure 2.3A,B). Because of these white regions where no contact occurs, it is not possible to compute the skin deformation by tracking points of interest in the non-contacting region because of ultrasonic levitation. To reconstruct the skin deformation in the whole contact area, a *dark-field light illumination* can be used (Figure 2.3C). In this method, the light illuminates the fingerprints at a shallow angle of 20° , allowing a visualization of the skin asperities even before entering in intimate contact with the plate.

2.1.4 Mechanical models of skin tissue

Modeling the skin tissue have many applications in drug delivery, vaccines and in cosmetic, and it can also be very useful to plan surgical incisions. The fields of tactile interface will also benefit from an accurate model of skin to design suitable stimuli [192, 99]. A fast and robust modeling of skin deformation can also serve to control robotic sensor and prostheses. Last but not least, it could allow a better understanding of how the mechanics of our finger contribute to human ability to touch and grasp. Modeling the interaction of a deformable object has already been a subject of numerous researches, which will be reviewed in this section.

Quasi-static model

Computational models of quasi-static deformation can be classified in two main categories: macroscopic and structural models. These both categories depends on the application.

In the macroscopic approach, skin is modeled as a homogeneous material, ignoring the layers and their mechanical properties. The aim of these models is to capture the macroscopic behavior, with mathematical relations describing the relationships between the applied loads and the resulting deformation under strictly normal loading. The simplest one is the linear-elastic model, as proposed by Hooke's law. It predicts the deformation of a fingertip in contact with a flat or a curved surface with a reasonable accuracy. Some studies modeled the skin as a bi-linear elastic material, based on the assumption that stress-strain relationship follows a Hooke's law with a Young's modulus E_1 for strain lower than ϵ_{eq} and E_2 for strain higher than ϵ_{eq} (see Figure 2.2B).

Knowing the interfacial pressure $p(x)$ and traction $q(x)$ distribution on skin surface, the model of Boussinesq & Cerruti [34, 26, 208] can be applied to reconstruct the stresses deep in the skin layers:

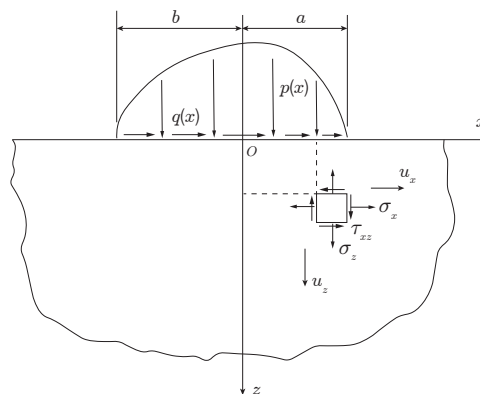


FIGURE 2.4: Skin modeled as a semi-infinite half plane

$$\begin{aligned}
\sigma_x &= -\frac{2z}{\pi} \int_{-b}^a \frac{p(s)(x-s)^2}{((x-s)^2+z^2)^2} ds - \frac{2}{\pi} \int_{-b}^a \frac{q(s)(x-s)^3}{((x-s)^2+z^2)^2} ds \\
\sigma_z &= -\frac{2z^3}{\pi} \int_{-b}^a \frac{p(s)}{((x-s)^2+z^2)^2} ds - \frac{2z^2}{\pi} \int_{-b}^a \frac{q(s)(x-s)}{((x-s)^2+z^2)^2} ds \\
\tau_{xz} &= -\frac{2z^2}{\pi} \int_{-b}^a \frac{p(s)(x-s)}{((x-s)^2+z^2)^2} ds - \frac{2z}{\pi} \int_{-b}^a \frac{q(s)(x-s)^2}{((x-s)^2+z^2)^2} ds
\end{aligned} \tag{2.6}$$

Higher accuracy has been obtained with models based on an incompressible fluid-filled membrane [206, 194, 214]. In these models, the finger was assumed to be an elastic membrane enclosing a fluid-like soft tissue, and the predictions fit well to in vivo experiments. Nevertheless, this model fails to capture the behavior when boundary conditions become complex, and they do not take into account non-linear skin elasticity.

In the structural approach, the skin is an assembly of microstructural elements with explicit characteristics. These models take into account the specific geometry of the skin layers, but also how they interact with each others [147] (Figure 2.5C). Finite Element Analysis have recently been seen more attractive because of advances in computing power. This method can take into account the geometry of the finger and model the strains inside the deeper layers of the skin [143]. In this approach, a finger section is modelled as a multi-layered structure using material properties of the finger tissue (Figure 2.5AB). Subject-specific geometry has been incorporated later in more detailed 3D-models [50, 212, 227] (Figure 2.5D).

Viscoelastic model

Even though everyday manipulation tasks nearly always includes movement, models of dynamic behavior of the finger emerged much later. Non-linear viscoelastic models of soft tissue could well describe pulp force-displacement [77]. Viscosity was implemented in 2D finite element models [240] and in 3D models using nonlinear and inhomogeneous materials [215]. These models allow to observe a time-dependent force responses of the fingertip.

However, the finite element methods incorporate too many parameters and therefore can be prone to overfitting and require a lot of processing power.

Friction modeling

Friction modeling affects a lot of areas, that is why numerous models were developed these last few years. Some of them are based on a spring-like relationship between frictional force and displacement. In this section, F_f and F_n will stand respectively for friction and normal force, μ for the friction coefficient. x will be used as the position and \dot{x} as the sliding speed.

Coulomb friction model is represented using the following equation:

$$F_f = F_c \cdot \text{sign}(\dot{x}) \text{ for } \dot{x} \neq 0 \tag{2.7}$$

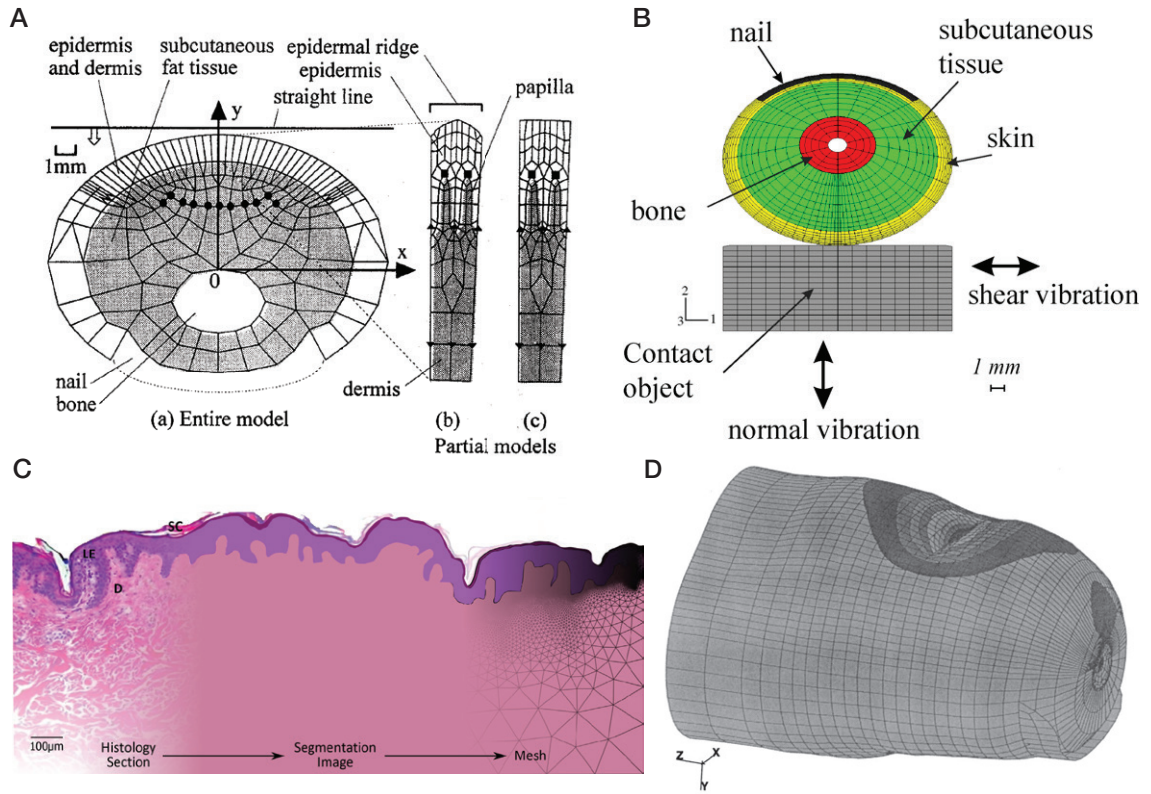


FIGURE 2.5: Structural mechanical models of human skin, from 2D to 3D, from general to subject specific. A. [143] B. [240] C. [147] D. [50]

F_c is the Coulomb friction force defined as $F_c = \mu F_n$. Viscosity can be added in Coulomb model by adding a linear part $k_v \dot{x}$, where k_v is the viscous coefficient. Although simple, the Coulomb model presents a discontinuous friction force which is not properly defined when $\dot{x} = 0$.

The first friction model that breaks with discontinuity was the Stribeck friction model, described in equation (2.8)

$$F_f = (F_c + (F_s - F_c)e^{-|\frac{\dot{x}}{v_s}|^i}) \operatorname{sgn}(\dot{x}) + k_v \dot{x} \quad (2.8)$$

F_s is the static friction force and v_s the Stribeck velocity.

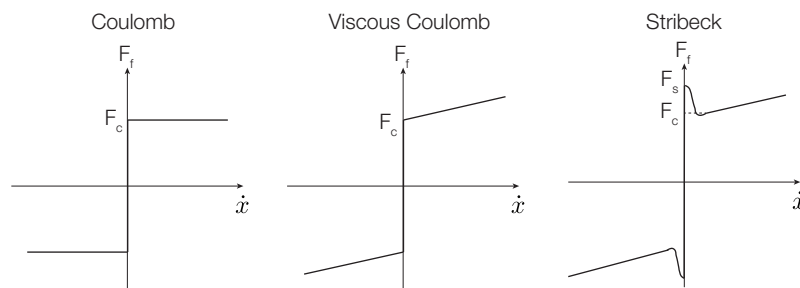


FIGURE 2.6: Coulomb, Viscous coulomb and Stribeck models of friction

Dahl model described the friction with an analogy of the stress-strain property

for materials [47]. For small displacements, objects returned to its initial position. Dahl modeled this elastic behavior by a spring. Larger displacements will cause plastic deformation, resulting in the object displacement.

$$\begin{aligned} \frac{dF_f(x)}{dt} &= \frac{dF_f(x)}{dx} \frac{dx}{dt} \\ &= \sigma_0 \left| 1 - \frac{F_f}{F_c} \text{sign}(\dot{x}) \right|^i \text{sign} \left(1 - \frac{F_f}{F_c} \text{sign}(\dot{x}) \right) \dot{x} \end{aligned} \quad (2.9)$$

σ_0 is the rest stiffness of the asperities at equilibrium point $F_f = 0$. i is an exponent that codes how ductile or brittle the material is. For more ductile material, the maximum stress before slippage will decline for increasing strain.

With this equation, Dahl takes into account pre-sliding and hysteresis. However, Dahl model does not predict the Stribeck effect.

LuGre model deals with this issue, adding a viscous term and the Stribeck function in Dahl equation [53]:

$$\begin{cases} F_f = \sigma_0 z + \sigma_1 \dot{z} + \sigma_2 \dot{x} \\ \dot{z} = \dot{x} - \sigma_0 \frac{\dot{x}}{g(\dot{x})} z \\ g(\dot{x}) = F_c + (F_s - F_c) e^{-|\frac{\dot{x}}{v_s}|^i} \end{cases} \quad (2.10)$$

z can be interpreted as the average deflection of the bristle. σ_0 is the contact stiffness, σ_1 the damping coefficient of the bristle and σ_2 the viscous friction coefficient. $g(\dot{x})$ takes into account the Stribeck effect.

The stress-strain curves of Dahl and LuGre models are shown in Figure 2.7A and B respectively. Hysteresis is observed in both models, but the curve is steeper for the LuGre model, meaning that the system react quicker to an external perturbation.

This section reviewed the mechanical bases of the fingertip. Time has now come for establishing a relationship between the stresses and strains and the neural responses [175] in order to understand how do humans encode skin mechanical deformation.

2.2 How do humans encode the mechanical deformation: Mechanotransduction

In the previous section, we show how the skin deforms during a mechanical event. This deformation is decoded through sensors located in different areas of the skin. The particular locations of these sensors is not arbitrary, but comes from the fact that the strain energy is concentrated at these locations [143]. The capture of electrical signals during a mechanical stimulation reveals the presence of four types of afferents or mechanoreceptors. These mechanoreceptors are able to transduce mechanical disturbances into actions potentials that are transmitted to the central

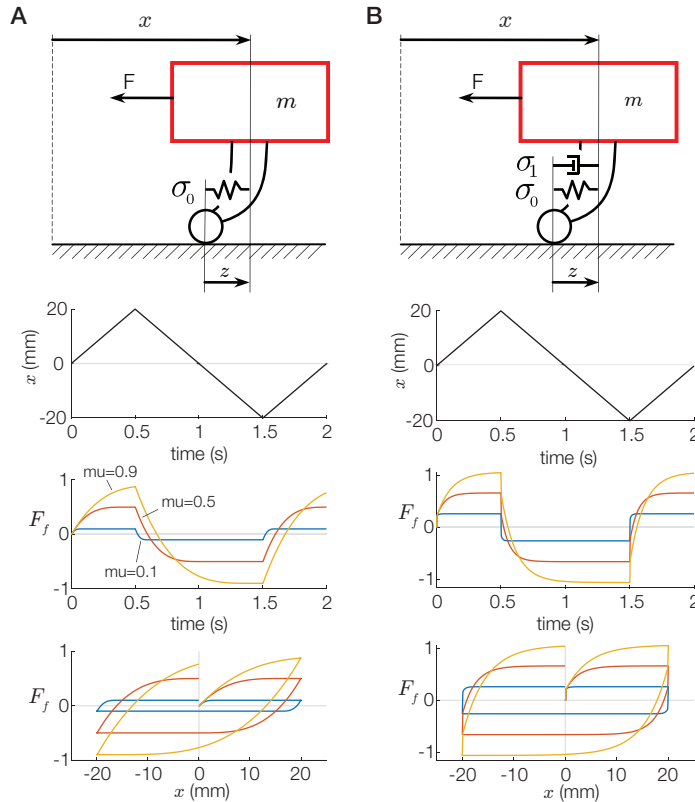


FIGURE 2.7: Mechanical equivalent of Dahl (A) and Lure (B) models (from [176]). Blue, red and yellow colors code friction coefficient of 0.1, 0.5 and 0.9 respectively.

nervous system through the nerves [58, 104]. Nerve endings can be free, allowing the perception of pain, or connected to one of these four types of afferents. They are classified according to two characteristics: the speed of adaptation to the mechanical events (slowly adaptive SA and fast adaptive FA) and the size and acuity of their receptive field (type I or type II). The word adapt here means that the mechanoreceptors stops sending signals to the brain. Although mechanoreceptors adapt differently, all of them adapt. For example, if you sit without moving, eventually the skin will stop feeling the pressure of the chair. This adaptation makes the sensitive system much more sensitive to a change than to a constant stimulus. The speed of adaptation was measured via electrophysiology via a probe clamp to the ulnar and median nerves running in arm (Figure 2.8).

2.2.1 Four types of afferents

SA type I afferents or Merkel cells

The Merkel's cells are located at the interface between the dermis and the hypodermis, on the ends of the ripples. They are distributed widely in the glabrous skin, and their density can reach 100 per cm^2 at the fingertip. Sensitive to the spatial component of deformation up to 1% [66], they respond to punctate pressure and

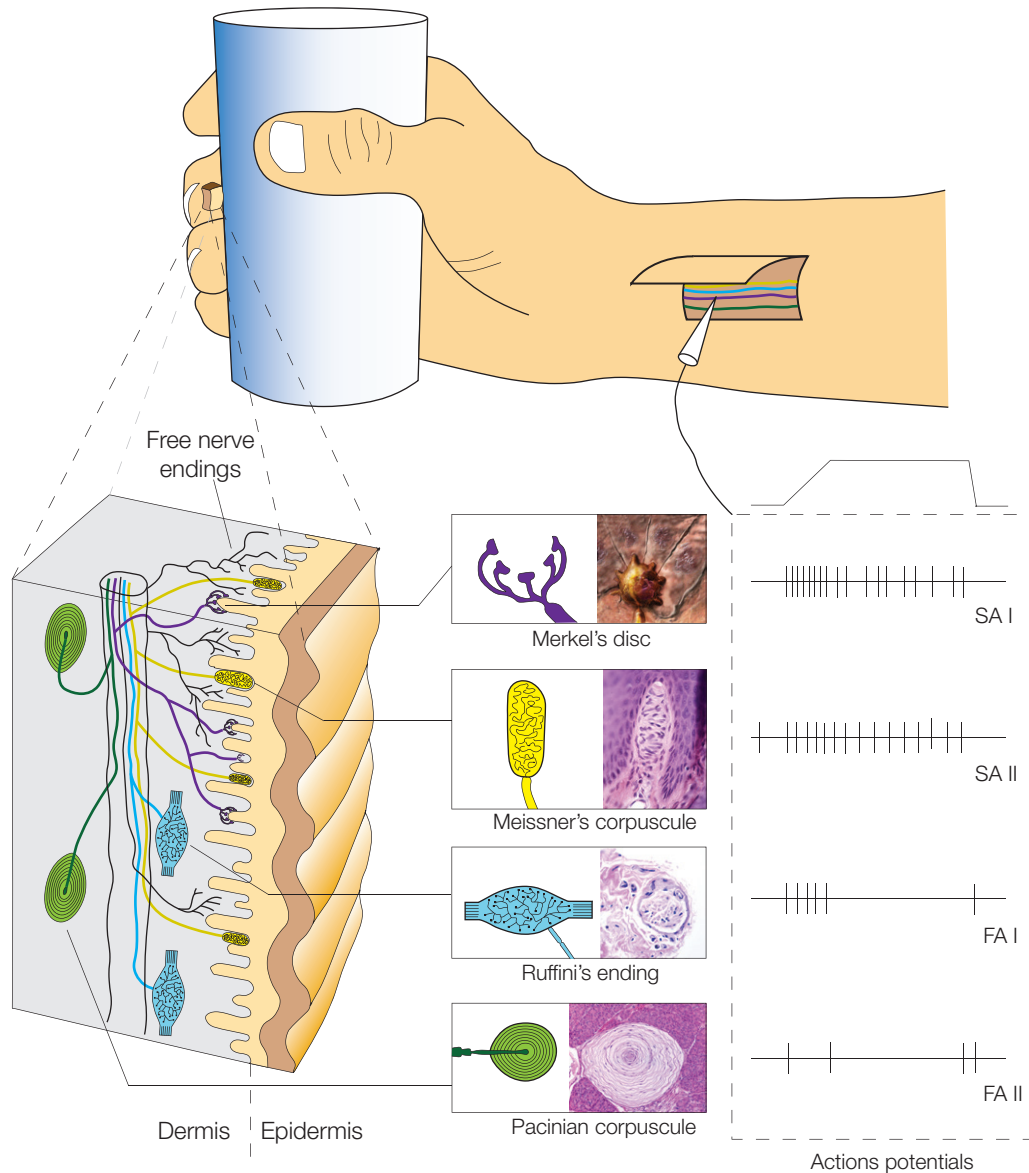


FIGURE 2.8: Four types of mechanoreceptors, their location (bottom left) and their action potentials (bottom right) (adapted from [51, 219])

are involved in the perception of edges [175], curvature [83, 126] and the coarsest textures [186, 110]. For a review, see [89].

SA type II afferents or Ruffini endings

The Ruffini endings are the mechanoreceptors whose role remains the least known so far [167]. Indeed, the latter were only very rarely observed in the human finger [105]. However, they are held responsible for the perception of lateral stretch of the skin and the lateral force during incipient slip. Thus, they are probably involved in friction perception, as human relies on tangential forces cues to assess friction [204]. They also contribute to the proprioceptive sense of the hand.

FA type I or Meissner corpuscles

Located in the glabrous skin, at the interface between the dermis and the epidermis, the Meissner corpuscles are rather found in the furrows unlike Merkel cells. They are composed of a stack of Schwann cells linked to the epidermal papillae with a connective tissue. They respond to stimuli with a radius of 3 to 5 mm and their sensibility is 4 times larger than the one of SA-I [109]. Insensitive to static stimulation, they are efficient to frequencies between 8 and 64 Hz [104] and are thus efficient in discriminating low frequency vibration. Therefore, the Meissner's corpuscles are very useful for the perception of slip and micro-slip occurring during object manipulation [207, 107]. Also, it has been shown that their firing rate change when skin strain rate is higher than 8%/s in dynamic on average [65]. Thus, they are probably responsible for grip force adjustment reflex [238]. For a review, see [168].

FA type II or Pacinian corpuscles

The Pacinian corpuscles are located deep in the layers of the dermis. They are oval in shape and composed of about thirty concentric lamellae separated by collagen fibers [16]. There are about 350 in the index finger and nearly 800 in the palm of the hand. They measure 1 mm long on average and can reach 4 mm in adults. Their size makes them the most studied mechanoreceptors. Receptive to displacements of 40 nm and efficient in a large range of frequency – from 40 Hz to 1 kHz – [224, 104], they are the most sensitive of the mechanoreceptors. At frequencies of 200 to 300 Hz, they readily respond to skin displacements on the order of 10-100 nanometers. Between 60 and 250 Hz, their sensitivity to vibration increases at a rate of 40 dB per decade, suggesting that they are sensitive to acceleration of the skin [25]. They have an excellent temporal acuity, but their spatial acuity are low, which make them good candidate for texture perception.

2.2.2 Summary

Table 2.2 summarizes the characteristics of human skin mechanoreceptors.

Each of these afferents is specialized to a spatial and a temporal frequency range and map the spatio-temporal space as illustrated in Figure 2.9.

In conclusion, the whole spatio-temporal space is covered by the four types of afferents, allowing for a good transmission of the stimuli presented. However, how the central nervous system deals with these thousands of action potentials to extract information is still at its infancy and will be reviewed in the next section.

	Fast Adapting	Slowly Adapting
Small Receptive field	Meissner corpuscles (FA I) Location: superficial skin Frequency: 8 to 64 Hz Receptive field: 22 mm ² Density: 150/cm ²	Merkel cells (SA I) Location: superficial skin Frequency: 0.4 to 10 Hz Receptive field: 9 mm ² Density: 100/cm ²
	Large Receptive field	Pacinian corpuscles (PC) Location: deeper tissue Frequency: 40 to 1 kHz Receptive field: 101 mm ² Density: 20/cm ²
		Ruffini endings (SA II) Location: deeper tissue Frequency: 15 to 400 Hz Receptive field: 59 mm ² Density: 10/cm ²

TABLE 2.2: Mechanoreceptors properties. Values reported here are average, they can differ between individuals

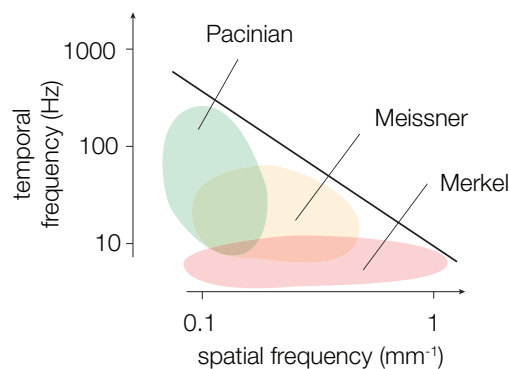


FIGURE 2.9: Spatio-temporal sensitivity of skin mechanoreceptors

2.3 How do humans perceive

The tactile perception is the ability to judge a physical reality or a sensation from what we sense. The perceived information are generally grouped into three categories: object shape properties (including curvature and edge), object material properties (including softness, friction, surface texture), and interaction information (including forces and slippage). In this section, I reviewed the tactile sensitivity to mechanical stimuli to quantify the range of sensations a human can perceive. In a second time, the detection of slippage and the perception of friction are explained in order to better understand the fast regulation of grip force during object manipulation.

2.3.1 Tactile sensitivity

Sensitivity to pressure and vibrations are first listed. Then, the spatio-temporal sensitivity to discrete stimuli is reviewed since it directly affects the object

recognition capability [62] and directional sensitivity [229].

Pressure sensitivity

Pressure sensitivity was measured as the small amount of pressure a body can sense. The pressure threshold does not vary much across body sites [230]. The highest value is under our feet where it reaches 31 mg. Women are more sensitive than men on average (mean values on the fingertips are 55 mg for men and 19 mg for women).

Vibrations sensitivity

To measure the sensitivity of the fingertip to vibrations, studies use a contactor separated from the surround to prevent any travelling-wave effects on the skin. Verillo [223] first described a two-limbed psychophysical function for vibrotactile threshold as a function of the frequency. At lower frequencies (25-40 Hz), the psychophysical function was relatively flat, meaning that the skin is not sensitive to this frequency. However, beyond that frequency range the psychophysical function was U-shape, with the threshold progressively declining up to approximately 250 Hz, at which point it began to increase up to 700 Hz. The smallest threshold was measured at 100 nm when the frequency of the contactor was 250 Hz. These results led to the proposition of a two-channel theory of vibrotactile sensitivity, the low-frequency (non-pacian channel) showing no spatial or temporal summation, in contrast to the high-frequency (pacian channel) which demonstrated both forms of summation.

Spatial sensitivity

The two-points threshold is defined as the smallest spacing between 2 points that can be identified as two different points by a person. It can give an idea on how finely innervated are the areas of skin and is widely used to assess tactile perception [199]. The typical values obtained depends widely on the body areas (Figure 2.10A), with a mean varying from 1.1 mm on the tongue to 36-75 mm on the back. These values place the tactile acuity between vision and audition. Tactile spatial acuity is also variable as a function of age, sex and laterality [230].

Although the two-points threshold is the most commonly used clinical method to assess the tactile spatial resolution, many researchers criticized this test for two main reasons [45]. Firstly, value of two-points threshold has been observed very variable both across and within subject. The value depends on the criterion subjects adopted for answering that they perceive one or two points. Secondly, people can use non-spatial cues to achieve the task. These non-spatial cues can be temporal if the 2 points are not perfectly simultaneously presented but also intensity cues [111]. For example, one point feels probably sharper than two nearby points [218] which will influence the neural responses of the mechanoreceptors [222].

Thus, alternative measures emerge, including gap detection and grating orientation task. In the gap detection test [209], a continuous or a discontinuous edge is presented randomly and subjects have to indicate if they feel a gap or not. But our mechanoreceptors are very sensitive to edges, which makes this task biased. In the grating orientation task, a horizontal or vertical is presented alternatively (Figure 2.10B). Subjects have to indicate the orientation of the grating as the width of the grooves and ridges decrease. This task gives a more accurate and less variable measure of spatial acuity [220]. Important is to notice that the grating orientation threshold is always smaller than the actual two-points threshold and reach 1 mm on average on the finger.

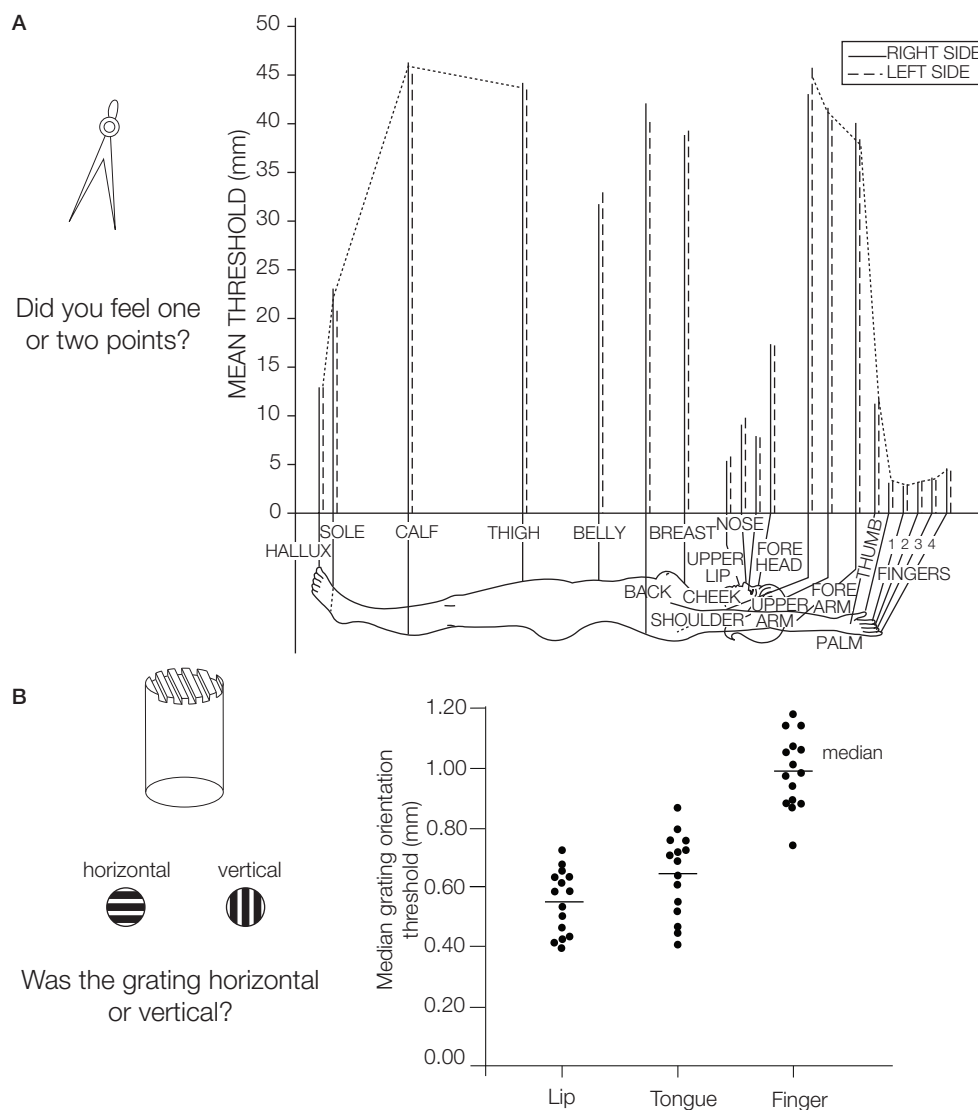


FIGURE 2.10: **A.** Two-point discrimination thresholds for different areas of the body. (from [230]) **B.** Grating orientation thresholds (groove width) at lip, tongue and finger required for 75% correct responses. (from [220]).

Temporal sensitivity

Searching for a specific coin in our pocket or reading braille are tasks involving a perfect sequential processing of the spatial patterns. Thus, temporal sensitivity has been studied for sixty years. The first study deals with the perception of temporal order [94]. Temporal separation of two contact events, at different locations, is needed as it helps in detecting the presence of multiple events. Mechanical taps were presented to the two index fingers, and subjects have to answer which location received the tap first. They found that 20 ms is required between the onsets of the taps to report correctly the temporal order.

A good way to measure temporal sensitivity can also be through the vibrations. Humans are able to detect vibrations up to 700 Hz [223]. More recently, the temporal sensitivity was measured through the ability to detect a silent interval between two vibrotactile stimuli called gap. The gap-detection threshold is expressed as the amplitude of the stimulus flanks required for 75% correct detection of the gap [221]. This gap detection threshold decreases with increasing gap duration [81].

As the two-points threshold in spatial, the gap-detection threshold in temporal is also criticized because of the same reasons. In 1990, Craig et al. [44] set up a test where subjects have to discriminate between a horizontal and a vertical stimulus (Figure 2.11B). He concludes that the temporal separation between two events at different locations on fingertips is on the order of 30-50 ms.

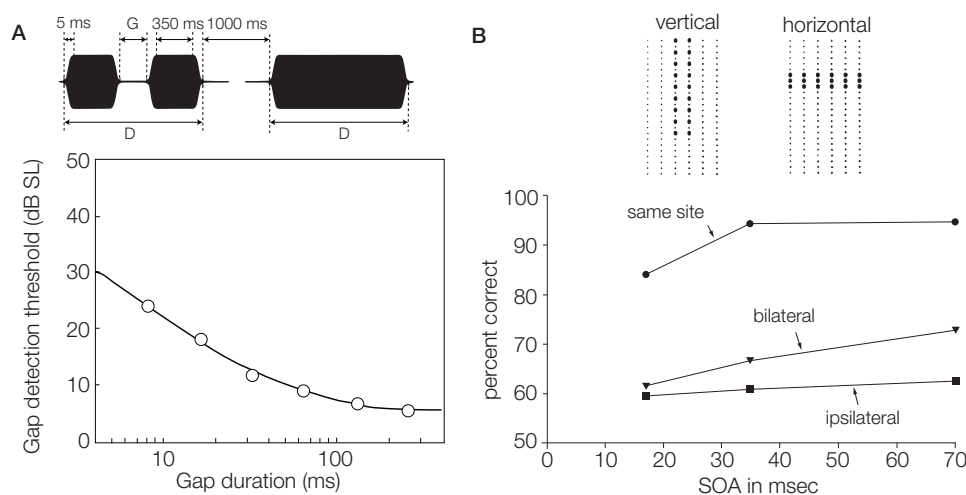


FIGURE 2.11: **A.** Gap-detection thresholds as a function of gap duration (from [221]). **B.** Performance at a temporal discrimination task (from [44]).

Spatio-temporal sensitivity: tactile motion

Stimulus movement across the skin can be detected by a passive observer in terms of direction [125, 78] and speed. Essick [70] found that brushing the arm at different speed yields to the Weber fraction of 25%. However, these results can be criticized

as the stimuli have limited length, therefore the actual velocity could have been determined by either speed or duration. Fixed duration of stimuli was applied in [59] and participants could not rely on time to assess the velocity. They also explored the effect of various textures on speed judgment, and it appears that speed estimates are varying with spatial period.

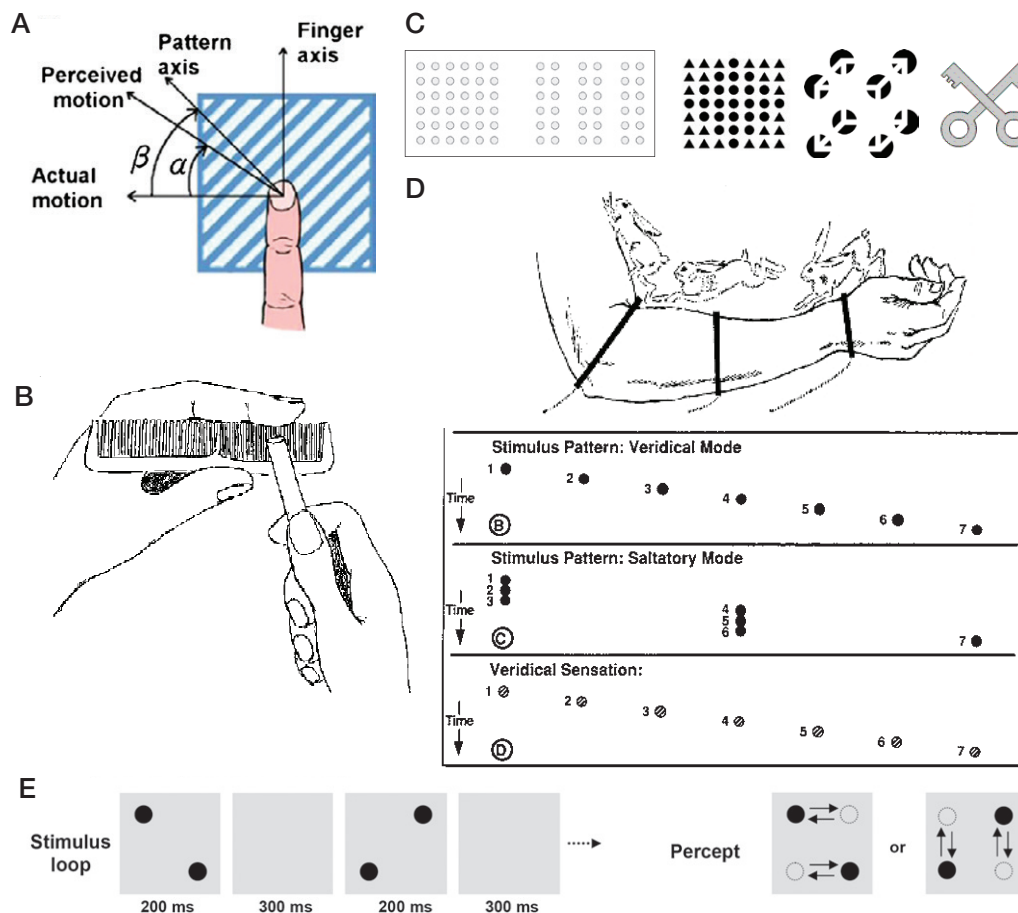


FIGURE 2.12: Tactile illusions of motion. **A.** Barber-pole illusion [21]. **B.** Comb illusion [91]. **C.** Gestalt principles of grouping: proximity, similarity, closure, continuation, connectedness. **D.** Saltatory effect or rabbit illusion [80, 39]. **E.** Tactile rivalry or apparent motion quartet [31].

The tactile counterpart of optic flow, referred to *tactile flow*, can be defined in terms of displacement of iso-strain curves [20]. An analogy can be drawn between the increase of the divergence in optic flow and the spread of the contact area in tactile flow, allowing for discrimination of a relative motion. Consenting the existence of a tactile flow would also give a possible explanation for several illusions, including the barber-pole illusion also known as the aperture problem [21]. When subjects touch a translating pads with oriented gratings, they perceived a direction of motion biased towards the orientation of the gratings (Figure 2.12A).

In addition to the sensation of tactile motion that results from real movement across the skin, an illusion of motion may also be produced. Vision researchers

have long known of highly robust illusion involving the visual perception of motion [3]. Even if it is sometimes assumed that vision is the main source of perceptual illusion, all senses, including touch, are subjected to illusions. An illusion occurs when there is a discrepancy between perception and reality. Studying tactile illusions allow gaining insight into the nature of touch and the cognitive process used by human to integrate the sensory information [129]. The illusion of apparent motion is experienced when observers fail to detect a missing portion of a raw sensory input, and it is produced by delivering a series of two pulses or more to adjacent locations in quick temporal succession. A simple experiment can be carried at home with a comb. If you hold the comb as pictured in Figure 2.12B and gently strokes the teeth back and forth, you might feel as if an embossing is running on your index finger. In this illusion, each individual motion is only few micrometers, but the resulting sensation is quite strong. Few studies try to quantify the maximal inter-stimulus onset interval (ISOI) –the time interval between two stimuli– to perceive an apparent motion. It was found that an optimal motion is obtained for a combination of a stimulus duration and a stimulus onset interval [197, 120]. For example, for a 25 ms stimulus, the interval between stimulus onsets should be less than 75 ms to feel a continuous motion. Interestingly, the curve of optimal movement is comparable to the one obtained for visual perception of motion [161], suggesting that similar brain mechanisms or neural circuits are shared by the senses. The contribution of spatial and temporal properties of a moving stimulus in the apparent motion illusion proves the complex neural integration of the spatio-temporal sequence of impulses [113, 78]. Most people failed to detect 2 mm gaps when the traversal time fell below 0.2 second. One possible explanation of this phenomenon is that predictions made by the brain are based on the previous exposure sensory, exactly in the same manner as the Occam's razor, which conducts to choose the simplest theory as the good one. More interestingly, when the brief temporal gaps inserted into a vibrotactile target were filled with vibrotactile noise, the target vibration was perceived to continue through the noise if the target vibration was sufficiently weak relative to the noise [121].

The apparent motion witnesses a strong interdependence between space and time, which can conduct to other kind of illusions. For example, the apparent distance between 3 equally spaced stimuli that are presented successively depends upon the inter-stimuli temporal interval [92]. If the time between the first and the second stimuli is shorter than the time between the second and the third stimuli, the distance between the first and the second stimuli will be judged as shorter. This illusion is called the *tau effect*. In the same way, the apparent temporal interval increase with increasing spatial separation, known as the *kappa effect* [210]. Similarly, it has been proven that we can convince the brain that a patch of skin does not exist if we are rapidly skipping over it [193]. The induced illusion of completion results in a length contraction to resolve the discrepancy between space and time. This experiment reveals the existence of Gestalt principle of grouping in

touch (Figure 2.12C).

Another interaction between space and time is the saltation effect also known as the rabbit illusion. This effect is produced when a series of short pulses are delivered successively at three different locations on the skin. The resulting sensation resembles a sweeping movement punctuated by taps [80], as if a tiny rabbit is hopping up their arms (Figure 2.12D). It has been proven that the number of taps to produce the optimal illusion lies between 3 and 6. More recently, Cholewiak and Collins [39] compared the veridical and the saltatory modes for drawing a good line in terms of length, smoothness, spatial distribution and straightness (Figure 2.12D). They found that effective lines were produced in both modes, and the two sets were perceptually equivalent when the interburst interval is higher than 10 ms.

Last but not least, our perception of apparent motion can alternate between possible interpretation of a stimulus. The best example is undoubtedly the rivalry. In vision, when pairs of dots are presented alternatively at the diagonal corners of a square, they will appear to jump either vertically or horizontally between the four corners locations (Figure 2.12E). However and surprisingly, the tactile quartet is perceived by the participants as a smooth motion [31].

Tactile perception of motion is important in textures [115] or shapes [130] recognition. Perceiving a relative movement between skin and a surface can also be useful in slip detection, which will be reviewed in the next section.

2.3.2 Slip detection

Detection of slip means to perceive the relative movement between the skin and a surface. Slip plays an important role in grip force control, as it produces feedback on the actual safety margin to apply to avoid loss of grip. When we lift an object, the tangential force increases gradually and if the forces start to be imbalanced, the object will start to move relative to the fingertips, which thus experiences incipient slippage of the object. Full slip is reached when the grip on the object is lost. But prior to full slip of the object, partial slips will develop at the fingertip-object interface, in the areas of contact where the pressure is minimal. Indeed, pressure and traction are unequally distributed on the finger surface (Figure 2.13), due to its shape and elasticity. Consequently, partial slips will start to develop at the periphery of the contacts with the formation of a *slip annulus* [7, 55]. This annulus of slippage then propagates to the center of the contact area, increasing in size with the tangential force until complete slippage. This phenomenon has been described mathematically by Cattaneo [32] and Mindlin [152]. They assumed a coulombic slip boundary condition ($\tau = \mu p$, for traction τ and pressure p), which leads to an axi-symmetric distribution of tractions as follows:

$$\begin{aligned}\tau_1(r) &= \frac{F_t}{2\pi a^2} \left(\frac{a^2 - r^2}{a^2} \right)^{1/2}, \quad r \leq a \\ \tau_2(r) &= -\frac{F_t}{2\pi a^2} \left(\frac{c}{a} \right) \left(\frac{c^2 - r^2}{c^2} \right)^{1/2}, \quad r \leq c\end{aligned}\quad (2.11)$$

where r is the radial coordinate with an origin in the center of the contact, a is the radius of the contact area and c the radius of the no slip area.

Even if this model succeeds to describe simply the overall behavior of the finger during incipient slippage, it does not fit well to in vivo experiment [213, 7, 1], especially for high normal force.

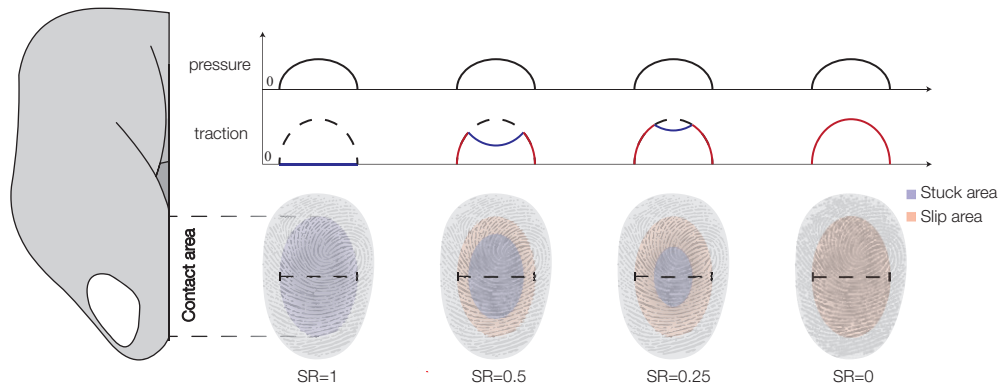


FIGURE 2.13: Incipient slippage visualization on a contact mechanics point of view. The pressure and traction distributions are shown in solid lines, while the dashed lines show the maximal traction that can develop. The stuck and slip areas, corresponding to several stick ratios SR, are marked in the views of the contact area in blue and red respectively. (adapted from "A Soft Touch on efficient neuromuscular control of the precision grip, Felix Roël")

The stick ratio is defined as the ratio between the no-slip areas to the total contact area. As the slip area increases, the stick ratio decreases until reaching zero during full slip. Thus, the stick ratio can quantify the partial slip progression during a manipulation task. However, during a slip-to-stick transition, the stuck region may disappear catastrophically [216], which could lead to a sudden slippage of the object. This phenomenon is mathematically consistent with the condition that the coefficient of dynamic friction is smaller than the static value.

It was thought since few decades that slip detection of a smooth glass is barely impossible. Indeed, the high frequency deformations of the skin caused by the relative motion of a fine surface texture along the fingertips, can be sensed by the Pacinian corpuscles to detect slippage before it occurs [106]. Thus, Srinivasan et al. [207] found that only a single 4 μm -high asperity is enough to detect a relative motion. However, FA-II afferents is known to rarely respond to partial slips, due to their lower frequency contents in comparison to full slips [106]. Hence, the detection of the moving surface features can be attributed more on the FA-I afferents or the SA depending on the dot height [127]. Furthermore, the subjects of

this study [207] applied a normal force lower than 0.2 N, inducing only very little skin deformation. Yet, for a normal force greater than 2 N, it has been observed that humans are able to detect slip on a smooth glass plate once the relative motion between the finger and the plate exceeds 2.3 mm [13]. This particular relative displacement induces a stick ratio of approximately 52% and results in a shear deformation difference between the maximal compressive and tensile strains of approximately 45% [56]. But to date, no study relates the influence of skin deformation on tactile encoding of incipient slippage.

To conclude, the transition between stick and slip is a mechanical event perceptible even in the absence of asperities on the surface. However, the complex dynamics of the skin during the onset of sliding makes it hard to understand with a simple model yet.

2.3.3 Friction perception

Friction underpins every single tactile interaction, from lifting a glass of water to perceiving the subtle wear of a fabric. It is essential to dexterously manipulate objects [87, 30, 162] and its variation during tactile exploration helps distinguish material properties [205, 85].

When the finger is sliding on a surface, the frictional strength of the contact is found by measuring the lateral force at which relative motion occurs [14], see section 2.3.2. The initial slip provides sufficient information for the central nervous system to be able to assess the friction coefficient of a smooth surface [204]. When exploring actively a varying friction glass surface, subjects are capable of ranking the friction accurately with a Weber index of 0.18 [184], meaning that they can detect an 18% reduction of the friction coefficient.

But even when no tangential force is exerted, there is evidence that the somatosensory system recognizes the frictional strength on first contact [107], since when lifting an object, humans adjust their grip force to friction before the development of the tangential force. However, the mechanisms responsible for this early perception are still unknown.

2.4 How do humans manipulate: Human hand's action

In the previous chapter, tactile perception and sensitivity to various stimuli was listed. However, perception and action are intimately linked together, and we cannot study one without looking at the other. To convince ourselves, we can take an example that you can do safely at home. Consider firstly moving your head; you are able to reconstruct your eye motion in the motionless world because the images of the external world move over the retina. And now, if you move your (closed) eye by pressing on it with a finger, you interpret the motion as a motion of the external world, showing that perception is intimately linked to self-motion.

2.4.1 Action and perception

Do we act to perceive, or do we perceive to act? On one hand, action is a means of acquiring perceptual information about the environment. It is known for decades now that hand motion is often necessary for perception [82, 130], such that moving your hand over an object's surface enables you to feel its shape and texture. But on the other hand, action responses are performed according to how we perceive our environment. For example, grip force adjustments are performed quickly after the observer detect a partial slippage of the object in his hand.

However, it was recently discovered that there is an independence between the neural mechanisms responsible for perception and action-related computations in the brain. In the well-known size-weight illusion, when lifting objects, large boxes are perceived to be lighter than small boxes of the same weight [157]. It was first hypothesized that the illusion was due to the manner of lifting the object. Since they expect a larger object to be heavier, they lift it with greater force, therefore the larger object is lifted more easily than the smaller one, causing it to be perceived as lighter. But further experiments showed that after several lifts, while the perceptual illusion persists, participants learned to scale their grip forces according to the true object weights, regardless of the object size [75]. Nevertheless, the illusion persists, suggesting that the sensorimotor system can operate independently of the cognitive and perceptual system. Interestingly, similar illusions also occur with differences in materials: metal containers felt lighter than wooden containers of the same size and mass [191]. Similarly, it has been found that adding a delay on the sensory inputs can create a discrepancy between the adjustment of the grip force and the perception of stiffness of an elastic object [133]. These results support the idea that there is a gap between perception and action.

2.4.2 Grip force control

A prehensile task, such as drinking from a cup, involves stably grasping an object, according to its inner properties (weight, texture, compliance). Stable grasp has been widely studied using the experimental setup developed by Westling and Johansson [231]. A schematic drawing is presented in Figure 2.14A. In this protocol, subjects were asked to lift a manipulandum between the thumb and the index finger. The forces exerted on the object by the two fingers can be resolved into two components: the applied grip force normal to the fingertip-object contacts, and the friction force that develops tangential to the contacts due to the local static friction. Temporal evolution of the forces are shown in Figure 2.14B. The process can be decomposed in 4 phases: the pre-loading phase corresponding to the formation of the grip, the loading phase in which grip force and load force increase in parallel, the transitional phase reached when the object is lifted to a given position and the static phase when the forces reach a steady-state.

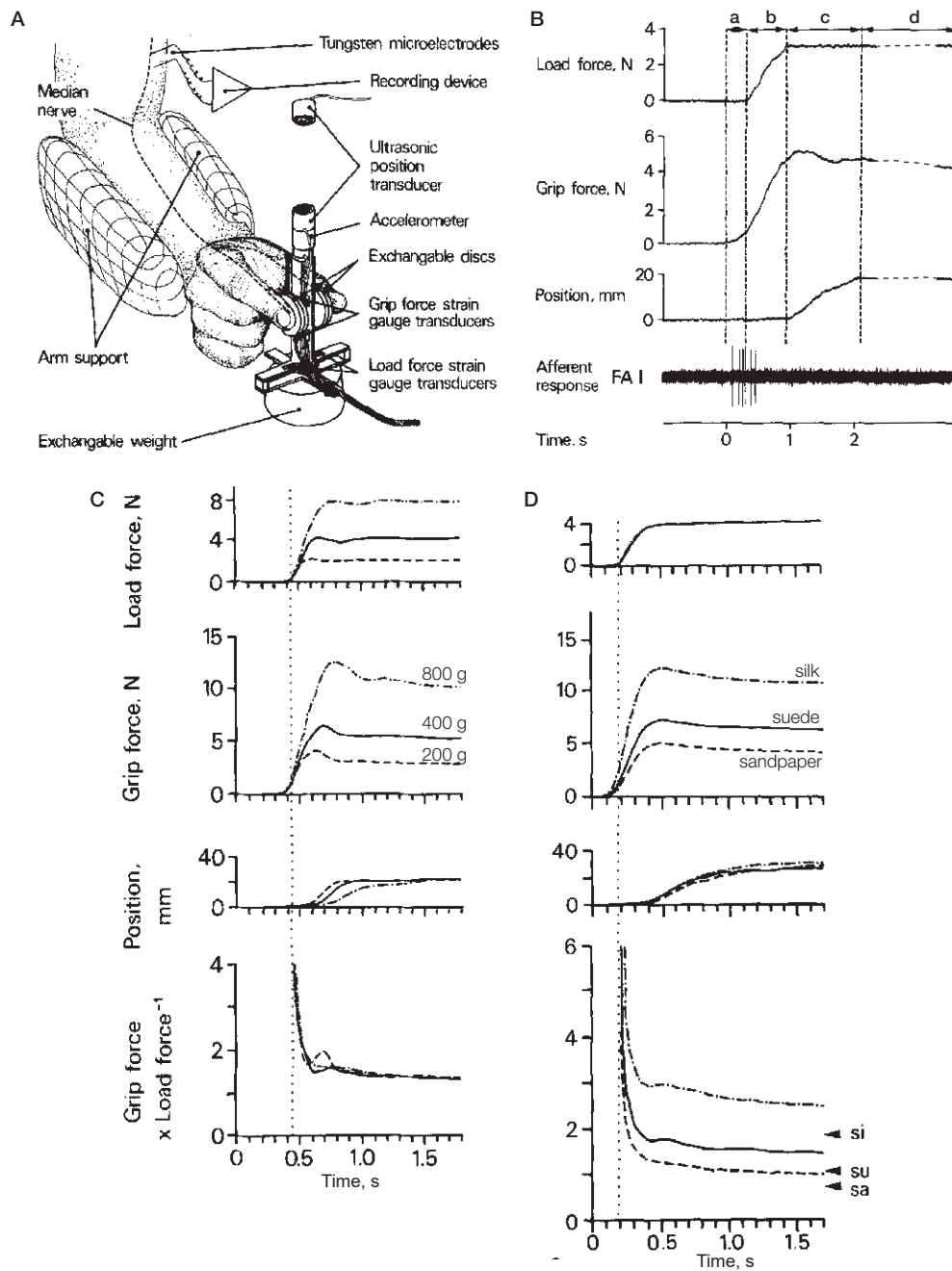


FIGURE 2.14: **A.** Schematic illustration of the apparatus to study grip force control. **B.** Phases of the lifting: (a) pre-load, (b) load, (c) transitional phase, (d) static phase. **C** and **D.** Forces coordination when lifting objects of different weights (200, 400 and 800 g) and different surface textures (silk, suede and sandpaper). Reprinted from [231, 107]

During a precision grip, the grip forces have to be large enough to compensate the weight and prevent the object from slipping between the fingers but not excessive to not cause damage to fragile objects and allow for object reorientation in the hands, necessary when we are washing our hands with a soap or when we are peeling an apple. The minimum force at which the object starts to slip, called the slip force, is proportional to the load force and varies with friction at the

interface [232]. The difference between the slip force and the actual grip force applied by the subject is known as the *safety margin* and is smaller in dexterous subjects. The grip forces required to lift an object are known to be unconsciously regulated to a value 20% above what would cause slippage [67].

The stability of the grasp is empowered by a real-time regulation of the grip force. Following a sudden load force perturbation, only 70 ms are necessary to react [106, 40]. This latency is smaller than the latency of a voluntarily initiated change in force (140 ms) but comparable in magnitude to long-latency reflex responses, meaning that the grip force regulation is presumably supraspinally mediated.

The prior experiences about the object play the first feed-forward role in the human's control system for applying initial grip force, and the estimation of change in friction force contributes to the adjustment of grip force. According to Johansson and Westling [107], the adjustment of grip force in humans begins once the contact is made, even before the appearance of tangential load. The initial grip force changes according to the frictional state of the contact surface. This result indicates that human may use early estimate of friction by applying of a simple normal pressure onto the object to adjust their initial grip force. These results were confirmed by Cadoret et al. [30], who proved that people rely on friction cues to optimize their grip force, regardless whether the friction comes from macroscopic surface features (texture) or a coating (talc or water).

When the finger are anesthetized, eliminating feedback from cutaneous mechanoreceptors, forces are no longer optimally adapted to the weight of the object and the friction at skin-object interface, and we observed larger safety margin than usual [88, 238, 8, 155]. These results suggest that tactile afferents play a critical role in the encoding of friction. Particularly, a change in friction has been proved to be most likely signaled by FA I afferents as they are sensitive to material properties [106].

2.4.3 Passive vs active sensing

A recognition task where the person is not able to move is known as passive sensing, whereas active sensing refers to an exploration where the user makes voluntary movements. These movements depend on the knowledge about objects you wanted to investigate. For example, if you want to know the object hardness you will better press on it, whereas if you want to know the texture of a material, you will probably slide over the surface. These movements were first described by Lederman and Klatzky [130] as *exploratory procedures* and are reported in Figure 2.15. Exploratory procedures are invariable to the object explored.

Active touch is estimated to be twice more accurate than passive touch. There are many reasons for that. Firstly, the mechanoreceptors activated with static stimuli are fewer [36]. Secondly, being passively touched tends to focus the observer's attention on his or her subjective bodily sensations, whereas contact resulting from active exploration tends to guide the observer's attention to

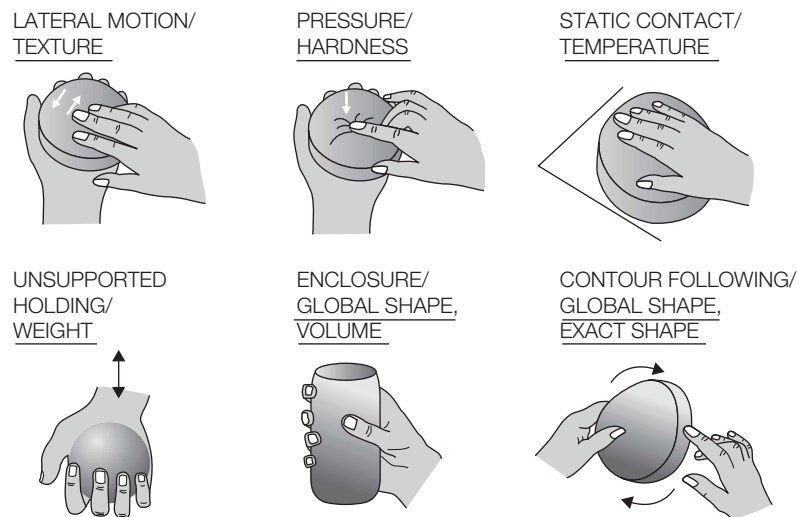


FIGURE 2.15: Exploratory procedures of for active tactile perception

properties of the external environment. Last but not least, when a motor signal is transferred from the central nervous system to the periphery, an efferent copy of this signal is generated and transferred to the forward model to predict the effect of an action [116]. The efferent copies make us insensitive to our own tickle because they inform the brain about the actual stimulation.

In opposition to a voluntary planned action, a reflex is a nearly instantaneous movement in response to a sudden stimulus. A reflex response is processed by the spinal cord before the impulse reaches the brain. The average reaction time for a tactile stimulus has been measured equal to 155 ms [156], in between the one for an auditory stimulus (140-160 ms) and a visual stimulus (180-200 ms). Below that threshold, the action is considered as spinally mediated and does not need any conscious thought.

2.4.4 Predictive coding

Predictive coding is a theory of brain function in which the brain is constantly generating and updating a mental model of the environment in vision [180], audition [189], and multimodality [68]. The mental model is constructed by making sense of the word as experienced by a top-down approach at various temporal and spatial scales. This model is making predictions (priors) which are compared against the sensory input (likelihood), yielding to a prediction error. If this error is larger than the level of expected statistical noise, the generative model will update so that it better predicts the sensory input in the future. If, instead, the model accurately predicts the sensory signal, activity at higher levels cancels out activity at lower levels, and the posterior probability of the model is increased.

Recently, Adams et al. [2] state that the motor actions are not commands but descending proprioceptive predictions, suggesting that the perceptual and motor systems are both involved to predict the sensory input.

2.5 Conclusion

This chapter reviews the state-of-the-art from tactile sensing to human hand actions. The Figure 2.16 illustrates the four most essential steps of the control loop towards dexterous human manipulation. When the finger enters in contact with an object, its soft skin deforms because of its mechanical properties. Our mechanoreceptors, buried inside the skin layers, are sensitive to this skin deformation and send actions potentials to the sensorimotor system. With this large amount of data, the brain is able to infer the physical properties as friction. This mechanism of perception provide enough information to regulate the grip force according to the object in contact and thus perform various different actions.

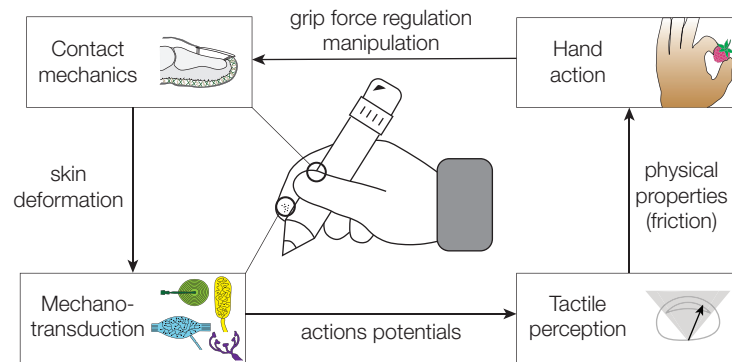


FIGURE 2.16: From object contact to human hand action.

Chapter 3

Mechanical model of skin deformation

Contents

3.1	Introduction	38
3.2	Finite-difference mechanical model	39
3.2.1	Dynamic equation	40
3.2.2	Sizing of the model	41
3.2.3	Contact modeling	42
3.3	Results of the simulation	43
3.3.1	Static deformation: comparison with the waterbed model	43
3.3.2	Ultrasonic clic caused by rapid changes in friction	44
3.3.3	Stick-slip transition	45
3.3.4	Bump exploration	45
3.4	Discussion	47
3.5	Conclusion	47

Preface to Chapter 3

THE tactile perception of shape, softness, or slipperiness stems from the deformation of the skin induced by the contact with an object. This mechanical deformation is encoded by mechanoreceptors embedded in the skin tissues and is subsequently interpreted as distinct tactile sensations, which allow environment perception as well as object manipulation. As a consequence, modeling how the skin deforms when subjected to external forces is paramount to understanding the pattern of deformation that leads to specific tactile sensations. Finite-element analysis or analytical models have shown that contact mechanics underpins tactile sensations such as softness or vibrations. However, these approaches are restricted in their ability to generalize: finite-element analysis comprises too many free parameters, and analytical models involve boundary conditions that are too restrictive. In this work, I describe a parsimonious finite-difference model which includes frictional effect and explains skin mechanics with a minimum of four parameters, while retaining a strong predictive power. This 2D-model was validated against several quasi-static and dynamic measurements reported in the literature. The model is both explainable and accurate, making it a powerful framework for predicting the deformation of the skin when being in contact with arbitrary surfaces. This ability has a wide range of applications, from the rendering of artificial tactile sensations to the control of robotic grippers.

3.1 Introduction

Tactile sensations are uniquely fitted to perceive facets of the environment that would be impossible to gather from vision or audition. Object exploration and manipulation induce skin deformation, which is relayed to the central nervous system via action potentials produced by thousands of mechanoreceptors [103, 109]. This deformation sends cues to the brain to infer properties of the object in contact such as the natural frictional resistance exerted by the object on our finger [219], and allows the central nervous system to adapt its grip force control to the lifted object [207, 8, 238]. Thus, skin mechanics play a fundamental role in the human sense of touch.

Let's take the example of a lifting task, in which the tangential force increases gradually. A collection of local stick-to-slip transitions occur progressively which are ignited at the periphery of the contact area [7, 55]. This annulus of slippage then propagates to the center of the contact area, increasing in size with the tangential force until complete slippage. The evolution of the amount of slippage is

materialized in the stick-to-slip ratio, which is the proportion of stuck skin to the total amount of skin on contact. The strain that travels through the skin during this slippage has been studied and modeled by Cattaneo [32] and Mindlin [152], for a description of the model see section 2.3.2. However, recent observations of in vivo measurements are in contradiction with Cattaneo and Mindlin's mathematical equations [212, 203]. Hertzian contact theory has been shown to predict the pressure distribution under light contact force [1], but fails for higher forces. Finally, recent optical measurements of surface strains of fingertip contact has shown an asymmetric strain profile which is in contradiction with the theories of Hertz and of Cattaneo and Mindlin [56]. The complexity of the skin dynamics during the onset of sliding makes it hard to capture in a simple model. However, studying skin behavior is key to understanding human slip detection, which could help mimic its performance in robotic grippers [95, 141].

On the other hand, modelling the relevant aspect of the contact and frictional behavior of the skin interacting with arbitrary surfaces in real-time models must be the solution for computation in robotics [86, 181] or for haptic rendering on 2D glass plates [182, 154]. Yet, to the best of our knowledge, none of the models available to date incorporate friction.

In this chapter, I built a 2D model of the fingertip that incorporates local deformations of a stiff skin supported by underlying tissues. The model captures the viscoelastic behavior of the skin using Kelvin-Voigt material and the local elastoplastic frictional interaction at the interface using Dahl friction model. We show that an elastic membrane supported by a bed of springs is mechanically sufficient to model the static deformation of the skin. This, combined with a model of friction, can explain the transition from stick to slip. With this model, we can simulate the temporal evolution of subject-specific skin deformation in any arbitrary contact conditions. With only four parameters (2 spring stiffnesses, 1 damping coefficient and 1 finger radius), this model is very simple but succeeds in capturing a wide range of skin behaviors in static and in dynamic conditions, making it more accurate than the Waterbed model [206]. Furthermore, its simplicity allows for a faster and more trustworthy execution than finite-element analysis. As speed is a key for robotics, our model could be used in the near future in control applications.

3.2 Finite-difference mechanical model

The model is composed of a chain of massless elements maintained together by elastic springs. This chain can be assimilated to the external layer of the skin (the epidermis). Its shape is maintained using elastic springs that connect the massless elements to a virtual bone, analogous to the mechanical behavior of the subcutaneous tissues. The both elements on the outside of the membrane are also attached to the bone and model the effect of the rigid nail. Overall, the model

resembles the discrete version of a curved elastic membrane on a spring foundation. The viscosity of the skin is modeled by dampers, connecting each particle to the mass of the system. All connectivities are represented in Figure 3.1A.

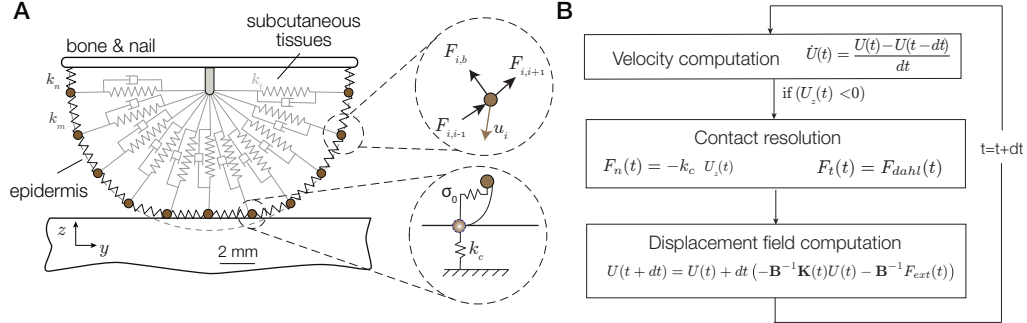


FIGURE 3.1: **A.** Sketch of the mechanical model with spring and dampers connectivities. **B.** Computational steps of the displacement vector.

3.2.1 Dynamic equation

Each spring applies forces to its endpoint particles i proportional to the length deviation (linear elasticity), discounted by a damping term proportional to the rate of length change. Let F_i be the forces acting on the particles i by all springs and dampers and U_i be the displacement of the particles i . Then the internal force on each element i can be written as follows:

$$F_i = -k_m(U_{i-1} - 2U_i + U_{i+1}) - k_t(U_i - U_b) - \zeta\dot{U}_i \quad (3.1)$$

where k_m is the stiffness of the external layer of the skin, k_t is the stiffness of the subcutaneous tissues and ζ is the damping coefficient.

Springs and dampers dependencies are then embedded in matrices \mathbf{K} and \mathbf{B} respectively. As mass and inertia are neglected [235], the equation of motion can be written as follows:

$$\mathbf{B}\dot{U}(t) + \mathbf{K}(U)U(t) + F_{ext}(t) = 0 \quad (3.2)$$

where U is the vector of normal and tangential displacements and F_{ext} is the vector of external forces.

The stiffness matrix \mathbf{K} is repopulated at each time-step to take into account the geometric changes, which influence the distance between each element. As it depends on the position of each element, the system of equations is essentially non-linear. The displacement vector U and the impedances are decomposed into a normal and a tangential component. For example, the normal and tangential components of spring stiffness are given by $k_m \sin \alpha$ and $k_m \cos \alpha$ respectively, where α is the angle between the surface and the spring.

The dynamic equation can be written in discrete time as follows:

$$\mathbf{B} \left(\frac{U(t+dt) - U(t)}{dt} \right) + \mathbf{K}(U) U(t) - F_{ext}(t) = 0 \quad (3.3)$$

$$U(t+dt) = U(t) + dt \left(-\mathbf{B}^{-1} \mathbf{K}(U) U(t) - \mathbf{B}^{-1} F_{ext}(t) \right) \quad (3.4)$$

The algorithm follows the procedure steps shown in Figure 3.1B. After resolving the contact, the forces are updated and displacements computed using Runge-Kutta algorithm at the fourth order.

3.2.2 Sizing of the model

Material properties of human skin have already been measured by several researchers [77, 143, 225] (see section 2.1.2). In [225], the effective Young's modulus of the external layer of the skin was measured by stretching the skin across the ridges. The resulting mean modulus was 1.54 ± 1.08 MPa.

Afterwards, the Young's modulus of the internal layers was adjusted so that the relationship between the load and the computed contact area corresponded with the one measured by [194]. When the Young's modulus is equal to 0.025 MPa, the computed contact width best fits Serina's observations (Figure 3.2A).

The value of the spring stiffnesses (k_m and k_t) are computed from the Young's moduli of membrane and subcutaneous tissue respectively:

$$k_m = \frac{E_m d e_m}{dL} \quad \text{and} \quad k_t = \frac{E_t \pi r^2}{2r} \quad (3.5)$$

where d is the diameter of the contact area, e_m is the thickness of the membrane, dL is the distance between two elements, and r is the radius of the finger. Consequently, the spring stiffnesses for the membrane and the internal layers were set to 2.5 kNm and 0.13kNm respectively.

The damping coefficient ζ was set according to a step response of finger traction as in [225]. The damping was chosen to obtain a time constant equal to 10 ms, corresponding to a damping coefficient of 0.1 (Figure 3.2B).

The time step must be small enough to ensure the stability of the system according to the damping coefficient, leading to the following equation for a sampled data system [41]:

$$\zeta > \frac{k_c dt}{2} \quad \text{thus,} \quad dt < \frac{2\zeta}{k_c} \quad (3.6)$$

According to this criterion, the sampling frequency was set to 400 kHz.

Moreover, the spacing between the elements should respect the Courant-Friedrich-Lewy (CFL) condition, which ensures the convergence of the system. The CFL condition links the spatial and the temporal stepping Δx and Δt through the following equation (3.7).

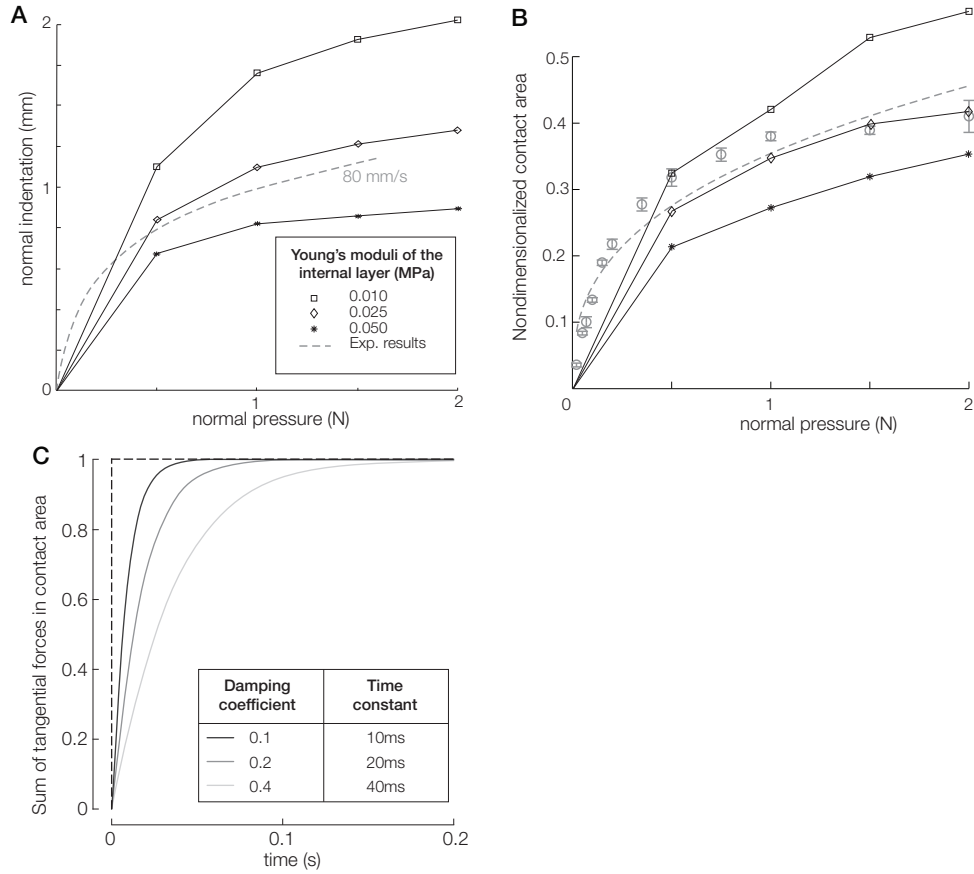


FIGURE 3.2: **A.** Variation of the normal indentation with normal pressure for 3 values of the Young's modulus of the internal layers. **B.** Variation of non-dimensionalized contact area with normal pressure for the same 3 values of the Young's modulus. **C.** Variation of global tangential force for 3 values of damping coefficient

$$C = \frac{v\Delta t}{\Delta x} \leq C_{max} \quad (3.7)$$

where v is the maximum magnitude of the velocity and C_{max} is method dependent. When the method is explicit, C_{max} is taken equal to 1. The maximum of speed magnitude approaches 440 m/s and the temporal discretization is defined equal to $2.5 \mu\text{s}$ according to equation (3.6). Then the spatial step should be higher than 1.1 mm. Taking 201 elements along this chain allows for the respect of this condition of convergence.

3.2.3 Contact modeling

To model the normal force developing when a finger makes contact with the surface, we used the penalty method by adding a high-stiffness spring k_c between one contact element and the surface.

Modeling friction is one of the most challenging tasks because of its nonlinearity (see section 2.1.4). Dahl [48] proposed a model to compute the friction

force in order to model presliding displacements in control applications. In most cases, the equation of the friction force can be written as follows:

$$\begin{aligned} \frac{dF(x)}{dt} &= \frac{dF(x)}{dx} \frac{dx}{dt} \\ &= \sigma_0 \left| 1 - \frac{F}{F_c} \text{sign}(\dot{x}) \right|^n \text{sign} \left(1 - \frac{F}{F_c} \text{sign}(\dot{x}) \right) \dot{x} \end{aligned} \quad (3.8)$$

where $F(x)$ is the friction force function, F_c is the coulomb friction force and σ_0 is the rest stiffness at equilibrium point $F = 0$, equal to $1e4$ here. n is a coefficient which codes how ductile or brittle the material is. Thus, $F(x)$ approaches the coulomb friction force F_c as long as $\dot{x} > 0$ and $-F_c$ when the direction of motion is reversed.

3.3 Results of the simulation

In the simulation, the external forces were applied on the bone and the stress-strain distributions of the elements in contact were resolved at each time step.

3.3.1 Static deformation: comparison with the waterbed model

The resulting static deformation was first compared with existing behavior from the literature. In Srinivasan's study [206], fingertips were indented in vivo using a line load and the resulting skin surface deflection profile was photographed and used to infer the mechanical behavior of the materials that make up the fingertip. The waterbed model was built to predict the surface deflection in the region of interest, less than 3 mm from the load.

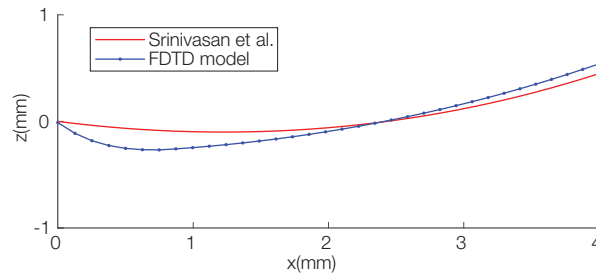


FIGURE 3.3: Surface deflection profile under a line load and comparison with the waterbed model

Figure 3.3 plots the skin deflection obtained with our model and with the waterbed model. The sum of the squared differences between our model and the waterbed model is very low ($7.8e^{-6}$ mm for the normal displacement and $8.1e^{-9}$ mm for the tangential one). These results show that the model follows theoretical profiles of skin deflection observed under line load. The small errors found lead us to conclude that the fingertip is mechanically equivalent to an elastic membrane supported by a bed of springs *in static*.

3.3.2 Ultrasonic clic caused by rapid changes in friction

Current touchscreen technologies developed for intuitive human computer interactions often lacks haptic feedback given by conventional input methods. In many tasks, one of the main issues for the virtual keyboard on screen is to reproduce the click sensation. Monnoyer et al. [154] have investigated the feasibility of modulating friction via ultrasonic vibration to simulate tactile feedback for keystroke. The vibrations of the ultrasonic lubrication are in the order of a micrometer and well outside the perceptual window of touch, but it has been shown that they decrease the friction, via a reduction of the area of contact [234, 237]. Remarkably, this behavior arises even in the absence of sliding or lateral forces, when the finger is static. In this study, they showed that participants can perceive sudden changes of friction while they are pressing down. Surprisingly, only a reduction of the friction coefficient leads to a robust percept. The physical mechanism that provides such tactile feedback remains elusive. In this section, we hypothesize that the percept is associated with the sudden release of a latent elastic strain upon activation of the friction-reduction device. A rapid change of friction, created using ultrasonic lubrication, results in a subtle skin deformation with enough amplitude to be detectable.

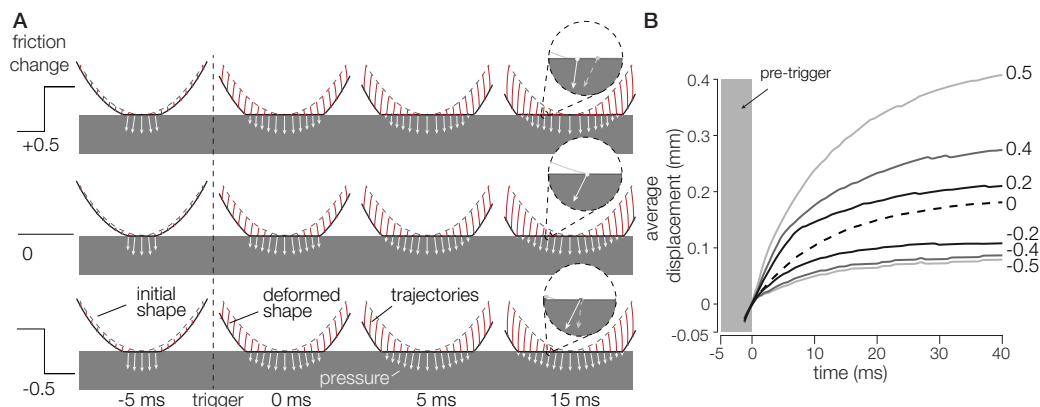


FIGURE 3.4: **A.** Simulated finger profile with a 0.5, 0 and -0.5 friction change. The black arrows represent the accumulated stresses on the surface, and the red lines correspond to the features trajectories. **B.** Simulated lateral displacements of skin points for no change (dotted line), falling friction (0.2, 0.4, 0.5), and rising friction (-0.2 , -0.4 , -0.5).

We simulated the interaction between the finger skin and a glass plate under 7 friction changes from -0.5 to 0.5 with a normal force of 4 N applied to the bone element. Results of the simulation are depicted in Figure 3.4A where displacements are represented in red and stresses in black. In the falling-friction condition, the lateral component of the interfacial pressure decreases significantly after the friction change, which happens at 0 ms. This release of the mechanical stress frees the lateral displacement of the skin in contact. However, in the rising-friction condition, the elements start to expand laterally before the mechanical detent, when the friction is low. Then, when we increase friction, the lateral component of the

interfacial pressure increases and locks the elements in place. The simulated median displacements are plotted on Figure 3.4B. They plateau in all conditions but despite this saturation, the median of all points displacement is 8 times higher in the maximal falling-friction condition compared to the rising-friction condition.

3.3.3 Stick-slip transition

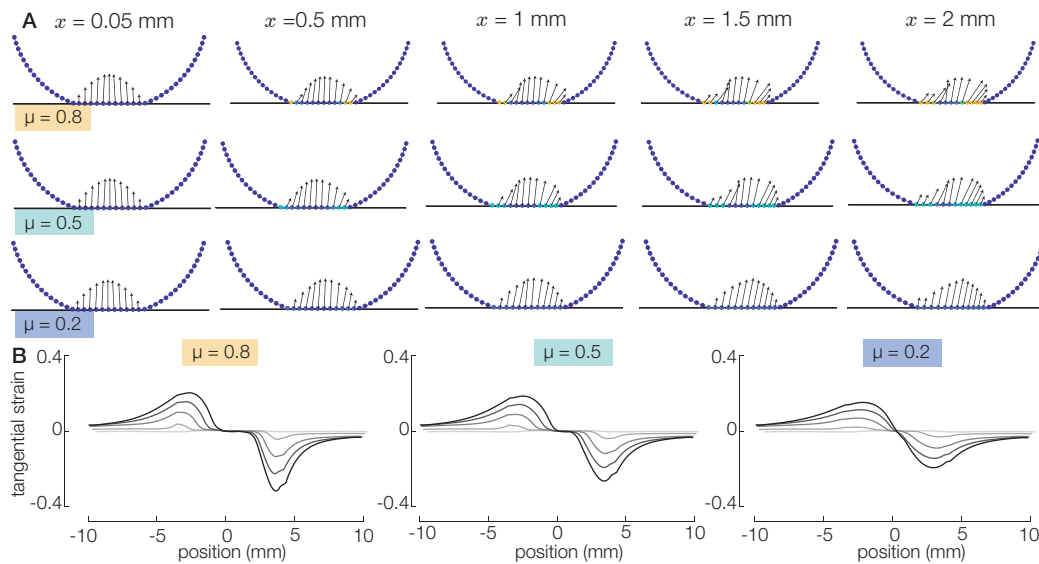


FIGURE 3.5: **A.** Simulated surface finger profiles for three friction coefficients. The blue arrows represent the pressure and traction acting on each element. **B.** The corresponding strain patterns at the same five positions are plotted below.

To validate the model in *dynamic*, we simulated finger slippages on a glass plate with various friction coefficients using the finite-difference mechanical model. A normal force $f_n = 1$ N was firstly applied on the bone, and once a balance was achieved, a tangential force $f_t = 1$ N was added to the bone. In Figure 3.5A, the surface profile is represented for 3 coefficients of friction from 0.2 to 0.8 at different positions.

The elements located on the periphery start to slip first, whereas the elements in the center are still stuck. Strain linear profiles are shown on Figure 3.5B. Their global behavior is the same for all friction conditions, with a compression ahead the stuck area and a dilatation behind it. However, their amplitude is highly dependent on friction and that from the very beginning of the incipient slip.

3.3.4 Bump exploration

Since the development of touchscreens 30 years ago and specially now because of the health crisis, we feel the need to experience vivid sensations when we touch a screen. Particularly, the simulation of 3D profiles and shapes on a 2D glass plate has been widely studied [134, 179, 128]. During an object exploration, it has been shown that geometry perception is highly correlated with the lateral forces applied

to the finger [182]. The principle consists in reproducing the 3D sensation of shape by modulating the lateral forces or their correlated variables (such as friction) on the subject's finger. If the friction force increases, the finger will feel more resistance, giving the sensation of climbing on a hill. Conversely, a reduction in friction force will simulate a hole. Thus, a 0.3 cm-high/deep and 4 cm-wide gaussian profile can easily be reconstructed virtually [182].

In this section, we simulated the exploration of a physical and a virtual bump. The displacement and interfacial pressure experienced by the skin are shown in Figure 3.6A and B respectively. The bump follows a sinusoidal curve with the period defined at 40 mm, corresponding approximately to a third of the contact area. The friction variation follows the same behavior but shifts in space (Figure 3.6C). The three curves plotted in Figure 3.6D represent the traction profile at three different locations (during the ascent, on the top of the bump and during the descent) for a physical and for a virtual bump.

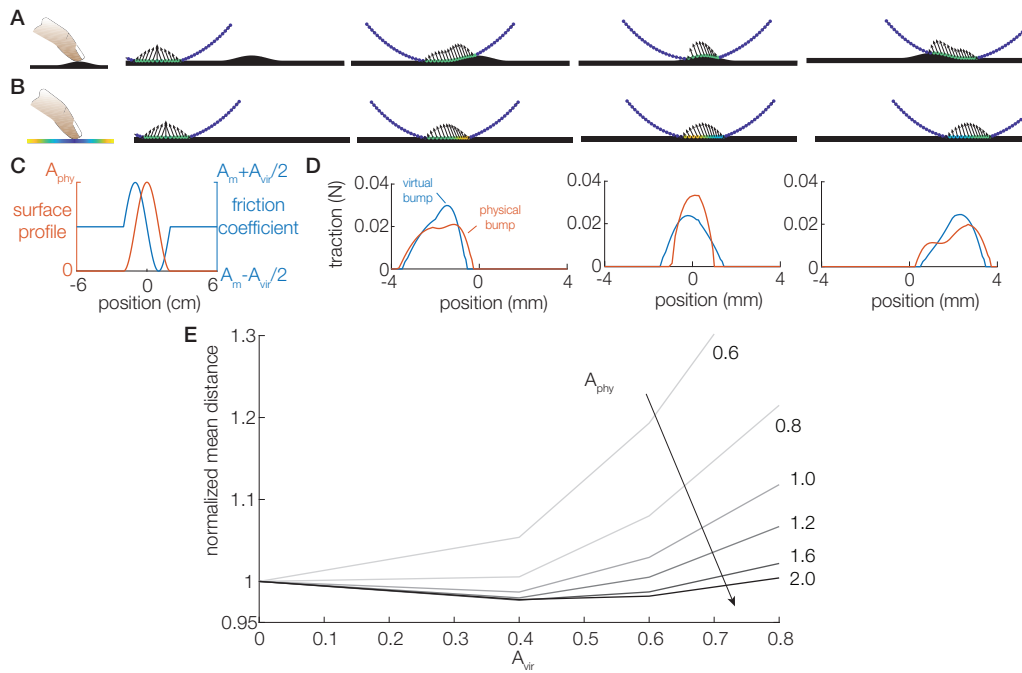


FIGURE 3.6: Interfacial pressures in the case of a physical bump (A) and a virtual bump (B). C. Surface profile and variation of static friction coefficient. D. Tangential strain profile at three locations (during the ascent, on the top of the bump and during the descent) for the virtual (blue) and physical (red) bumps. E. Normalized distance (according to the distance for the uniform-friction condition) between the traction for a physical and a virtual bump.

We computed the mean distance between the traction profiles (blue and red) to determine a quantitative indicator for assessing whether a surface with a spatial variation of the friction coefficient can create a realistic tactile representation of a physical bump. The normalized distances (according to the uniform-friction distance) are plotted on Figure 3.6E for a bump height from 0.6 to 2.0 mm and a

friction variation from 0.2 to 0.8. We found a minimum distance when the physical bump height exceeded 0.8 mm. The optimal friction variation is then equal to 0.4.

3.4 Discussion

The results given in this chapter show the validity of our mechanical model of human skin in static and in dynamic. The structure of the fingertip was proved to be mechanically equivalent to an elastic membrane supported by a bed of springs. This mechanical model ensures a minimal number of parameters to predict and match available experimental data. It is demonstrated that this simple model gives us an acceptable prediction of surface deflection [206]. Moreover, damping matches the viscoelastic response of the skin and particularly the relaxation time of 10 ms [171]. Finally, the discrete-time implementation of Dahl model is reliable to the dynamic evolution of the friction force and guarantees continuity and convergence.

The model can be used to highlight the ultrasonic click perception and the tactile shape illusion occurring when the friction state varies along the surface. Indeed, for bumps higher than 0.8 mm, a friction change of 0.4 ensures a more similar frictional stress profile than no friction variation. These findings can be useful to design tactile interfaces.

Nonetheless, this model has been shown to be computationally efficient in 2D compared to the finite-element analysis models. However, future work will focus on developing it in 3D to take into account for the longitudinal deformation as well.

3.5 Conclusion

In this chapter, we proposed a numerical finite-difference model of the finger cross-section. Finger geometry and material properties data were used to reconstruct a stress/strain profile that was as realistic as possible. This model can help future researchers to understand the mechanisms involved throughout an interaction with an object. Investigating such mechanisms will enhance future developments of the next generation of sensory-controlled prosthetic and robotic manipulators. Indeed, in the field of robotics, detecting the friction coefficient will allow us to control the normal force so that the tangential force is within the friction cone to avoid any slippage.

The simulated skin surface deformation obtained with the mechanical model presented in this chapter matches the basic case from the literature. In the next chapters, we will show that this model predicts a trend quantitatively similar to the experimental data acquired for different friction conditions not only on initial contact (Chapter 4) but also when the finger is sliding on a surface (Chapter 5). The model will be used as a strong predictor of the stress experienced by the surface layers and thus, by the mechanoreceptors buried inside the dermis (Chapter 6).

Chapter 4

Mechanics of friction perception

Contents

4.1	Introduction	50
4.2	Materials and Methods	51
4.2.1	Participants and protocol	51
4.2.2	Setup	52
4.2.3	Data analysis	55
4.3	Results	58
4.3.1	Empirical skin deformation	58
4.3.2	Friction discrimination performance	59
4.3.3	Friction influences skin deformation	60
4.3.4	Skin deformation and friction perception	62
4.3.5	Influence of the kinematics of the exploratory procedure	63
4.3.6	Strain energy and mechanoreceptors thresholds	64
4.3.7	Ideal Observer Analysis	66
4.4	Predictions from the mechanical model	67
4.5	Discussion	69
4.6	Conclusion	71

Adapted from Willemet, L., Kanzari, K., Monnoyer, J., Birznieks, I. & Wiertlewski, M. (2021). Initial contact shapes the tactile perception of friction. *Proceedings of the National Academy of Sciences*.

Preface to Chapter 4

HUMANS efficiently estimate the grip force necessary to lift a variety of objects, including slippery ones. The regulation of grip force starts with the initial contact, and takes into account the surface properties, such as friction. This estimation of the frictional strength has been shown to depend critically on cutaneous information. However, the physical and perceptual mechanism that provides such early tactile information remains elusive.

In this chapter, we elucidate the effects of the frictional properties of objects during initial contact. We found a correlation between participants' conscious perception of friction and radial strain patterns of skin deformation. The results provide insights into the tactile cues made available by contact mechanics to the sensorimotor regulation of grip as well as to the conscious perception of the frictional properties of an object.

4.1 Introduction

We lift glasses of water, regardless of whether they are empty or full and whether they are dry or wet. The sensorimotor mechanisms responsible for this astonishing performance are far from being understood. The grip forces required to lift an object are known to be unconsciously regulated to a value typically 20% above what would cause slippage [67]. Remarkably, this regulation starts from the moment our fingers touch the surface. It has been shown that just a hundred milliseconds of contact with a surface is enough to start adjusting fingertip forces to friction. Humans provide larger grasping forces if the surface is made of slippery silk but smaller if it is made of sandpaper since it provides better grasp [107, 30]. It has been further demonstrated that it is friction and not texture, which determines these adjustments [30]. Since 1 mm of indentation of the fingertip is sufficient to reach 80% of the final gross contact area, and that fingers move faster than 10 mm/s toward an object, within these 120 ms the sensorimotor system already should be able to extract some estimates of the frictional properties from the initial deformation of the finger pad.

On a physical level, the overall so-called *frictional strength* of the contact is given by the number of asperities in intimate contact and their individual shear strength [17, 63, 160]. It is the measure of the maximum lateral force on the contact that will lead to slippage. This frictional strength is the main determinant in regulating grip force applied to lift an object of a given weight [30]. Failure to properly assess the frictional strength of the surface at initial contact –due to the

presence of gloves or anesthesia for instance– is followed by larger than usual grip forces, consequently increasing the real area of contact [238, 8, 155].

Despite its crucial importance, the mechanical deformation that underpins the encoding of the frictional strength on initial contact remains unclear. It is well known that the timing of the impulses of tactile afferents encodes the information related to force direction [22], local curvature [102], edges [177], shapes [122] and also contains information about the frictional strength [119, 117]. One hypothesis suggests that, at the mechanical level, micro-slip events at the finger-object interface induce vibrations of the skin [190, 93]. Another hypothesis postulates that the sensation of friction is mediated by a radial pattern of skin strain within the contact area. The magnitude of the strain induces internal stresses, which are 21% smaller on slippery surface than on high-friction surface [103].

Interestingly, roboticists have leveraged these findings to estimate friction on initial contact from the gradient of the lateral traction field. This metric is used to control the force applied by robotic grippers to soft and fragile objects [137, 37, 142]. In haptic rendering it is possible to produce tactile sensations by releasing the accumulated stress using ultrasonic friction modulation [154]. However, the perception of the frictional strength with a single normal motion is not as salient. Khamis et al. recently showed that participants were unable to differentiate a 73% reduction in friction of a glass plate when it was pressed against their fingertips by a robotic manipulator [118].

Friction is consciously perceived in a passive condition only when the plate starts sliding [85, 184, 6, 207]. The change in the frictional state from stuck to sliding is perceived after a global lateral displacement of 2.3 mm [13]. This transition induces large deformations of the skin along with a particular strain pattern [56, 217, 6, 212]. These results suggest that large or rapid deformations can elicit a tactile sensation, but the quasi-static radial strain pattern is too subtle to induce a reliable percept.

We hypothesize that the frictional strength can be perceived when actively touching the surface. Active exploration is known to promote acuter sensitivity than passive touch [202, 139, 82]. We present evidence that during the first instant of contact between the finger and an object, a radial strain pattern exists. Its magnitude is affected by the interfacial friction and correlates with the perception of friction. Combined with the results of the motor control literature, a picture emerges explaining the mechanical basis upon which friction is encoded.

4.2 Materials and Methods

4.2.1 Participants and protocol

Fourteen right-handed volunteers (3 females and 11 males), ranging from 19 to 55 years old, participated in the study. They were naive to the purpose of the experiments and had no previous experience with haptic devices. None of them reported having any skin conditions or perceptual deficits. The study was

conducted with the approval of Aix-Marseille University's ethics committee (2019-14-11-003), and the participants gave their informed consent prior to the procedure.

Participants sat in a chair in darkness and wore noise-cancelling headphones projecting pink noise, blocking any visual or auditory cues. The last phalanx of their left index finger was connected to a vertical linear guide, preventing any lateral movement (Figure 4.1A). The approach angle of the finger was maintained at 30° . The entire session was composed of 2 blocks of 20 min, separated by a 10-min break. Participants were asked to compare the slipperiness, a correlate of the friction coefficient, of the same surface presented with different levels of friction. The friction of the plate was set by the amplitude of ultrasonic vibrations. After pressing twice, they stated which stimulus was the most slippery using dedicated buttons.

4.2.2 Setup

The apparatus combining a friction plate and a custom-made optical system is shown in Figure 4.1B,C.

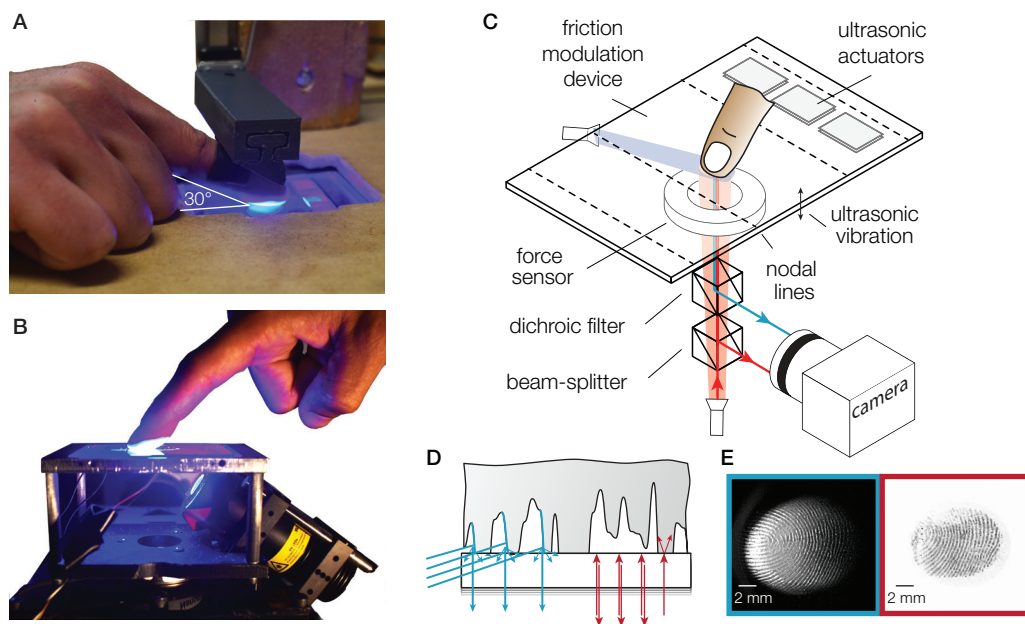


FIGURE 4.1: **A.** Linear rail to maintain the angle between the finger and the surface constant equal to 30° . **B.** Friction reduction device with custom-made optical system. **C.** Experimental setup. The friction between the fingertip and glass plate is reduced in the presence of flexural ultrasonic waves. A dual-illumination setup where blue light illuminates the skin at a 20° angle, and red light is normally incident to the glass surface. **D.** Close-up view of the illumination combining a dark-field blue light to highlight the fingerprint ridges, and a red light, coaxially oriented with the camera, to illuminate only the asperities of the skin in intimate contact with the glass plate. **E.** Typical images of the fingertip profile (left) and the asperities in intimate contact (right).

Optical system

In order to accurately measure the plate-fingertip interaction, we used a bespoke illumination apparatus that highlights the topography of the skin, while synchronously showing the micro-junctions that comprise the real area of contact. A 450 nm blue light (Thorlabs M455L3) illuminates the fingerprints at a shallow angle of 20° . A 660 nm red light (Thorlabs M660L4) is shone via a beam-splitter, so its principal axis is orthogonal to the surface of the glass and parallel to the optical axis of the camera. This type of illumination used in [212] leverages the frustration of the 4% reflection of the glass surface by the skin to image the asperities in great details. A dichroic filter (Thorlabs DMLP 550) and a set of mirrors spatially separate the two illumination sources. The images were captured at 300 frames per second by a high-speed camera (Phantom VEO E310) with a resolution of 512x640 pixels covering a total area of 16x21 mm.

The interaction of the light sources at the skin-plate interface is illustrated in Figure 4.1D, and the resulting images are shown in Figure 4.1E.

While participants were pressing down, the motion of individual points on the surface of the skin was tracked using the images from the blue grazing illumination. The high-contrast images created with the coaxial red illumination show the micro-junctions formed by the contact at the interface, providing a temporal reference of the instant when a particular point was in intimate contact.

Ultrasonic lubrication

The frictional resistance of the plate against the skin was controlled by ultrasonic lubrication [234], allowing for repeatable stimuli where the surface topography and physicochemistry remained unchanged. The friction reduction device uses a flexural standing wave to induce micrometric levitation of the skin of the fingertip. The device is composed of a rectangular glass plate vibrating at a frequency of 29.194 kHz in the 1×0 mode, with dimensions of $67 \times 50 \times 5$ mm³. The plate is mounted onto an aluminum frame attached to a 6-axis force sensor (ATI Nano 43) to measure forces exerted by the finger with 10 mN accuracy.

To demonstrate the ability of the plate to reduce friction, participants were asked to slide their finger over the surface while the amplitude of the ultrasonic carrier was modulated with a 4 Hz sinusoid. The evolution of the normal and tangential forces was measured with a custom-built tribometer. The tribometer relied on a rigid elastic structure, which nanometre-scale deformation was measured via a Fabry-Perot interferometer, see [18] for construction details. This high-precision sensor can resolve forces with amplitudes lower than 1 mN. Participants were asked to keep the normal force steady around 0.5 N on average. The epochs where the finger was moving from the right to the left and the vibration envelope increased were selected (Figure 4.2A). The friction coefficient was computed from the ratio of lateral to normal forces for each separate epoch (Figure 4.2B). When the finger was steadily

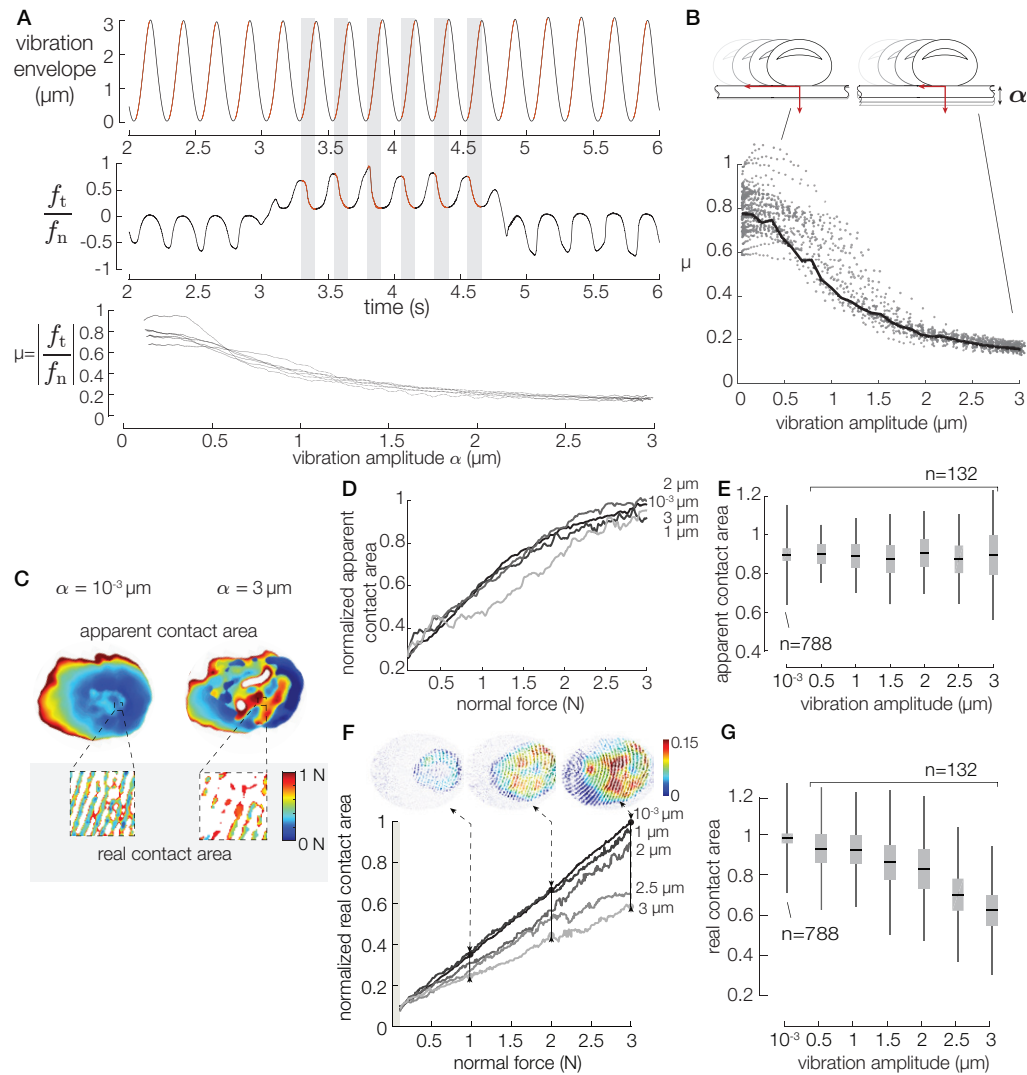


FIGURE 4.2: **A.** Typical trial during the measurement of sliding friction. Subsets of time series were selected when the finger was moving from right to left and the vibration envelope was increasing. **B.** Friction coefficient reduction for increasing ultrasonic amplitude across all trials. The black line represents the median friction coefficient. **C.** Vignettes showing the force at which contact is fully made for a high- and a low-friction condition respectively. The apparent contact areas are shown on top and the real contact areas on the bottom. **D.** Evolution of the normalized apparent area of contact with the normal force. **E.** Median normalized apparent contact area for a normal force of 3 N. Black lines and grey boxes represent mean \pm SD. **F.** Influence of the vibration amplitude on the normalized real area of contact. Images of contact area differences between the higher and lower levels of friction are shown for 1, 2, and 3 N. **G.** Median normalized real contact area for a normal force of 3 N. Black lines and grey boxes represent mean \pm SD.

sliding and the amplitude of the ultrasonic wave was changed from $\alpha = 10^{-3} \mu\text{m}$ to $\alpha = 3 \mu\text{m}$, the coefficient of friction varied from $\mu = 0.81$ down to $\mu = 0.18$ when the maximum amplitude was applied, leading to a 78% relative reduction in friction (Figure 4.1C).

Since no frictional forces were present during the normal indentation by the participants during the 2-Alternative Forced Choice (2-AFC) procedure, the friction coefficient cannot be computed from the force ratio. Thus, we used the area of contact as a proxy measurement for friction. The area of contact of skin on glass can be characterized in two ways; the apparent area of contact, which is the macroscopic area due to the gross deformation of the tissues; and the real area of contact, which is made by summing the contribution of the microscopic scale junctions between the asperities of the skin and the glass plate.

The forces at which contact is fully made were computed to see the impact of friction reduction by ultrasonic vibration amplitude. After applying a Gaussian filtering to blur the image, we computed the time instant from which the brightness of the contact image reached the mean value of the brightness for each pixel. These values of time instants gave us the heatmaps shown in Figure 4.2C. The contact between the finger and the glass plate initially started towards the center and expanded radially, for all trials. The center of the contact in the low friction case experienced ultrasonic levitation, creating the white areas where asperities were never in intimate contact.

The observed contact areas varied significantly across participants with values ranging from $84.7 \pm 21.5 \text{ mm}^2$. The variation is attributed to differences in skin reflectance, humidity, and fingertip size. The contact areas were normalized to the median size of each individual to compare the results across all participants. The apparent contact area is not affected by the ultrasonic levitation (Figure 4.2DE), as previously shown by Wiertlewski et al. [234]. However, the normalized real contact area evolved almost linearly with the normal force (see Figure 4.2F), and the slope of the relationship was negatively correlated with vibration amplitude (Spearman's coefficient = -0.28, $p < 0.0001$). The correlation is illustrated in Figure 4.2G, in which the maximal vibration amplitude of $3 \mu\text{m}$ caused a 38% reduction in the contact area, consistent with ultrasonic lubrication theories [234] and with friction theories [27]. It reveals that fewer asperities were in intimate contact, thus potentially allowing more lateral movement of the skin unimpeded by friction.

4.2.3 Data analysis

Force data

Force data were synchronized to the images via a signal that triggered when the normal force exceeded 0.7 N and was interpolated to match the time vector of the images and denoised with a zero-lag 50 Hz second-order low-pass filter.

Real contact area

Gathering the real contact area followed a three-stage process (see Figure 4.3A): i) The raw image of the contact area was first normalized to a reference image containing only the illumination function. ii) Once the uniformity of the light was

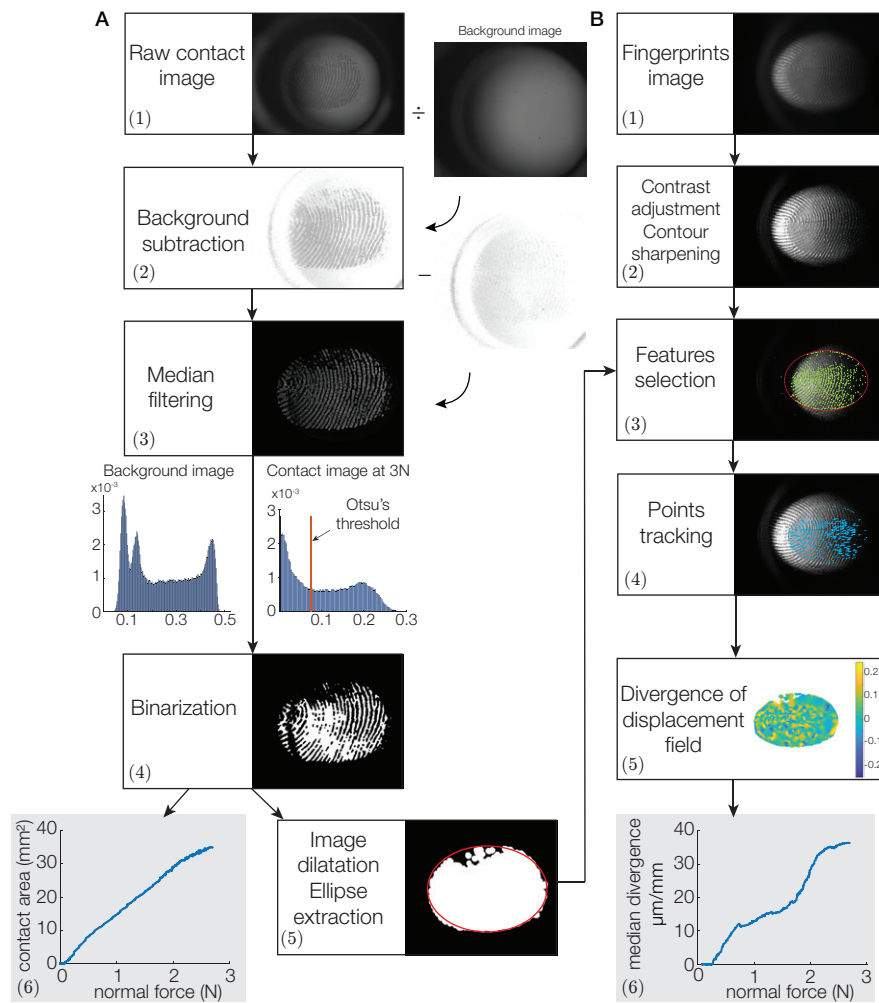


FIGURE 4.3: **A.** Processing stages of the contact area: (1). Raw image of the contact. (2). Raw image normalized by the background image to correct the non-uniform lighting. (3). Contact image subtracted from the image at the first instant of contact and filtered with a median filter of radius 5. (4). Binarized image with Otsu's threshold obtained from the histogram of the filtered image of contact. (5). Opened image (dilated with circle of radius 8) using grayscale mathematical morphological transform of Matlab and ellipse extraction. (6). Contact area in mm² as a function of the normal force. **B.** Processing stages of the divergence: (1). Raw image of the full finger. (2). Processed image of the full finger with contrast adjustment and contour sharpening. (3). Optimal features selection at the first instant of contrast. (4). Features tracking using Lucas & Kanade algorithm. (5). Computation and interpolation of the divergence in the apparent contact area. (6). Median of divergence as a function of the normal force.

restored, a 2d median filter with a 9x9 kernel removes salt and pepper noise. iii) The denoised and illumination-corrected images were thresholded using Otsu's method to measure the number of asperities in intimate contact. The contact surface in mm² was computed by summing the number of white pixels scaled by pixel resolution in mm/px. The pixel resolution was computed for each subject and

ranged between 0.032 and 0.037 mm/px.

Displacement field

Once the image of the contact was found, we computed the deformation field from the topographic image obtained with the blue grazing light (Figure 4.3B). Robust features of interest that lied in the apparent area of contact were tracked. To do so, the image of contact was registered according to the topographic image, using a calibration object containing 3 non-aligned points. The registered image followed the same treatment as the one used to compute the contact area. At the end, the binarized contact image was dilated with a radius of 8 pixels and an ellipse was extracted from this image.

Contrast of the topographic image was adjusted, and the contour was sharpened. The algorithm of Shi & Tomasi [198] was used to select 700 optimal features to track inside the ellipse of contact. Then, these features were tracked using Lucas & Kanade algorithm [140]. The tracker tracks each point from the previous to the current frame and computes the bidirectional error, which is the distance in pixels from the original location of the points to the final location after the backward tracking. If the maximal bidirectional error exceeds 1 pixel, the point is considered to be not reliably tracked.

The 700 most salient features of the fingerprint were tracked from the start until the normal force reached 3 N. The image showing the micro-junctions formed by the contact at the interface provides a temporal reference to mark when the tracked points were in intimate contact. Subtracting the position of each point once it first touches the plate, we obtained the 2-dimensional displacement field. The displacements of these features are interpolated on a uniformly sampled rectangular grid to compute the divergence using equation (4.1) and the *gradient* function in Matlab.

$$\int_S \nabla \cdot \vec{u}(x, y) dS = \int_S \frac{\partial u_x}{\partial x} + \frac{\partial u_y}{\partial y} dS \quad (4.1)$$

where u_x and u_y are the x and y components of the displacement vector $u(x, y)$ respectively, and S is the apparent area of contact.

The evolution of the median of the divergence field quantified the observed expansion.

The global displacement was computed for each trial by summing all the displacements in the apparent contact area. Trials in which the global displacement exceeded 0.3 mm were removed from the divergence analysis to prevent participants from using this cue for the discrimination task. Seventy-nine trials out of 840 were removed.

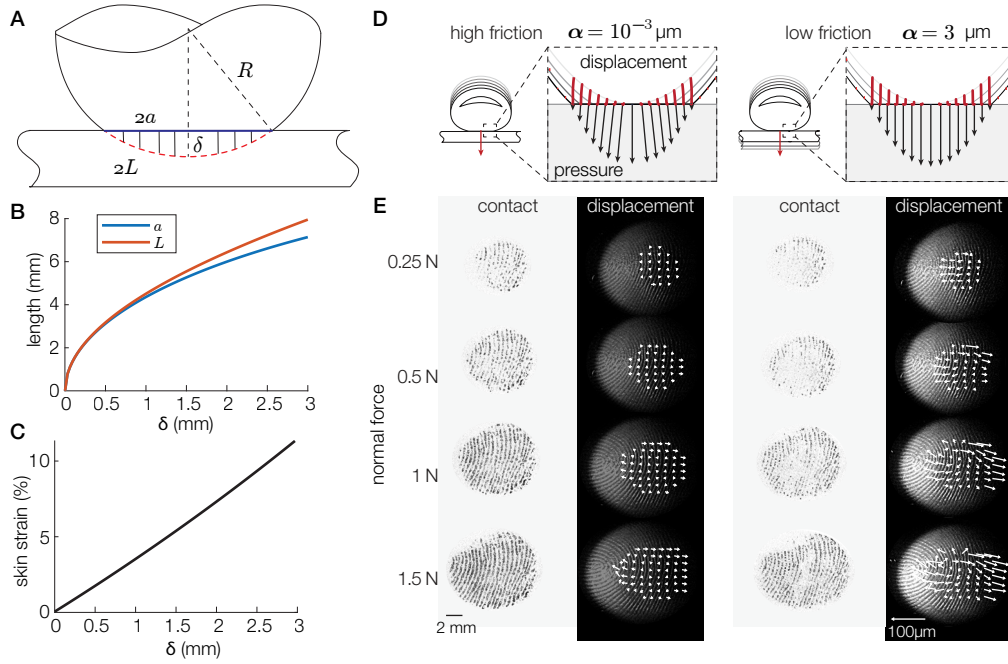


FIGURE 4.4: **A.** Geometrical model of the finger, $2L$ is the length of the arc of the skin and $2a$ is the length of the contact area. **B.** Lengths L and a as a function of the normal indentation δ . **C.** Skin strain in % as a function of δ . **D.** Presumed deformation of the skin when pressed against the surface in high- and low-friction conditions. Points trajectories are shown in red. The black arrows represent the pressure and traction exerted by each point on the surface. **E.** Images of the intimate contact and skin deformation for increasing normal forces (top to bottom) and the highest (left) and lowest (right) friction. The white arrows show the displacement of reference points, scaled up tenfold.

4.3 Results

4.3.1 Empirical skin deformation

We can build an intuitive understanding why the skin experiences a radial lateral stretch by considering that the fingertip is geometrically approximated to a deformable half-sphere. Upon compression against a flat surface, the skin of the fingertip changes from a quasi-hemisphere to a flat disk (Figure 4.4A). If the friction is considered to be infinitely high, the elements in contact are locked in place and are not able to move laterally. Thus, the length of the arc of the skin L is compressed to fit within the contact area a . Both of these dimensions can be estimated from the finger radius R and the normal indentation δ , which depends on how much the finger is pressing on the surface (4.2). Figure 4.4B plots both lengths as a function of δ .

$$L = R \arccos\left(\frac{R - \delta}{R}\right) \quad (4.2)$$

$$a^2 = (R^2 - (R - \delta)^2)$$

Skin strain ϵ can be computed with (4.3). For a 3 mm normal indentation, this model estimates a 10% lateral compression (Figure 4.4C).

$$\epsilon = \frac{L - a}{L} \quad (4.3)$$

It ensues a volume reduction, which can build-up stress at the interface, if friction is high. Conversely, if the surface is slippery, a noticeable deformation is observed (see Figure 4.4D).

The mechanical behavior of the finger observed during the experiment is qualitatively consistent with the prediction of the geometrical model. Figure 4.4E shows the evolution of the *real* area of contact constituted by the micro-junctions and the movement of the skin in a high-friction and a low-friction condition for a typical trial. Notably, the real area of contact, shown against a white background, grows with increasing normal force, and its brightness depends significantly on the level of friction reduction. This observation is consistent with previous works and with the adhesive theory of friction, in which the sliding friction force is a function of the real area of contact made by all the individual asperities in intimate contact [234, 24].

The displacement vector fields $\vec{u}(x, y)$ are computed from the difference in position between the final image and the moment when a particular point is detected to make contact. For typical trials a noticeable difference in skin movement between the high- and the low-friction conditions is found, see Figure 4.4E.

4.3.2 Friction discrimination performance

During the 2-Alternative Forced Choice procedure, the reference stimulus was the highest friction when the plate vibrates with a 10^{-3} μm amplitude. The comparison stimuli covered the range of amplitudes from 0.5 to 3 μm at intervals of 0.5 μm , with each stimulus appearing 10 times. The reference and the comparison were presented in random order. After pressing twice on the surface, participants had to indicate which stimulus they felt was the most slippery, following a typical 2-alternative forced-choice protocol. The procedure is depicted in Figure 4.5A.

We computed the probabilities of responding that the comparison stimulus was the most slippery, and the mean friction discrimination performance for all subjects is reported in Figure 4.5B. Despite the considerable inter-subject variability, there is a significant effect of plate vibration amplitude on the mean success rate (Repeated measures ANOVA, $F(5,55) = 4.77$, $p = 0.0011$). The results were fitted with a psychometric function, with which we could extract the 75% detection threshold. Participants were able to discriminate the difference of friction, with differences in vibration amplitude as low as 1.13 ± 0.69 μm , which corresponds to a reduction of the real contact area of only 8%. As the number of asperities in contact decreased, the skin could freely expand in the lateral direction, see Figure 4.5C.

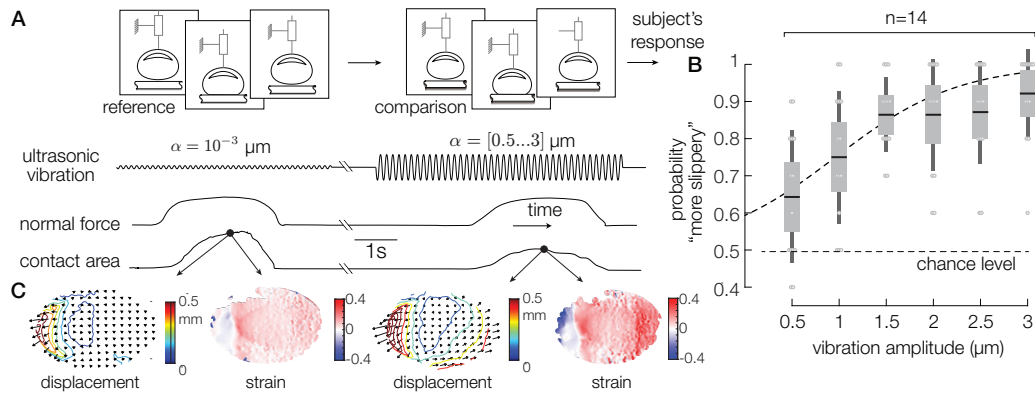


FIGURE 4.5: **A.** Experimental protocol. Participants were asked to compare the slipperiness of two surfaces. The reference and comparison are presented in random order. **B.** Probability of a participant perceiving the difference in friction as a function of the amplitude of vibration of the ultrasonic lubrication. The higher the amplitude of ultrasonic vibration is, the lower the friction coefficient. The dashed line represents the fit with a psychometric function. Individual performances are represented as grey dots. The chance level is represented by the dashed line. **C.** Displacement and resulting strain of the skin for the cases of high friction (left) and low friction (right).

4.3.3 Friction influences skin deformation

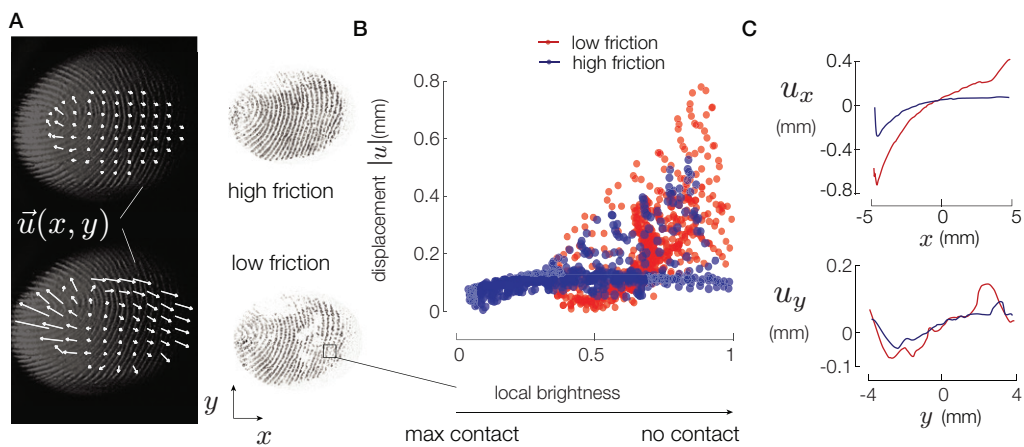


FIGURE 4.6: **A.** Typical images of the high- and low-friction trials. **B.** Displacements of a grid of points plotted against the local brightness. Displacements and local brightness are positively correlated. **C.** Displacements of this typical grid of points along the x- and y-axes.

The contact area and displacement field in both high- and low-friction conditions are shown in Figure 4.6A. In the low-friction case, the regions where the contact was virtually non-existent matched the locations of the regions of maximal displacement of the tracked points. The amount of contact area was measured via the local brightness of a 10-pixel radius circle around each of the tracked points. The displacement of each point positively correlates with the local brightness, hence with the local density of asperities in intimate contact (Spearman's coefficient

of 0.58, $p < 0.0001$). The data are shown in Figure 4.6B. This relation provides evidence that at the scale of fingertip features, friction does influence the lateral mobility.

The lateral displacements of the skin along the x and y axes are shown in Figure 4.6C for the low- and high-friction cases. The projection along the central axis reveals that the center of the contact experiences a deformation gradient whose value depends on the frictional state.

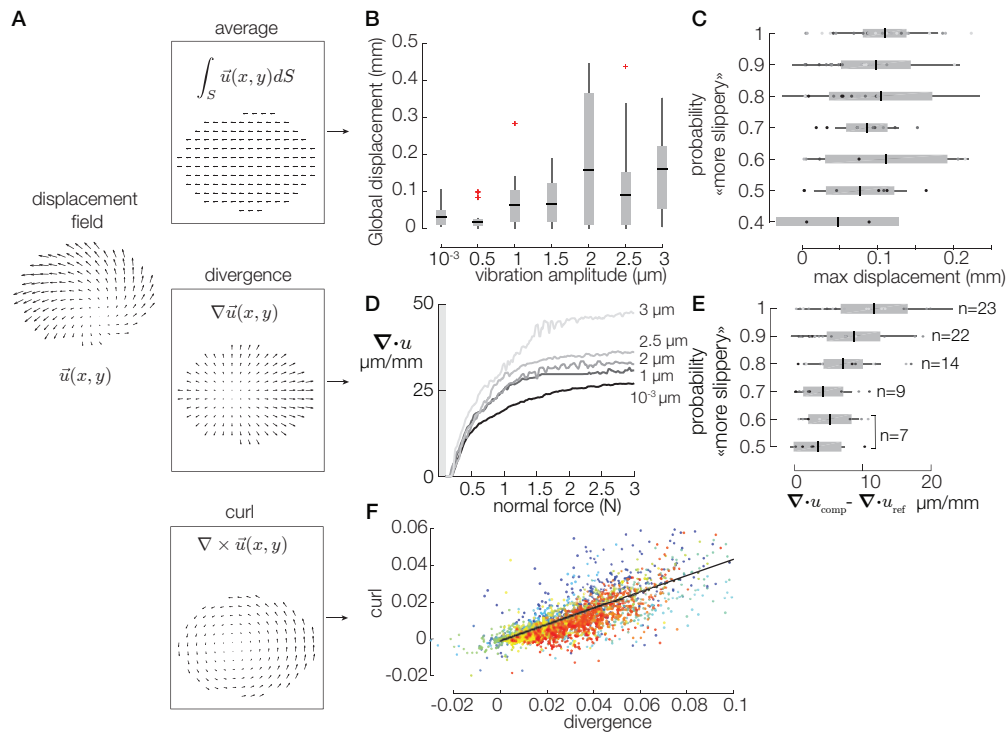


FIGURE 4.7: **A.** Decomposition of a displacement field into its conservative components. **B.** Global displacements of all trials as a function of the vibration amplitude. **C.** The probabilities to answer comparison is "more slippery" are plotted against the median of maximal global displacements. The color of the dots represents the vibration amplitude. The darker there are, the smaller the vibration amplitude. **D.** Median divergence for each vibration amplitude. **E.** The probability to answer comparison is the most slippery are plotted against the median divergence differences. Darker colours represent the smaller vibration amplitudes. **F.** Correlation between median curl and median divergence. Each color stand for a participant.

To explore the effect of friction on the displacement field, we decomposed it into a constant field, a divergent field and a rotational field (see Figure 4.7A).

Lateral global displacements were estimated by computing the median of all vectors in the apparent contact area at each time instant. They represent the constant part of the deformation field. Global displacement takes relatively small values (avg=0.08 mm \pm 0.10 mm SD) (Figure 4.7B).

Figure 4.7D plots the median across trials of the average divergence for increasing plate vibration amplitude. Intuitively, the averaged divergence of a

vector field captures its outward or inward flux. A positive divergence implies that the finger expands radially. The divergence grows with the normal force. The rate of growth is positively correlated with the vibration amplitude (Spearman's coefficient = 0.115, $p < 0.0001$). The growth of the average divergence is notable at the early stage of fingertip compression and hits an inflection point after 1 N. After this inflection point, the dependence on friction is more pronounced. Above 2 N, the curves flatten, likely due to saturation of the compression of the fingertip pulp [194, 172]. Despite the saturation above 2 N, the differences in average divergence are significant (ANOVA, $F(6,1569) = 4.85$, $p = 10^{-5}$), with values twice as large for the low-friction case ($3 \mu\text{m}$) than for the high-friction case ($10^{-3} \mu\text{m}$). Large divergence reflects that the skin moves significantly without friction. In the high-friction case, the low divergence values signal the presence of residual radially distributed stress of the skin.

The curl is a vector denoted infinitesimal rotation of a vector field. In our case, the curl is directed along the z-axis and is computed as following:

$$\int_S \nabla \times \vec{u}(x, y) dS = \int_S \frac{\partial u_y}{\partial x} - \frac{\partial u_x}{\partial y} dS \vec{z} \quad (4.4)$$

As the divergence, curl is computed for each point of the apparent contact area. Taking the median curl of all points gives the speed of rotation of the finger around itself. We found that divergence and curl follows the same global evolution against the normal force. Both metrics are positively linearly correlated with a Pearson's correlation coefficient of 0.7726 ($p < 0.0001$) (see Figure 4.7F). A possible explanation of this phenomenon postulates that fingerprints align with the direction of the stimulus, as observed in [56].

4.3.4 Skin deformation and friction perception

The global lateral displacement of the skin, computed from the median of the vector field at each time instant, did not significantly influence the response of the participant (Spearman's coefficient = 0.14, $p = 0.2$), see Figure 4.7C.

Nonetheless, the probability of correctly identifying the most slippery stimulus was positively correlated with the amount of diverging skin deformation observed (Spearman's coefficient = 0.28, $p = 0.009$). Figure 4.7E shows the difference in divergence between the reference stimulus and the comparison stimulus as a function of participants' discrimination performance. While the correlation is weak, friction was unambiguously discriminated when the skin experienced the largest inter-stimulus difference in divergence. Correlation does not imply causation, however, in the next part, we were focusing on finding the best predictor of participant's answer.

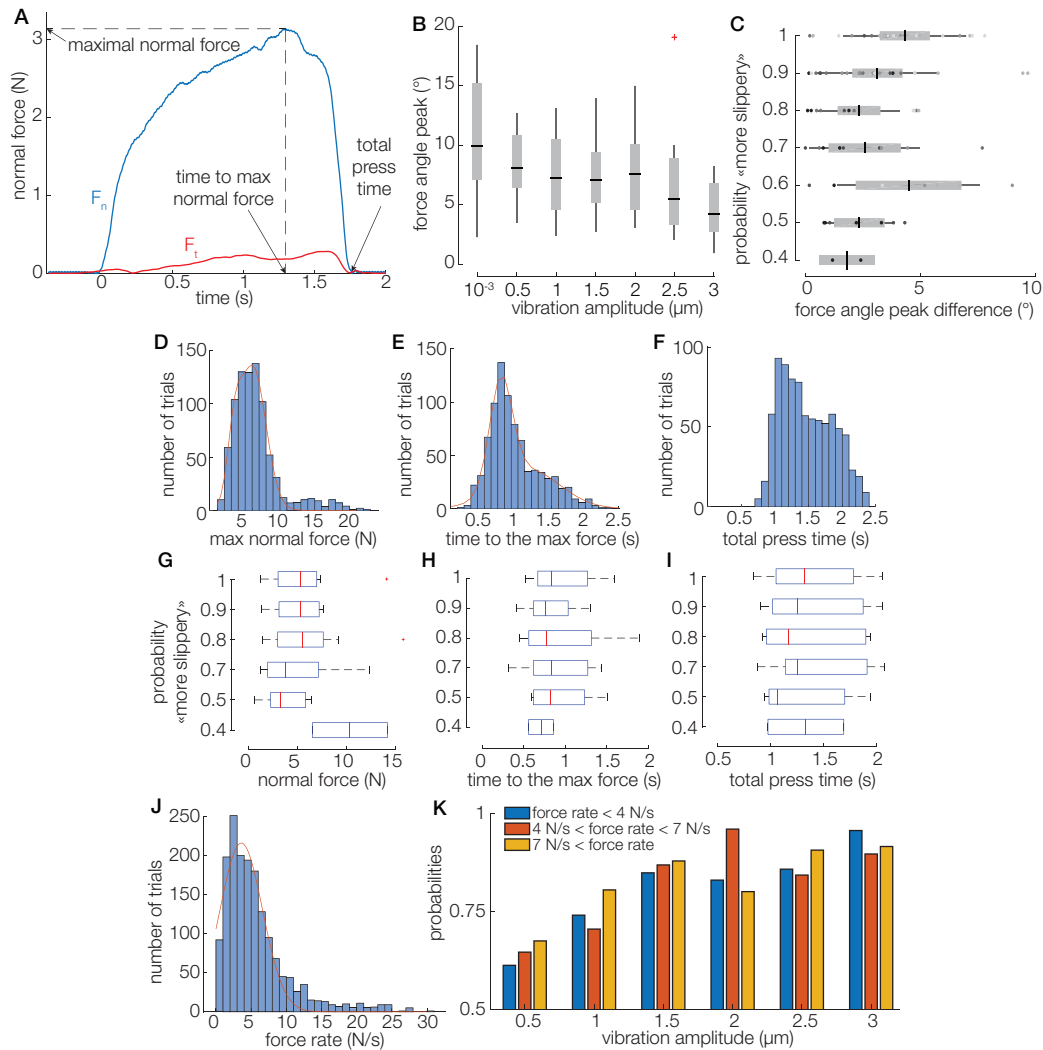


FIGURE 4.8: **A.** Typical normal force time series for one trial. **B.** Force angle peaks of all trials as a function of the vibration amplitude. **C.** The probabilities to answer comparison is "more slippery" are plotted against the peak force angle difference. Distribution of normal force **D**, time to reach the maximal force **E** and total duration **F** for all trials. **G H I.** Influence of these metrics on the probabilities to answer comparison is "more slippery". **J.** Distribution of maximum force rate for all trials. **K.** Influence of the maximum force rate on the probability to answer comparison is "more slippery" for each vibration amplitude.

4.3.5 Influence of the kinematics of the exploratory procedure

Normal pressure results in a force vector angle which depends on the vibration amplitude (ANOVA, $F(6,1593) = 67.9$, $p < 0.001$) (Figure 4.8B). The peak force angle is on average $9.9^\circ \pm 4.9^\circ$ SD when the friction is high and $4.2^\circ \pm 2.1^\circ$ SD when the friction is low. This suggests that in high-friction cases, tangential forces induced at the interface limit the global displacement of the finger, whereas in low-friction cases, tangential forces are released and micro-slips occur. However, the force vector angle is not correlated with the participants' answers (Spearman's coefficient

= 0.24, $p = 0.03$), which suggests it was not used as a cue to assess friction (Figure 4.8C).

Participants were free to press at any normal force and as long as desired. Consequently, the recorded normal forces (avg = 5.5 ± 3.5 N) and the time to reach it (mean = 1.47 ± 0.39 s) showed significant variations (Figure 4.8D and E). The total duration of every trial varies from 1 s to 2.5 s (Figure 4.8F). In any case, the amount of force applied or the duration of the trial were not significantly correlated with participants' answer (ANOVA, $p = 0.31$ for normal force, $p = 0.99$ for time to max force and $p = 0.91$ for total duration) (Figure 4.8G, H and I). Nonetheless, large normal forces were found to be associated with low probabilities. Our hypothesis is that when participants haven't any valuable cues to discriminate friction, they press harder to induce larger skin deformation.

The force rates applied by the participants follow a normal distribution of mean 3.6 N/s and standard deviation 3 N/s (Figure 4.8J). In the bar plot in Figure 4.8K, the probability that participants will identify the comparison stimulus as most slippery is shown as a function of the force rate for each vibration amplitude. We found that the force rate has a significant influence on the participants' answers for the vibration amplitude $\alpha \leq 2 \mu\text{m}$ (Linear Mixed Model, $p = 0.018$). The faster the indentation speed, the more the chance to detect correctly the most slippery stimulus. Thus, the kinematics of the exploratory procedure play a significant role for the low vibration amplitudes.

4.3.6 Strain energy and mechanoreceptors thresholds

It is worth considering whether the amount of skin deformation is enough to induce a supraliminal response. We estimate the stimulation of the mechanoreceptors by computing the strain components, according to the following method.

Strain computation

The strain components were obtained via the same procedure as in [56]. A Delaunay triangulation was first constructed with the 700 tracked points, only considered once they enter in contact with the plate. This triangulation is illustrated in Figure A.1A and C. Then, we used the following formulas to compute the strain components of each triangle.

$$\begin{aligned}\epsilon_{xx} &= \frac{\partial u}{\partial x} + 0.5 \left[\left(\frac{\partial u}{\partial x} \right)^2 + \left(\frac{\partial v}{\partial x} \right)^2 \right] \\ \epsilon_{yy} &= \frac{\partial v}{\partial y} + 0.5 \left[\left(\frac{\partial u}{\partial y} \right)^2 + \left(\frac{\partial v}{\partial y} \right)^2 \right] \\ \epsilon_{xy} &= 0.5 \left[\frac{\partial u}{\partial y} + \frac{\partial v}{\partial x} \right]\end{aligned}\tag{4.5}$$

The strain energy densities u_d were computed for each triangle based on average values of Young's modulus and Poisson's ratio, respectively equal to 1 MPa and 0.4.

Note that these values can nonetheless vary from one participant to another.

$$u_d = \frac{E(1-\nu)}{2(1+\nu)(1-2\nu)} (\epsilon_{xx}^2 + \epsilon_{yy}^2) + \frac{E\nu}{(1+\nu)(1-2\nu)} \epsilon_{xx} \epsilon_{yy} + \frac{E}{1+\nu} \epsilon_{xy}^2 \quad (4.6)$$

The total strain energy on the whole contact area was obtained by integrating the strain energy densities on a volume, assuming that the strains are uniform for a given depth of 2 mm [56].

$$U = \int u_d dV \approx 0.002 \int u_d dS \quad (4.7)$$

Mechanoreceptors sensitivity

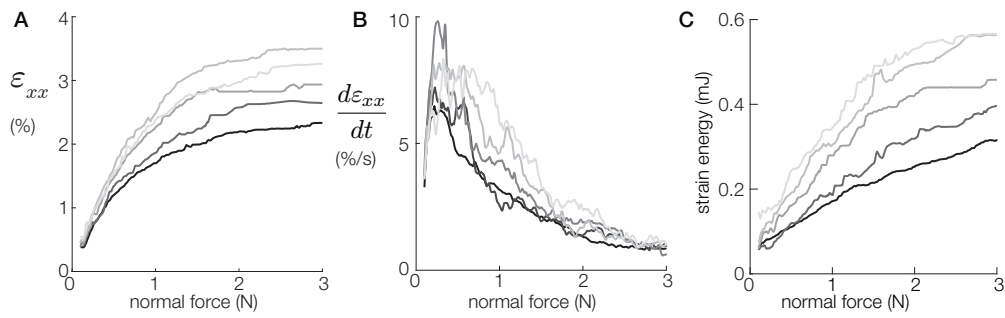


FIGURE 4.9: **A.** Median longitudinal strain for each vibration amplitude. **B.** The strain-rate peaks after 0.4 N for each vibration amplitude. **C.** Evolution of the strain energy for various coefficient of friction.

Strain components are shown for a low- and a high- friction case in Figure 4.5C. Median longitudinal strain components for each vibration amplitude are plotted in Figure 4.9A. They are all positive, suggesting a skin expansion once the contact is made, both in the high- and the low-friction condition. Nonetheless, the data show that the participants' skin is subjected to a longitudinal strain whose magnitude depends on the vibration amplitude (Spearman's coefficient $\rho = 0.17$, $p < 0.0001$). The strain magnitude estimates fall between 2 and 4%, which is sufficient to change firing rate in FA and SA afferents [66]. The median strain rates were computed for each of the vibration amplitudes by differentiating the longitudinal strain component with respect to time. Similarly, the dynamics of the stimulation shows significant differences between friction condition (Figure 4.9B). They peak at the very beginning of the normal indentation when the normal force reaches 0.37 ± 0.7 N. This is compatible with the evidence in literature that a stimulation with a strain rate higher than 8%/s elicits a response in all afferent types [65].

The strain energy densities along the skin surface were computed using (4.6). Total strain energy follows the same behavior as the divergence with a plateau after 2 N (Figure 4.9C). The action of pressing down against the surface stores mean= 0.32 ± 0.52 mJ of strain energy. As for strain components, there is a strong

correlation between the total strain energy and the vibration amplitude (ANOVA, $F(6,1481) = 3.2$, $p = 0.004$).

Finally, median longitudinal strain (Figure A.1H) and resulting strain energy differences (Figure A.2E) are not correlated with participants' answers. However, we found a weak correlation between the strain rate and the probability of answering that the comparison is "more slippery" (ANOVA, $F(5,70) = 2.12$, $p = 0.023$), suggesting that a sufficient deformation speed is required to enable subjects to sense frictional differences [65].

4.3.7 Ideal Observer Analysis

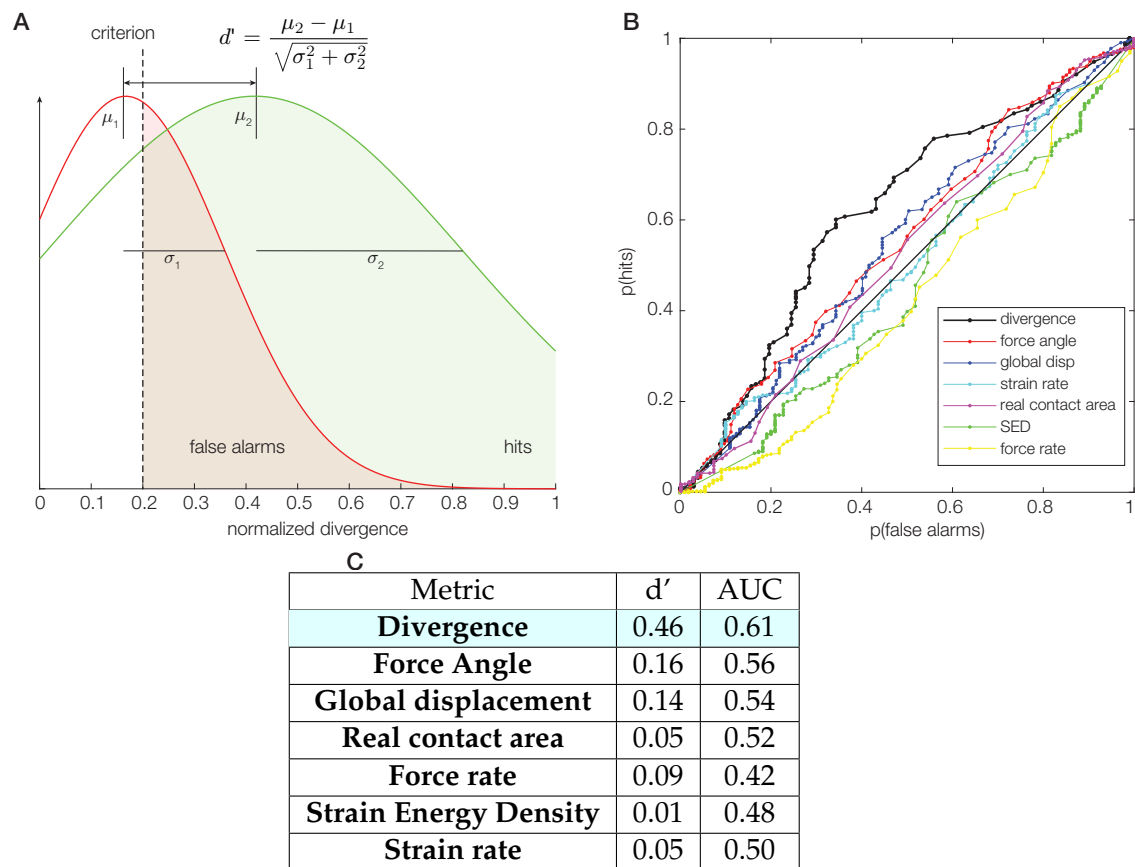


FIGURE 4.10: Ideal Observer Analysis. **A**. Fitted gaussian curve of the number of trials when participants are answering reference (red) and comparison (green) as a function of the normalized divergence. **B**. Receiver Operating Characteristics, representing the probability of answering the comparison when the metric is higher than a criterion ($p(\text{hits})$) as a function of the probability of answering the reference when the metric is higher than a criterion ($p(\text{false alarms})$). **C**. The table gathers the sensitivity index d' and the area under the ROC curve (AUC) for each metric listed.

To test the contribution of each variable as a predictor of friction differentiation ability, we computed the performance of an ideal observer. The following variables were tested: divergence, force angle, global displacement, strain rate, strain energy

density, force rate, and real contact area. Since global displacement and force angle were undesired in the experiment, the other metrics were set to NaN (not a number) for trials that present a global displacement higher than 0.2 mm, in order to evaluate the contribution of these variables when no other cues were available. The incorrect trials (i.e. when participants answered that the reference was more slippery) were first separated from the correct trials, (i.e. when they answer the comparison was more slippery). Each of the variables was normalized according to the 0.9 quantile and grouped in bins of 0.05. We counted the correct/incorrect instances in each bin and fit a normal distribution to it. The sensitivity indexes (d') were extracted from the means (μ_1 and μ_2) and standard deviations (σ_1 and σ_2) of the Gaussian distributions of the normalized variables for correct (green) and incorrect (red) trials, as represented in Figure 4.10A.

The probability of hits is given by the proportion of correct trials for which the variable produces a response greater than a criterion, whereas the probability of false alarms is the proportion of incorrect trials for which the variable exceeds the criterion. The receiver operating characteristics (ROC) were computed from the probability of hits as a function of the probability of false alarms when the criterion ranges from 0 to 1. The ROCs are shown in Figure 4.10B for all tested variables. The larger the area under the curve, the better the predictor. The sensitivity index d' and the area under the curve (AUC) of the ROC are summarized in table 4.10C. The performance of the ideal observer was on a par with the performance of the participants of the psychophysics experiments. Amongst all tested variables, the divergence metric leads to the highest sensitivity index and the highest AUC, suggesting that it is the best predictor amongst the others studied. It is followed by the force angle and the global displacement, indicating that undesired minor lateral motion present in some trials also facilitated the friction discrimination task. On the contrary, the low values of d' and AUC obtained for real contact area, strain rate, SED, and force rate, mean that the participants perform at chance according to those metrics, or they possibly may even interfere with correct judgement, confirming our findings that the divergence was the most relevant metric predicting participants performance. Note that in the case of an ideal observer, choosing a criterion of 13.1 $\mu\text{m}/\text{mm}$ for the divergence leads to a probability of hits of 75%.

4.4 Predictions from the mechanical model

We developed an axisymmetric spring-damper model presented in chapter 3, to estimate the stress experienced by the skin. The model captures the large deformation of the skin, its viscoelastic behavior using Kelvin-Voigt material and the local elastoplastic frictional interaction at the interface.

We simulated the interaction with a plate surface under four different coefficients of friction from 0.1 to 0.6, with a normal force of 3 N applied to the bone

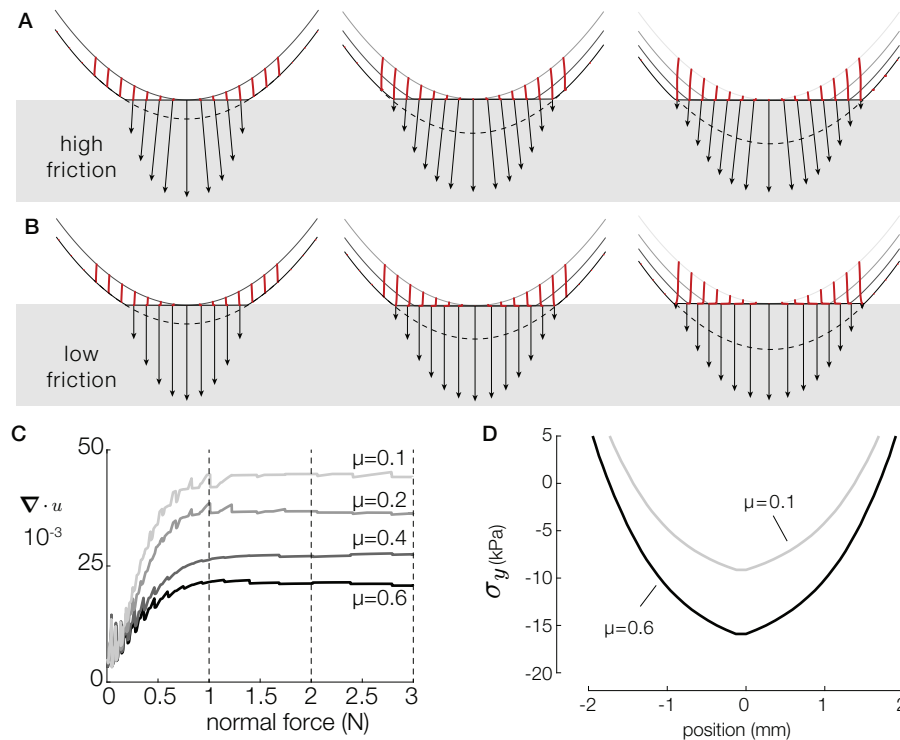


FIGURE 4.11: Surface deformation profiles when in contact with a low- **A** and a high- **B** friction surface for 1, 2 and 3 N. Points trajectories are shown in red. The black arrows represent the pressure and traction exerted by each point when brought in contact with the surface. **C**. Total divergence of the contacted skin as a function of the normal force for friction coefficients varying from 0.1 to 0.6. **D**. Stress profiles at 3 N of normal force for a high- and a low-friction condition.

element. The simulation was initiated before contact and ran until it reached static equilibrium. The simulated displacements and interfacial pressure in response to an external normal force of 1, 2 and 3 N for $\mu = 0.1$ and $\mu = 0.6$ are shown Figure 4.11A and B respectively. Figure 4.11C shows the simulated divergence of skin displacement for all friction coefficients. The divergence varies from $\nabla u = 0.02$ for a coefficient of friction $\mu = 0.6$ to $\nabla u = 0.04$ for $\mu = 0.1$. The model predicts a trend quantitatively similar to the experimental data.

These observed lateral displacements can be explained by the stress acting on each element because of friction. We estimated those lateral traction in the case of a low- and a high-friction contact. The normal component of the interfacial pressure remains identical across frictional conditions. However, the lateral component directly depends on the friction, with the high-friction case seeing 40% larger tangential stress (Figure 4.11D). The maximum of the stress is located in the center of the contact area and is consistent with the traction observed in [103, 142]. In the low-friction case, the low tangential traction results in a free lateral displacement of the skin as the skin flattens in contact with the plate. In this case, every point moves outward such that the contact length approaches the initial curved length of the fingertip (dashed line). Conversely, in the high-friction case, the tangential traction

constrains the motion of skin in contact. The elements are secured in place once they touch the plate, resulting in little displacement and a 40% increase in stored elastic stress compared with the low-friction case.

4.5 Discussion

A short one-second haptic normal force contact was sufficient to allow participants to discriminate the frictional strength of a surface. When pressing, the skin conformed to the surface, and the observed deformation was directly tied to the frictional strength of the surface. The results demonstrate that no gross lateral motion of the whole contact area was necessary to elicit the perception of friction. The observers fundamentally relied on cutaneous cues, involving a particular spatio-temporal pattern following an outward expansion, quantified by the divergence of the skin deformation.

The deformation of the skin is caused by the absence of friction at the interface, unfettering the lateral motion of the skin while it is compressed against the surface. Under low-friction conditions, fewer asperities are in intimate contact, and therefore, they cannot hold the lateral force, inducing local slippage. Conversely, in high-friction conditions, the asperities make sufficiently large contact and thus restrain lateral relaxation of the skin, which causes an accumulation of the elastic stress. Psychophysics experiments demonstrated that the magnitude of friction reduction effect correlates with likelihood of subjects identifying the most slippery surface. Such frictional effects are accompanied by corresponding skin deformation changes, which we were able to describe by a biomechanical model. As there were no net lateral forces present, the pattern of outward skin expansion characterized by divergence was the decisive factor to assess friction when other cues are not available.

We estimate that the action of pressing down against a high-friction surface stores approximately 0.3 millijoules of potential elastic energy in the skin (Figure 4.9C). This amount is 10 times lower than what was found when detecting slippage during relative motion, where the strain can reach 25%. This result suggests that information about the frictional strength is available well before slippage is detected [13, 56].

The amount of lateral skin deformation during pressing is sufficient to trigger a significant difference in the activation of all types of tactile afferents [57, 117, 98]. Since the action is faster here, the relative speed between the skin and the glass plate at the periphery of the contact is larger than 10 mm/s. This speed, combined with the spatial nature of the deformation pattern, suggests that fast adapting afferents predominantly contribute to the encoding of friction upon initial contact.

An early estimation of the frictional strength has been associated with early adjustment of the grip force during precision grasping tasks. New evidence obtained in the current study extends these findings showing that in a

well-controlled perceptual task, abolishing all additional contributing factors like lateral force and texture cues, friction discrimination was possible perceptually. This indicates that information about the initial skin deformation pattern can be sufficient to obtain frictional information. However, during object manipulation beyond initial touch, when load forces develop, more sensory signals become available, improving force coordination and making overall adjustments to friction more accurate [117, 103]. Gloves and other mechanical filters are well known to affect the regulation of grip forces, resulting in an overcompensation of the safety margin increases regardless of the friction of the surface [8, 103, 119]. The presence of this mechanical filters might remove the ability to gauge the divergence of the field during the first instant of contact, hence defaulting motor control to a more robust grasping state.

The skin deformation increases with the applied normal force, and its rate of increase is a function of the friction of the surface. Despite growing at different rates, the divergence of the displacement field reaches a plateau at 2 N of normal force for all friction conditions, which is similar to the level of grasping force at which friction starts to influence the rate of grip force increase [107]. This result suggests that during the first instant of contact, grasp control may rely on the measured divergence of the skin deformation.

Interestingly, the perception of the softness of an object during active touch is correlated with the rate of growth of the contact surface [19]. Since friction influences the rate of change in the elastic energy, we can conjecture that cross-coupling might exist between softness and friction, with slippery surfaces appearing more compliant to the touch.

Despite having similar levels of friction variations and observed skin displacement up to 0.2 mm in magnitude, previous studies in which participants passively perceived the stimuli showed that the discrimination of friction is a challenging task [118]. In contrast, the active exploration procedure of this study, even if constrained, resulted in a fundamentally more successful discrimination of the frictional conditions. The stark difference could be explained using predictive coding theory [29]. To determine friction, the observer has to assess the total deformation separating at least these two components, one encoding the indentation magnitude and another related to the lateral deformation encoding the frictional strength. In the active case, observers possess an efferent copy based on which they could predict the dynamics of gross deformation of the fingertip. The ability to predict sensory consequences of own actions (reafference) would enable the nervous system to better extract and isolate sensory signal features related specifically to the diverging deformation pattern, and thus focus attention on frictional cues.

Alternatively, it is possible that a difference in indentation speed may have played the major role determining detectability of the frictional differences. Khamis et al. [118] report a force rate of 1.7 ± 0.3 N/s, whereas in this study the force rate is

3.6 ± 3 N/s, which would provide a more potent activation of fast adapting afferents (Figure 4.8K).

This study establishes the link between skin deformation and performance in a friction discrimination task. Similar to the suggestion in [56], an artificial tactile stimulation stretching the skin radially while the user is pressing down, could indicate the amount of friction. These cues could facilitate the manual control of teleoperated devices or render a virtual sensation of slipperiness. The biomechanics can also inspire the control of robotic grippers and prostheses based on radial lateral skin stretch [137].

4.6 Conclusion

Humans have the remarkable ability to manipulate a large variety of objects regardless of how fragile, heavy or slippery they are. To correctly scale the grip forces, the nervous system gauges the slipperiness of the surface. This information is present at the instant we first touch an object, even before any frictional force develops. This study demonstrates that a radial tensile strain of the skin is involved in the perception of slipperiness during this initial contact. These findings can inform the design of advanced tactile sensors for robotics or prosthetics and for improving haptic human-machine interactions.

Chapter 5

The mechanical basis encoding stick-slip transition

Contents

5.1 Introduction	74
5.1.1 Encoding of slippage	76
5.1.2 Efficient coding hypothesis	76
5.1.3 Rationale behind dimensionality reduction	77
5.2 Materials and Methods	78
5.2.1 Data collection	78
5.2.2 Dataset of spatio-temporal skin deformation	79
5.3 Results	81
5.3.1 Empirical strain patterns	81
5.3.2 Model validation	82
5.3.3 Dimensionality reduction	82
5.3.4 Tactile encoding efficiency of the safety margin	84
5.4 Discussion	86
5.5 Conclusion	87

Adapted from: Willemet, L., Huloux, N., & Wiertelowski, M. (2022) Efficient tactile encoding of object slippage.

Preface to Chapter 5

TACTUALLY detecting incipient slippage swiftly can be the difference between a secure grasp and dropping an object. In less than 200 ms, tactile information is processed to determine the frictional strength of the contact from the deformation of the skin and react accordingly. Given the thousands of afferents innervating the fingertips, it is unclear how the nervous system can process the large influx of data in a sufficiently short time span to make a robust decision whether the grip force needs to be increased. In this study, we measured the deformation of the skin during the initial stages of incipient sliding for a wide range of frictional conditions. We show that the dominant patterns of deformation are sufficient to estimate the distance between the frictional force and the frictional strength of the contact. From these stereotypical patterns, a classifier is able to predict if an object is about to slide during the initial stages of incipient slip. The prediction is robust to the actual value of the interfacial friction, showing sensory invariance. These results suggest that the nervous system efficiently encodes tactile information by projecting the measured deformation of the skin onto a compact basis of deformation patterns, that we call *Eigenstrains*. Our findings suggest that only 6 of these Eigenstrains are necessary to classify the slippage sensed by tens of thousands of afferents. These findings are relevant to the understanding of the unconscious regulation of grasp, and the insights are directly applicable to the design of robotic grippers and prosthetics that rapidly react to external perturbations.

5.1 Introduction

Dexterous tasks, such as picking fruits or writing with a pen, continuously recruit sensorimotor feedback to detect and avoid slippage. The amplitude of the grasping forces applied to the object rely on cutaneous afferents, which encode the deformation of the skin. Using this information, the sensorimotor system continuously balances between applying enough force to keep the object steady, while at the same time having a light enough touch to permit posture adjustments. During this process, a margin of safety between the frictional strength of the contact (i.e. the maximum admissible lateral force before slippage) and the external load forces acting on the object is maintained [107]. This safety margin sets the grip force 10% to 20% higher than the minimum admissible force, depending on the unpredictability of the forces at play [87]. The typical evolution of the forces during grasping an object is shown in figure 5.1A.

To maintain this safety margin, tactile afferents which encode the spatio-temporal deformation of the skin are continuously monitored [106]. As a

cogent evidence, in the absence of tactile sensations following anesthesia, the dexterity of the participants is drastically degraded because they struggle to regulate their grip forces [8, 238]. Grip force adjustments are likely triggered by early signs of incipient slippage of the object in contact with the skin. At a mechanical level, during incipient slippage, the contact transitions from a state where it is completely stuck, to an intermediate state where the outer region of the contact slips. This slip region grows to eventually encompass the entire contact area, at which stage the stuck area vanishes and the object fully slips [7]. This transition, predicted by Cattaneo-Mindlin theory [212] and illustrated in figure 5.1B, induces stereotypical patterns of skin deformation [13], leading to a compression of the tissues on the leading edge and to a stretch on the trailing edge [56].

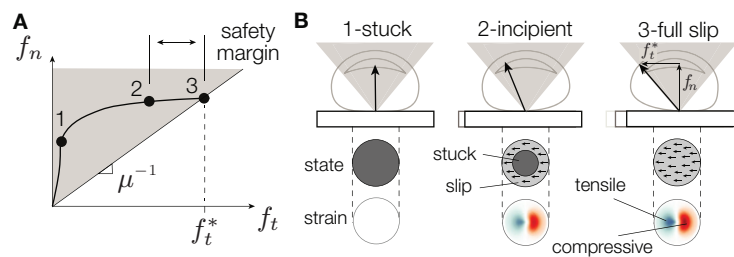


FIGURE 5.1: **A.** Normal and tangential component of the lateral force in a typical grasping task. To avoid slippage, the nervous system regulates the grasping force f_n to keep a safety margin from the maximum load bearing capacity $f_t = \mu f_n$. **B.** Typical evolution of the interaction force, area of contact and skin deformation during the transition from stick to slip.

Reacting quickly to incipient slip requires processing signals sent by thousands of afferents to detect a specific pattern in the spatio-temporal deformation. In addition, the deformation depends on the friction of the surface, but since the safety margin is independent of friction [30], the detection has to be friction-invariant. Given the complexity of the task, how can the nervous system process efficiently the afferent signals in a swift amount of time to quickly detect slippage, regardless of the friction of the surface, in order to avoid a catastrophic loss of grip?

In this article, we formulate the hypothesis that the nervous system must compress the peripheral information by projecting it on a compact basis of functions. This compression removes the redundancy and promotes perceptual invariance to friction when detecting incipient slippage. To test this hypothesis, we extracted a compact dictionary of deformation patterns from a large dataset containing the spatio-temporal evolution of skin strains during the transition from stick to slip at different frictional conditions. We show that the dictionary is crucial to efficiently decode the safety margin from the pattern of strain produced during slippage. These results reveal the contribution of skin mechanics to the detection of incipient slippage, and can inspire reactive control of robotic grippers based on tactile events [95, 141].

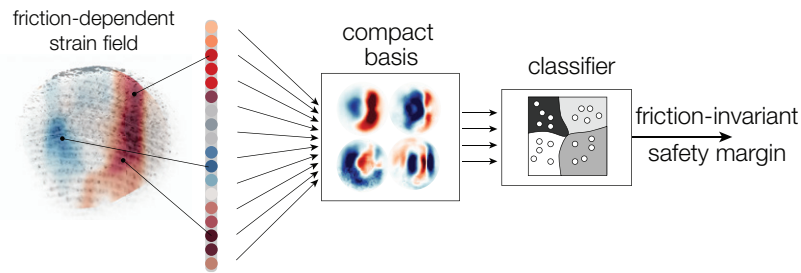


FIGURE 5.2: Steps of perceptual computation from a friction-dependent strain field to a friction-invariant estimate of the safety margin.

5.1.1 Encoding of slippage

At the onset of sliding, the deformation of the skin likely stimulates upward of thousands of mechanoreceptors, whose neural activity propagates toward the central nervous system [105, 119, 109]. The timing and the number of the first spikes of neural activity produced by this deformation contain crucial information, which is exploited by the nervous system to adapt the safety margin for a stable grasp [219, 102]. External perturbations elicit responses within 100 to 150 ms [40] during which central processing only accounts for approximately 15 ms of the total time [102]. This latency is comparable in magnitude to long-latency reflex responses, suggesting that the grip force regulation is mediated supra-spinally [149].

Given the speed of the reaction, the number of stimulated mechanoreceptors, and the limited capacity of the brain, the nervous system likely compresses the information contained in the afferents. One possible compression mechanism involves projecting the incoming skin deformation pattern onto a *compact* dictionary of strain primitives. A dimensionality reduction that reduces the high-dimensional space of the neural information –from upward of 1,000 afferents in the fingertip down to few principal components– can enable a swift estimation of the safety margin to determine if more grip force should be applied (Figure 5.2).

5.1.2 Efficient coding hypothesis

The dimensionality reduction conjecture derives from the efficient coding hypothesis, first introduced by Barlow [11]. Efficient coding postulates that information is transmitted from the sensory organs to the nervous system with a minimal number of action potentials, using a *compact* lexicon that minimizes the neural activity by removing the information redundancy. Moreover, this lexicon must be independent of the friction coefficient, since the same reflexive behavior can be observed on objects having surfaces of various frictional strength [57].

How can we gain access to a likely candidate of this compact lexicon? Considering that the sensory system evolves in the natural world, a representation must be created where natural stimuli are encoded efficiently [15]. Therefore, by

distilling the lexicon from a large sample of natural stimuli, we can find a compact function decomposition by maximizing the sparsity of the signal. The sparsity assumption allows us to extract useful patterns from big datasets and, thus, reduce the computational cost. In the specific case of detecting incipient slippage, these stimuli are the strain patterns, representative of the deformation of the skin. Similar dimensionality reduction approaches have been successful in distilling sparse representation of natural images [163] and audio signals [135]. The sparsity condition ensures that the information is embedded in a population code with a minimum number of neurons active at any one time, leading to a more than 20-fold compression of images or audio waveforms without losing perceptual accuracy [242]. Similar efficient coding strategies have been observed in touch, and facilitate the classification of hand gestures from vibrotactile surface wave propagation [196] or to identify material properties from the vibrotactile signal they produce [151].

5.1.3 Rationale behind dimensionality reduction

Amongst the numerous dimensionality reduction methods, matrix factorization methods can efficiently compress natural stimuli. For instance, independent component analysis finds features separating the signal in statistically independent parts. When applied to natural images, it recovers a functional basis that resembles Gabor filters [15], hinting at a possible structure of the computation used in the early stages of the visual processing. Similarly, Non-negative Matrix Factorization [131] has been popular for explaining sensory processing since it promotes basis functions that capture local features. As an example, this factorization trained on a database containing human faces leads to a dictionary containing representations of the mouth and the nose.

In our specific case of decoding the safety margin from the skin deformation, we postulate that the nervous system uses a compact set of basis patterns (i.e. that includes only a minimal amount of projective axes) to accelerate the processing. This compact set of bases should capture the most variance of the skin deformation patterns and should maximally decorrelate the output signal. This set of requirements makes the principal component analysis the most suited method. Principal component analysis can be computed by taking the Singular Value Decomposition of the entire database of strain patterns and truncating the result to conserve only the first most representative principal components [166, 73]. For an overview of the dimensionality reduction methods and how it applies to our specific case, refer to Appendix C.

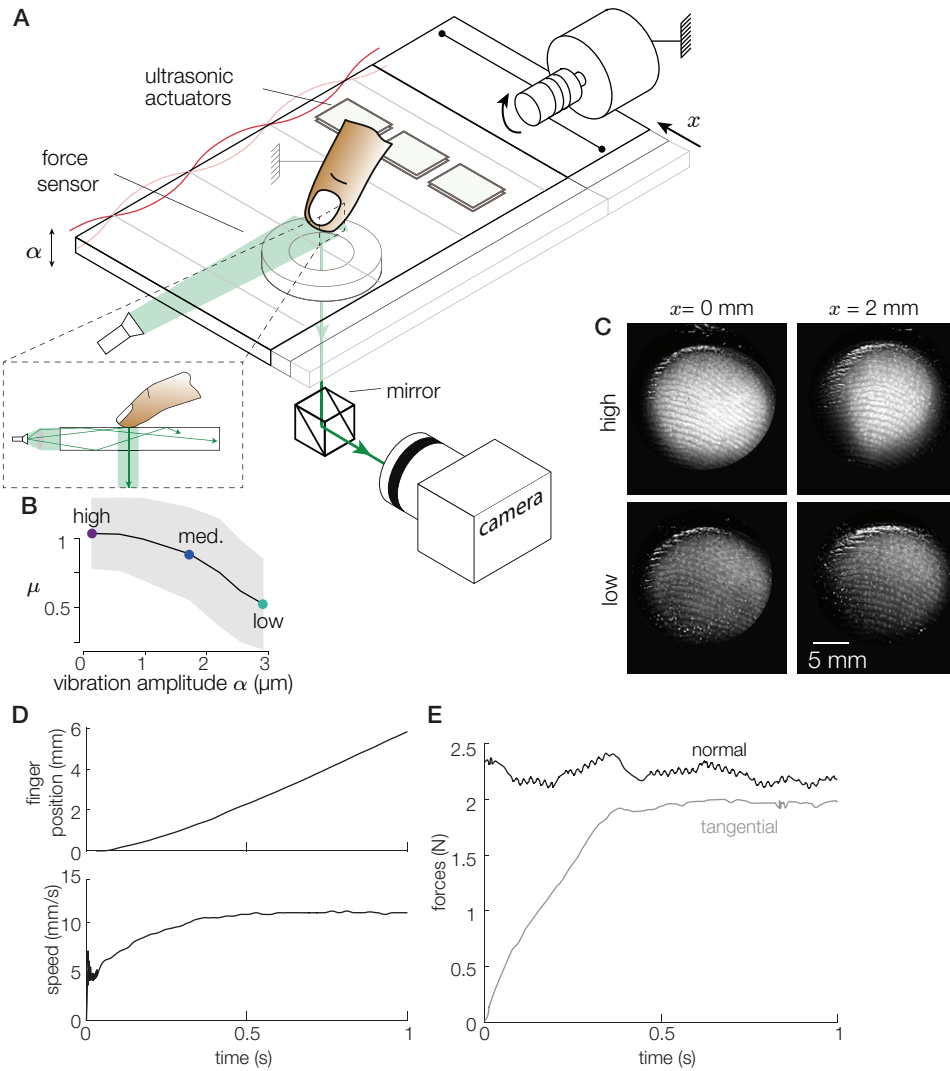


FIGURE 5.3: **A**. Experimental apparatus combining ultrasonic friction reduction and FTIR imaging of the contact (inset). **B**. Ultrasonic vibration reduces the sliding friction coefficient. **C**. Typical images for two lateral deformations and two amplitudes of vibrations. **D**. Time series of finger position and speed respectively. **E**. Normal and tangential forces applied by the finger.

5.2 Materials and Methods

5.2.1 Data collection

Twelve volunteers participated in the study. They gave their informed consent prior to the experiment. Their fingertip was secured in a dedicated 3D printed plastic shell to ensure a constant angle between the finger and the glass plate around 20° . The frictional resistance of the plate against the skin was controlled by ultrasonic lubrication [234]. The device uses a flexural standing wave to induce a micrometric levitation of the skin of the fingertip, thereby reducing the interfacial friction. The rectangular glass plate vibrated at a frequency of 29.97 kHz in the 3×0 mode, $68 \times 120 \times 11$ mm³. The friction of the plate could be changed from high, medium and

low friction, corresponding to average coefficients of sliding friction of 1.1, 0.8 and 0.5 respectively for vibration amplitudes of 0.17, 1.6, and 2.9 μm (Figure 5.3B).

Images of the fingertip were captured at 300 frames per second by a high-speed camera (Phantom Miro M110). Frustrated Total Internal Reflection (F.T.I.R) was used to highlight the asperities of the skin in intimate contact with the glass plate, while darkening everything that is not touching the plate [100]. This technique create highly contrasted images of the skin asperities at pixel resolution, that is 0.0535 mm. An illustration of the apparatus can be found Figure 5.3A and typical images for a high- and low-friction case are shown in Figure 5.3C.

The plate moved in the radial direction with a speed of 10 mm/s, for a total displacement of 20 mm, ensuring that the finger reaches a full slippage (Figure 5.3D). The normal force was maintained constant by a balance mechanism, and the lateral force was servo-controlled by a current-controlled coreless motor (Maxon RE 36) through a capstan transmission (Figure 5.3E).

The haptic surface is mounted onto an aluminum frame attached to a 6-axis force sensor (ATI Nano 43). Force data was synchronized to the images using a digital trigger also used to start the movement. The time-domain data were interpolated to match the time vector of the images. The force data were filtered using a zero-lag 50 Hz second order low-pass filter. The glass plate displacement was measured with an encoder attached to the shaft of the DC-motor.

5.2.2 Dataset of spatio-temporal skin deformation

The deformation of the skin was measured from the images of the contact illuminated by frustrated total internal reflection (FTIR). Contrast of the image was adjusted, and the contour was sharpened. 3000 optimal features were selected within a fitted ellipse of contact, extracted from the binarized image. The selected features were nearly equally spaced with a minimum spacing of 10 pixels, to be sure the entire population of features is equally distributed inside the ellipse of contact. Then, these features were tracked frame by frame with a sub-pixel accuracy. The relative displacement of each feature was obtained by subtracting its current position to the initial value found before the movement started. For good measure of plate displacement, a checkboard pattern was printed on the glass plate to get an external reference of the relative motion.

The strain fields were obtained via the same procedure as in [56]:

$$\epsilon_{xx} = \frac{\partial u}{\partial x} + 0.5 \left[\left(\frac{\partial u}{\partial x} \right)^2 + \left(\frac{\partial v}{\partial x} \right)^2 \right] \quad (5.1)$$

The longitudinal strain components ϵ_{xx} were computed from 0.05 to 6 mm every 0.2 mm of relative position between the finger and the plate during the slippage. Strains were then interpolated on a grid of size 76×101 .

To find the set of basis function that encodes incipient slippage, we collected the spatio-temporal evolution of the skin deformation when the participants' finger

touched the plate that slid from left to right. We captured the temporal evolution of the strain pattern of the index fingertip of 12 participants, using 7 levels of frictional conditions and 4 repetitions, resulting in 336 individual videos. We selected 30 frames of these videos, totaling in 10,080 data points. For each data point, the spatial strain field of the fingertip was matched to the safety margin S_m . First, the static friction limit f_t^* was identified from the lateral force time series by considering the average force when the finger was fully sliding. Then, the safety margin was computed for all instant in time from:

$$S_m(t) = \frac{f_t^* - f_t(t)}{f_t^*} \quad (5.2)$$

The data set of skin strains is represented by a $m \times n$ matrix, ϵ , where m is the number of spatial positions at which the strain is interpolated (7,676) and n is the number of recorded trials times the number of relative positions between the finger and the plate at which the strain is computed (10,080).

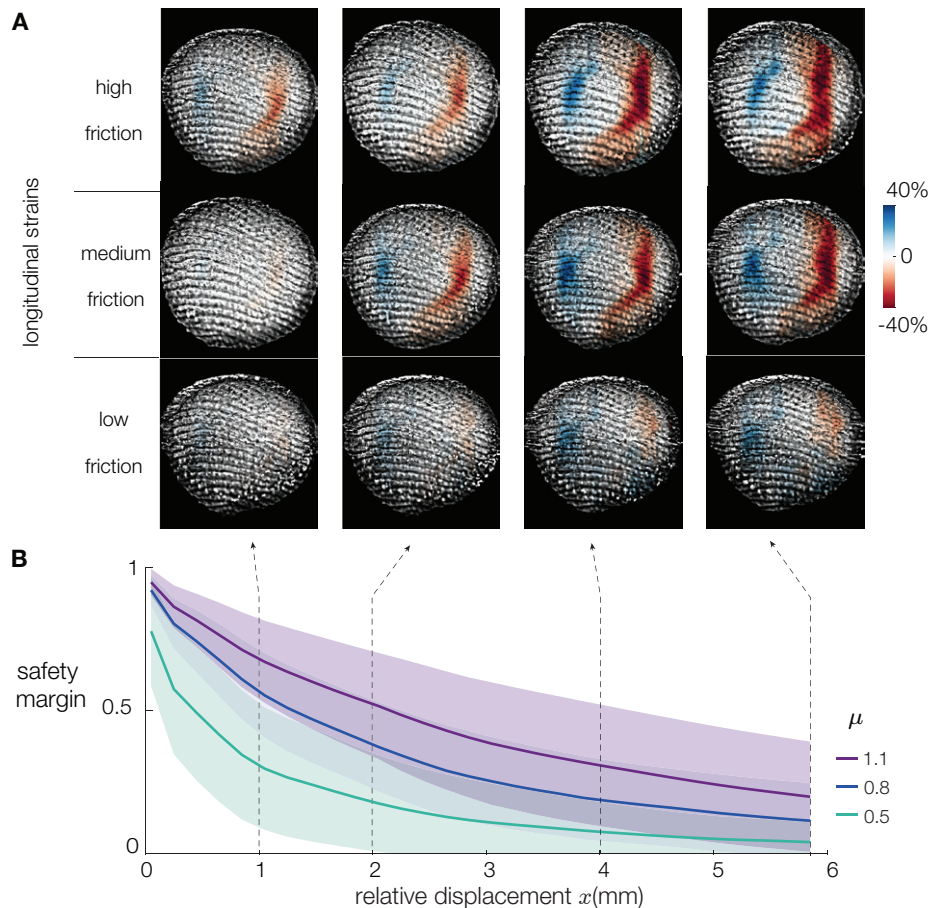


FIGURE 5.4: **A.** Experimental deformation of the skin when the finger is sliding on the surface in high, medium and low-friction conditions for relative displacements of 1, 2, 4 and 6 mm. **B.** Safety margin as a function of the finger position for the same 3 friction conditions. The solid lines and shadings stand for mean \pm std.

From the start of plate motion and until full slippage is reached, the finger experiences longitudinal strains, whose amplitude depends on the frictional strength of the contact as shown in Figure 5.4A.

5.3 Results

5.3.1 Empirical strain patterns

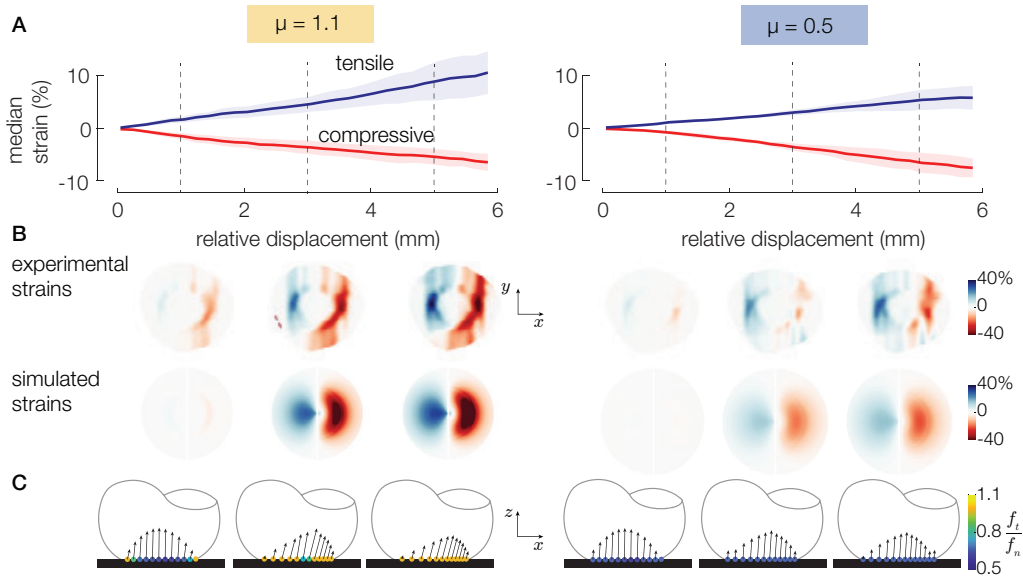


FIGURE 5.5: Typical trial. **A.** Compressive and tensile strains for 3 different friction conditions as a function of the relative position between the finger and the plate. The solid lines and the shadings represent the mean \pm std. **B.** Experimental and simulated strain profiles for the 2 different friction conditions at five positions on the plate from 1 to 5 mm. **C.** The corresponding simulated surface finger profile when $x = 2$ mm and 4 mm. The blue arrows represent the pressure and traction acting on each element, and the color of the dots represent the local force ratio $\frac{f_t}{f_n}$.

During the transition from stick to slip, the finger deforms and the strain field propagates from the periphery to the center of the contact area. The largest values of the strain are located at the periphery of the contact. The strain wave is always compressive ahead of the stuck area (red in figures) and tensile on the trailing edge (blue in figures) consistent with previous observations [56], see Figure 5.5B. For all friction conditions, as the plate displacement increases, the magnitude of the tensile and compressive longitudinal strains increases (Figure 5.5A). The magnitude of the compressive strain increases significantly with increasing vibration amplitudes (ANOVA, $F(6,329)=2.18$, $p = 0.045$), whereas the magnitude of the tensile strain decrease with increasing vibration amplitudes (ANOVA, $F(6,328)=6.3$, $p = 0.0091$), see Appendix B. For a high-friction condition, the maximum compressive strain experienced by the finger is on average 25% larger than when friction is low.

5.3.2 Model validation

To better understand the influence of friction on the skin deformation during sliding, we simulate the interaction using a finite-difference time-domain model capturing the viscoelasticity of the stratum corneum and soft cutaneous tissues as well as the local frictional behavior. The details of the implementation are presented in the chapter 3. The model is composed of a chain of massless elements linked by high-stiffness springs ($2.5 \text{ kN}\cdot\text{m}^{-1}$). The full chain lies on a bed of soft springs ($31.5 \text{ N}\cdot\text{m}^{-1}$) attached to a rigid element modeling the bone to which the external forces are applied. A normal force $f_n = 1 \text{ N}$ was first applied on the bone to compress the tissues. Once the static equilibrium is achieved, a tangential force $f_t = 1 \text{ N}$ is added on the bone. The resulting simulated strain profiles are shown in Figure 5.5B. The simulated strain fields follow a similar trend than the experimental ones, with a compressive part ahead of the stuck area and a dilatation behind it.

The fingertip model allows us to observe the pressure and traction fields at the interface between the skin and the surface that cannot be accessed by experimental means, see Figure 5.5C. During the transition from stick to slip, we observe that the elements on the outer edge are the first to slide, since the interaction pressure is collinear with the friction cone. In the high friction condition, the lateral motion of the elements is constrained, resulting in a larger skin strain. Conversely, in the low friction condition, the outside layer experiences lower tangential traction, and the lateral stress is released for smaller lateral displacement.

5.3.3 Dimensionality reduction

We postulate that the strain field must contain information about the safety margin before slippage. Since this estimate of the safety margin exists before gross sliding occurs, the estimate is likely independent of the actual friction coefficient of the surface. While we do not have access to the neural encoding of the afferent to find a base of neuronal activation, we can infer it from the skin displacement. Our dataset allows us to find a potential set of basis patterns expressed in terms of strain fields.

To find the *Eigenstrain* patterns, we performed a Singular Value Decomposition (SVD) of the 10,080 individual strain patterns contained in the dataset. The method outputs a set of orthogonal eigenvectors $u_i(x)$ representing the dictionary of strain patterns, and eigenvalues σ_i , whose magnitude relates to the variance explained. The weight of each Eigenstrain as a function of time is embedded in $v(t)$, such that each vector v_i reveals the temporal evolution of the i^{th} eigenvectors. To compress the information, we selected the first r elements of the set. The original evolution of the skin strain can be recovered by adding these eigenvectors, weighted by time-dependent vectors, $\alpha_i v_i(t)$ as follows.

$$\hat{\epsilon}(x, t) = \sum_{i=1}^r u_i(x) \alpha_i v_i(t) \quad (5.3)$$

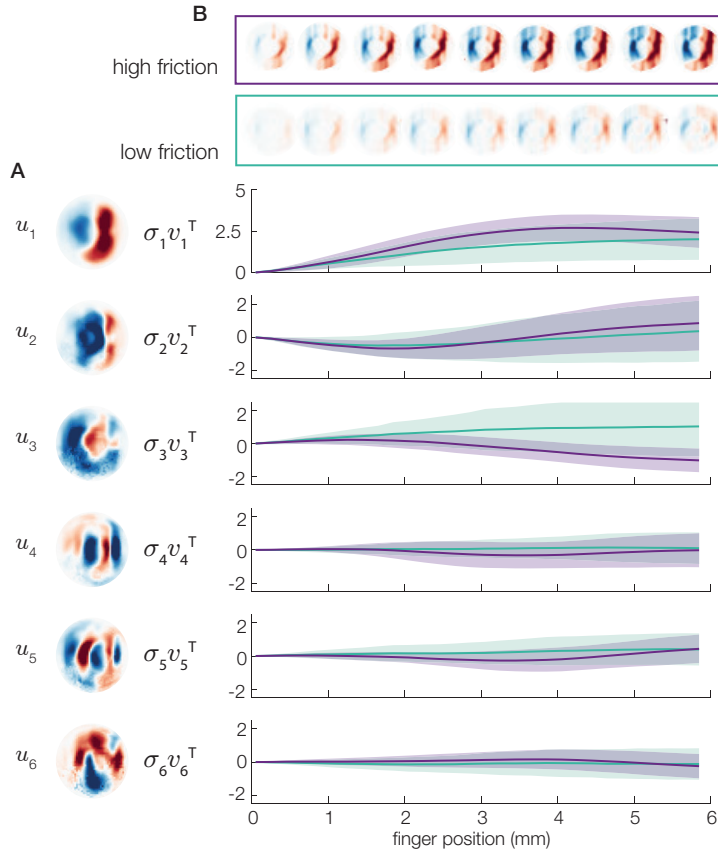


FIGURE 5.6: **A.** Six first bases u_i . **B.** Temporal evolution of the weights of the six bases for a low and a high-friction condition (in violet and green respectively).

The first six primitives are shown in Figure 5.6A. u_1 is the major principal component, illustrating the typical pattern of compression ahead of the stuck area and stretching behind it. u_2 and u_3 include higher frequency details at the periphery of the contact, whereas the following bases improve the details at the center of the contact area.

The figure 5.6B shows the recruitment of each basis $\alpha_i v_i^T$ as a function of time, for the high and low friction coefficients. The recruitment of the first basis differs between high and low friction conditions from the early stages of the slippage, when the finger has moved 0.25 mm relative to the plate (Spearman's correlation, $\rho = -0.17$, $p = 0.0024$). The amplitude of the first basis captures the intensity of the skin deformation. On the other hand, the recruitment of bases 2, 4, 5 and 6 are not significantly impacted by the level of friction. Similarly, the recruitment of the third basis changes significantly with friction when the relative displacement is higher than 1 mm (Spearman's correlation, $\rho = -0.21$, $p = 8.4 \times 10^{-5}$). $\alpha_2 v_2^T$ do not significantly differ between the friction conditions, suggesting that the friction does not significantly influence the tensile pattern embedded in u_2 .

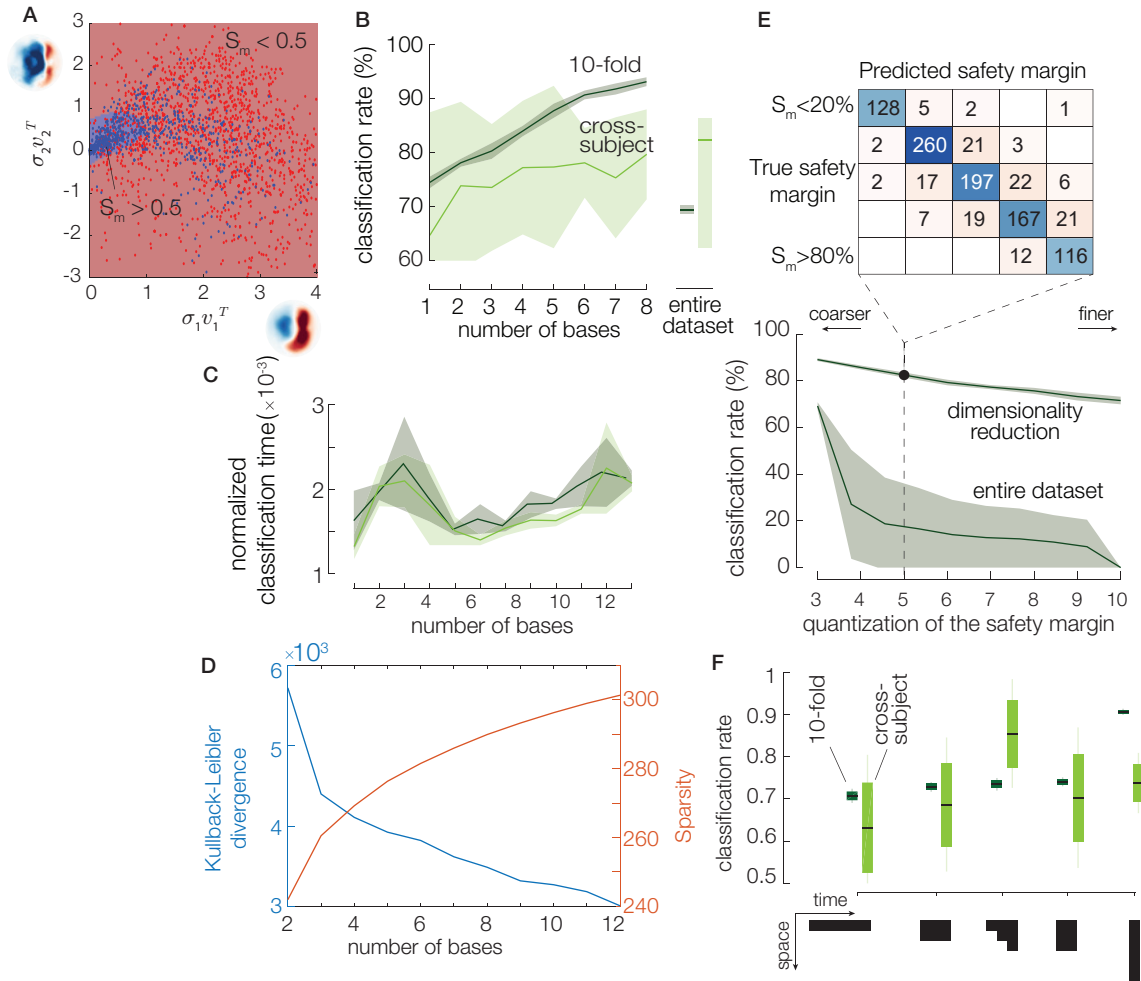


FIGURE 5.7: **A.** 2-dimensional mapping of 2 classes of the safety margin S_m (higher and lower than 0.5). **B.** Classification rate of the safety margin into 2 classes as a function of the number of bases. The dark green line corresponds to a ten-fold testing when taking 90% of the data for training and 10% for testing, and the light green line corresponds to a cross-subject testing when only one subject among 14 is used for testing. The solid lines and shaded areas stand for mean \pm std. Classification rates using the whole strain matrix ϵ are given inside the dotted box. **C.** Time needed for the classification using ΣV^T normalized by the time using the whole matrix of strains for the cross-subject and the 10-fold classifier. **D.** Kullback-Leibler divergence and sparsity of the V matrix for an increasing number of bases. **E.** Effect of safety margin quantization on the classification rate when using 6 bases for the decomposition. The confusion matrix is shown for 5 classes. **F.** Effect of time and space contributions to the classification rate from 6 temporal values to 6 spatial values (bases).

5.3.4 Tactile encoding efficiency of the safety margin

We trained two support-vector machine classifiers to predict the safety margin from the recruitment of the basis αv^T . The first one was trained using 90% of the whole dataset (10-fold) and the second one with data of the whole subjects, except one which was used for testing (cross-subject). The prediction map using the first two

bases with the 10-fold classifier is shown in figure 5.7A for 2 classes of safety margin: higher and lower than 0.5.

Compressing the tactile information with only 2 bases leads to a classification rate of 70%, whereas this number increases with the number of bases and exceeds 90% of accuracy for 6 bases (see Figure 5.7B). Adding more than 6 bases leads to marginal increase of the classification rates, and the performance of the 10-fold classifier drops when using the entire dataset. The classification rates for cross-subject classifiers are lower and present larger standard deviations than the one with a ten-fold training, due to the high inter-subject variability.

Since humans react in a remarkably short amount of time, we qualitatively compared the speed of each classification approach, by studying the influence of the number of bases on the computational effort. To get a qualitative estimate of the computational effort, we computed the time needed for the cross-subject and 10-fold classifiers to perform the prediction, normalized by the time of classification using the whole matrix of strains (Figure 5.7C). For both classifiers, the predictions using a limited number of bases are performed more than 600 times faster than using the entire strain data; the latter takes around 23 s. Moreover, the relative classification time between the limited number of bases and the entire strain matrix is minimum when considering only 6 bases. This minimum of computational effort suggests that the 6-bases kernel provides an efficient estimation, while preserving accuracy.

This value matches the tradeoff between precision and compactness of the bases. Kullback-Leibler divergence quantified the dissimilarity between $\epsilon(x, t)$ and $\hat{\epsilon}(x, t)$ as follows:

$$D_{KL}(\epsilon, \hat{\epsilon}) = \sum \left(\epsilon(x, t) \ln \frac{\epsilon(x, t)}{\hat{\epsilon}(x, t)} - \epsilon(x, t) + \hat{\epsilon}(x, t) \right) \quad (5.4)$$

A small value of divergence means that u_i accurately captures the information contained in the strain data in all conditions. Divergence decreases with the truncation rank r and plateau for $r = 9$ (Figure 5.7D), denoting that a higher number of bases leads to more accurate estimate of the strain fields. On the other hand, the number of bases that need to be activated, should also be restricted to promote compactness of the information. The compactness can be measured with the sparsity, expressed as the l_2 norm of the matrix V for each value of the rank r , as follows:

$$S(v) = \sqrt{\sum_i v_i^2} \quad (5.5)$$

A higher number of basis increases the complexity of the computation since the V matrix become sparser (Figure 5.7D). A sparse matrix may result in a spreading of the main information on many primitives, which will be hard to capture in few milliseconds. Overall, selecting less than 6 bases lacks of estimate accuracy, whereas considering more than 6 bases leads to a recruitment matrix V not compact enough, which is less efficient to process

To increase the accuracy of safety margin estimates, we reduced the interval

quantization of the safety margin by increasing the number of classes from 3 to 10 (Figure 5.7E). The classification rate using 6 bases decreases when the number of classes increases, but stays higher than 0.7 even when the safety margin was predicted with a 0.1-precision using 10 classes. Increasing the discretization of the safety margin comes with a significant tradeoff in the classification rate.

We also studied the influence of adding short-term memory to the classifier. We trained the classifier with knowledge of the short-term evolution of the recruitment of each basis. We find that the accuracy of the safety margin estimation using the 10-fold classifier trained with the contribution of the 6 bases at a given time instant was 20% higher than using the contribution of the first basis at 6 consecutive instants. However, adding priors on the weight of the first and second bases increases the accuracy of the cross-subject classifier by 10%, in comparison with exclusively spatial or exclusively temporal values (Figure 5.7F).

5.4 Discussion

The findings suggest the existence of a pre-neuronal compression of the tactile information of incipient slippage. The six strain primitives obtained with the singular value decomposition enable a reduction of the dimensionality of the tactile signal while keeping a sufficient accuracy of the predictions. We found a major contribution of the compressing strain in the encoding of friction, which has recently been shown to excite the response of fast adapting afferents of type 1 (FA-I) [57].

The first 6 bases were found to optimally encode the safety margin, leading to a 90% accuracy of the safety margin quantized over 2 classes. This estimation is reliable compared to the 76% accuracy obtained with a similar classifier for colon cancer detection [4]. When the safety margin was quantized with more than 7 classes this accuracy decreased to 85%. Globally, if the number of bases exceeds the number of classes, the classification rate obtained is higher than 80%. However, since the goal of the sensorimotor system is to react to an excessive reduction of the safety margin, a quantization with only two classes is a perfectly acceptable hypothesis.

The safety margin was estimated at specific time stamps, without taking the history of the deformation that led to a particular strain pattern. Taking dynamical effects into account could help improve the prediction of an impending slippage. Since the adjustment of the grip force is a continuous process, it is likely that the nervous system constantly monitors the time differences in strain to make a judgment. Assuming that the detection of slippage makes use of predictive coding, the evolution of the strain could be associated with priors on the weight and material property to lead to a robust classification [35].

The classification rate of the 10-fold classifier is 10% lower when the prediction is made with exclusively temporal evolution of the first base compared to purely

spatial one. Future investigations will include several scanning speeds to properly study the influence of the skin dynamics to the classification of the safety margin.

It is worth noting that the mechanics dictating the skin deformation is strongly influenced by the friction of the surface. Large friction coefficients lead to large compressive and tensile strain of the skin, in line with previous findings. The strain profiles observed when the finger is sliding on a friction-modulated glass plate matched with the previous one observed in the literature with a slip annulus forming at the periphery first [56, 1, 7]. The classifier successfully removes the dependence to friction, suggesting that the information of the safety margin is contained not in the magnitude of the strain, which is strongly influenced by friction, but in the relative recruitment of the different Eigenstrains.

In this study, the database is constituted with data acquired in constrained conditions when the plate is moving in the ulnar direction to mimic a slippage of an object due to gravity. Since it is known that the direction of the slippage has a significant influence on the strain experienced by the finger [56], future studies will take into account all directions along which the safety margin can be estimated. Another limitation is that the glass plate used for this experiment is perfectly flat, contrary to most of the objects manipulated in everyday life, which are textured and curved. To extend these results to the robotic field to control reactive grippers, the effect of material properties, curvature and texture must be investigated.

Interestingly, the optimal basis of strain pattern resembles a collection of Gabor filters, containing alternative patterns of compression and tension. While the first basis has only one cycle of alternating strains, the higher order pattern contains a higher frequency feature that captures finer details of the interaction. It has been hypothesized that a bank of Gabor filters is used to encode tactile features [delhaye2019rapid]. Our experiment only studied one direction of stimulation, which would follow that of gravity in a grasping task, but it is likely that different orientations might be encoded in the nervous system. These filters are central to the perception of movement in the visual system, and their presence in the tactile perceptual system suggests that their function is shared across modalities.

5.5 Conclusion

The corresponding temporal evolutions of the recruitment of each of the six bases, compactly represent the evolution of the strain field. By virtue of its compactness, this code simplifies and accelerates the decoding by the nervous system, which is needed to react in a timely manner while avoiding slippage of an object in hand. Even if the existence of this compact lexicon in the human nervous system still needs to be confirmed, the *Eigenstrain* decomposition can be directly used to design efficient control policies for robotic grippers that can manipulate object while preventing slippage [james2018slip, 137].

Chapter 6

Space-time fusion of discrete tactile events

Contents

6.1 Introduction	90
6.2 Viscoelastic model of the skin	91
6.2.1 Spatial stress distribution	91
6.2.2 Temporal attenuation of strain	92
6.3 Mechanical stresses and strains at the depth of the mechanoreceptors	92
6.3.1 Influence of friction on strains during a simple press	92
6.3.2 Evolution of strains during the transition from stick to slip	92
6.4 Tactile persistency	95
6.4.1 Spatio-temporal model	95
6.4.2 Materials and Methods	96
6.4.3 Results	96
6.5 Conclusion	98

Adapted from: Willemet, L., Cochelin, B. & Wiertelowski, M. (2019). Mind the spatiotemporal gap: Skin deformation limits our perception of discontinuous motion.

Preface to Chapter 6

IN the previous chapter, the strains experienced by the finger skin surface when interacting with objects with various friction coefficient was quantified via imaging methods. However, the mechanoreceptors, buried inside the skin layers are subjected to a filtered version of these strains since the skin is a viscoelastic medium acting as a mechanical filter. In this chapter, I expose a new model based on contact mechanics to quantify the sensitivity of the mechanoreceptors to the patterns of skin deformation highlighted in the first two chapters. This model also correlates with the perceptual thresholds that limit the resolution of both spatially distributed events, also known as the two-point threshold, and temporally distinct events, known as the gap-detection threshold. Thus, in the second section, I am interested in how these limits impact the perception of discrete moving stimuli that evolves both through time and space. We found that the spatiotemporal gap of stimulation can be masked, hinting at the potential role of skin mechanics in an *illusion of continuity*.

6.1 Introduction

Our ability to perceive dynamic simulations on our skin is essential for interacting with our environment. However, the sense of touch, like vision and audition, is not a perfect sensor. In vision, two stimuli sparsely spaced in space and time give us a persuasive impression of motion because the visual system blurs discrete images as a continuous moving scene [3]. The present study is interested in understanding whether similar behavior in touch is caused by the viscoelastic behavior of the skin that applies a spatio-temporal filter to the mechanical signal on the surface.

Touch is subject to finite spatial and temporal acuity. The spatial acuity depends on body location: two points threshold experiments report that two indentations of the skin spaced lower than 2 mm in the fingertip and 20 mm in the forearm can be felt as one [144]. Similarly, in time two successive stimuli can be felt as one if they are less than 30 ms apart, it is called the gap-detection threshold [169]. One hypothesis is that the mechanoreceptors, buried several millimeters deep in the tissues, receive a degraded image of the mechanical interaction that happens at the surface. This degradation is caused by the viscoelastic properties of the skin that diffuse and delay stimulation, therefore acting as a mechanical filter to surface pressure.

Considering this spatio-temporal filtering, Kitagawa et al. [121] have already proved that the illusion of continuity exists in the vibrotactile domain. Moreover, Cholewiak et al. [39] showed that the feeling of continuous motion depends on two parameters, the burst duration and the interburst interval. In this chapter, I propose

to study whether the spatio-temporal sensitivity of human is caused by the viscoelastic properties of their skin or not, with the help of a viscoelastic model.

6.2 Viscoelastic model of the skin

To estimate the stress inside the tissues, the skin can be modeled as a viscoelastic semi-infinite half plane [225]. In this context, the spatio-temporal stimulation at the surface is spatially filtered by continuum mechanics, which diffuses stresses $\sigma(x, t)$ deeper in the soft tissues, where the mechanoreceptors are located. These stresses change consequently the local strains, following a linear first-order viscoelastic relaxation, resulting in a temporal filtering of the original stimulation (Figure 6.1A,B).

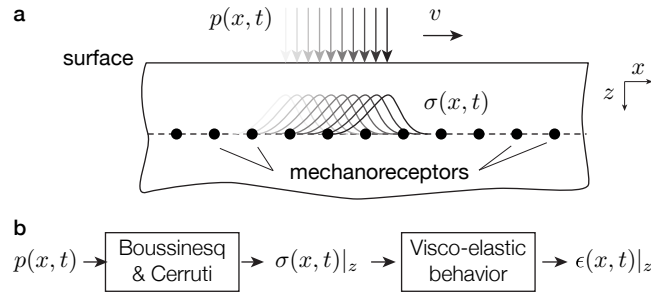


FIGURE 6.1: **A.** Infinite half-plane model of the skin. The stress deep in the skin is a filtered version of the stimulus applied on the surface. **B.** Computation steps of the strains deep in the skin

6.2.1 Spatial stress distribution

To compute the strain to which the mechanoreceptors are sensitive to [208], the model first calculates the stress using Boussinesq and Cerruti equation [108]. This model considers the skin as a semi-infinite homogeneous elastic medium on which a localized normal pressure $p(x, t)$ and tangential traction $q(x, t)$ are applied. The equation (6.1) leads to the shear and orthogonal normal stresses as a function of their position x and depth z as follows:

$$\begin{aligned}\sigma_x &= -\frac{2z}{\pi} \int_S \frac{p(s, t)(x-s)^2 ds}{((x-s)^2 + z^2)^2} - \frac{2}{\pi} \int_S \frac{q(s, t)(x-s)^3 ds}{((x-s)^2 + z^2)^2} \\ \sigma_z &= -\frac{2z^3}{\pi} \int_S \frac{p(s, t) ds}{((x-s)^2 + z^2)^2} - \frac{2z^2}{\pi} \int_S \frac{q(s, t)(x-s) ds}{((x-s)^2 + z^2)^2}\end{aligned}\quad (6.1)$$

If only a localized normal pressure P is applied on the skin, then the equations become:

$$\sigma_x = -\frac{2P}{\pi} \frac{x^2 z}{(x^2 + z^2)^2} \quad \text{and} \quad \sigma_z = -\frac{2P}{\pi} \frac{z^3}{(x^2 + z^2)^2}\quad (6.2)$$

These equations result in a blur of the pressure profile on the surface which diffuses the stresses on a larger area and removes the high spatial frequency content of the stimulation [226].

6.2.2 Temporal attenuation of strain

The stresses induce a deformation of the body which follows the viscoelastic Hooke's law. The compressive and shear strains ϵ can be expressed, in the Laplace domain, as a function of the local stresses:

$$\begin{bmatrix} \mathcal{L}(\epsilon_x) \\ \mathcal{L}(\epsilon_z) \end{bmatrix} = \frac{1}{E^*} \begin{bmatrix} 1 & -\nu \\ -\nu & 1 \end{bmatrix} \begin{bmatrix} \mathcal{L}(\sigma_x) \\ \mathcal{L}(\sigma_z) \end{bmatrix} \quad (6.3)$$

where \mathcal{L} is the Laplace transform, ν is the Poisson's coefficient and $E^* = E + s\eta$ is the complex Young modulus of the skin layers, with $E = 1.1$ MPa the elastic modulus and η is the viscosity of the skin and s the Laplace operator. Time variation of the strain is computed numerically using a 4th-order Runge-Kutta solver. The viscoelastic behavior leads to a low-pass filtering of the surface pressure with a cut-off frequency set to $E/\eta = 100$ Hz.

6.3 Mechanical stresses and strains at the depth of the mechanoreceptors

6.3.1 Influence of friction on strains during a simple press

The pressure and traction applied on the skin surface during a simple press on a high and a low friction surface were computed with the mechanical model detailed in 3 and plotted in Figure 6.2A,B. The stress profile deep in the skin tissue are shown in Figure 6.2C. Thus, the mechanoreceptors located 2 mm under the skin surface will be subjected to a resulting stress 20% higher in the high-friction than in the low-friction case (Figure 6.2D).

The tangential strains 2 mm below the skin surface are plotted in Figure 6.2E and Figure 6.2F shows the time evolution of the total strain at the interface, which is 20% higher in the high-friction case. This 20% difference between a high and a low friction case is in the same order of magnitude of the just-noticeable difference typical for the somatosensory system, suggesting that signalling differences between two frictional conditions is possible.

6.3.2 Evolution of strains during the transition from stick to slip

The same mechanical model was used to compute the stress the skin is subjected to when sliding on a high- and a low-friction surface (Figure 6.3A). Pressure and traction distribution on the skin surface (Figure 6.3B) creates a stress diffusion deep in the skin layers (Figure 6.3C), due to Boussinesq & Cerruti model. The stress

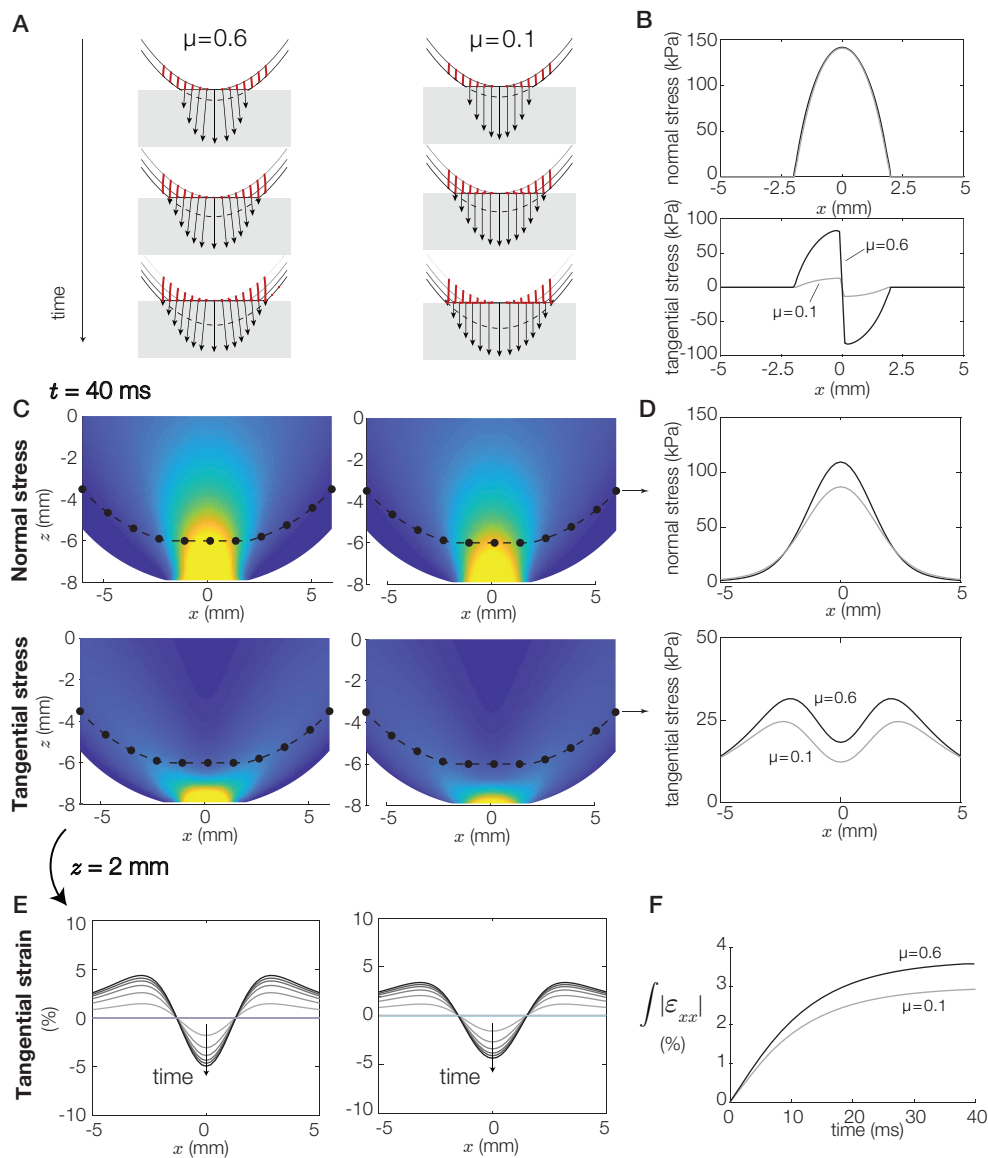


FIGURE 6.2: Influence of friction on in-depth strains during a simple press. **A.** Evolution of interfacial pressure and skin deformation. **B.** Normal and tangential stresses for a high- and a low-friction condition. **C.** Spatial stress distribution inside the finger skin. The black dots correspond to the position of the mechanoreceptors, separated by 1.2 mm and 2 mm below the skin surface. **D.** Normal and tangential stresses at the mechanoreceptors' depth. **E.** Temporal attenuation of the strains 2 mm below the skin surface. We can see a dilatation of the central part and a compression aside. **F.** The internal layer of the skin is almost 20% more compressed in the high-friction case.

profiles 2 mm below the skin surface are highly asymmetric especially for the high-friction condition.

The tangential strains 2 mm below the skin surface show a maximal compression of 30% in the center of the contact area and a dilatation of the skin on both sides of the contact area (Figure 6.3E). The time evolution of the total strain at the interface is 18% higher in the high-friction case than in the low one (Figure 6.2F).

Recent findings showed that slippage could be detected on a perfectly flat surface, if the compressive strain of skin surface is larger than 25% [13, 56]. We can now affirm that it corresponds to a threshold of 15% at the depth of the mechanoreceptors.

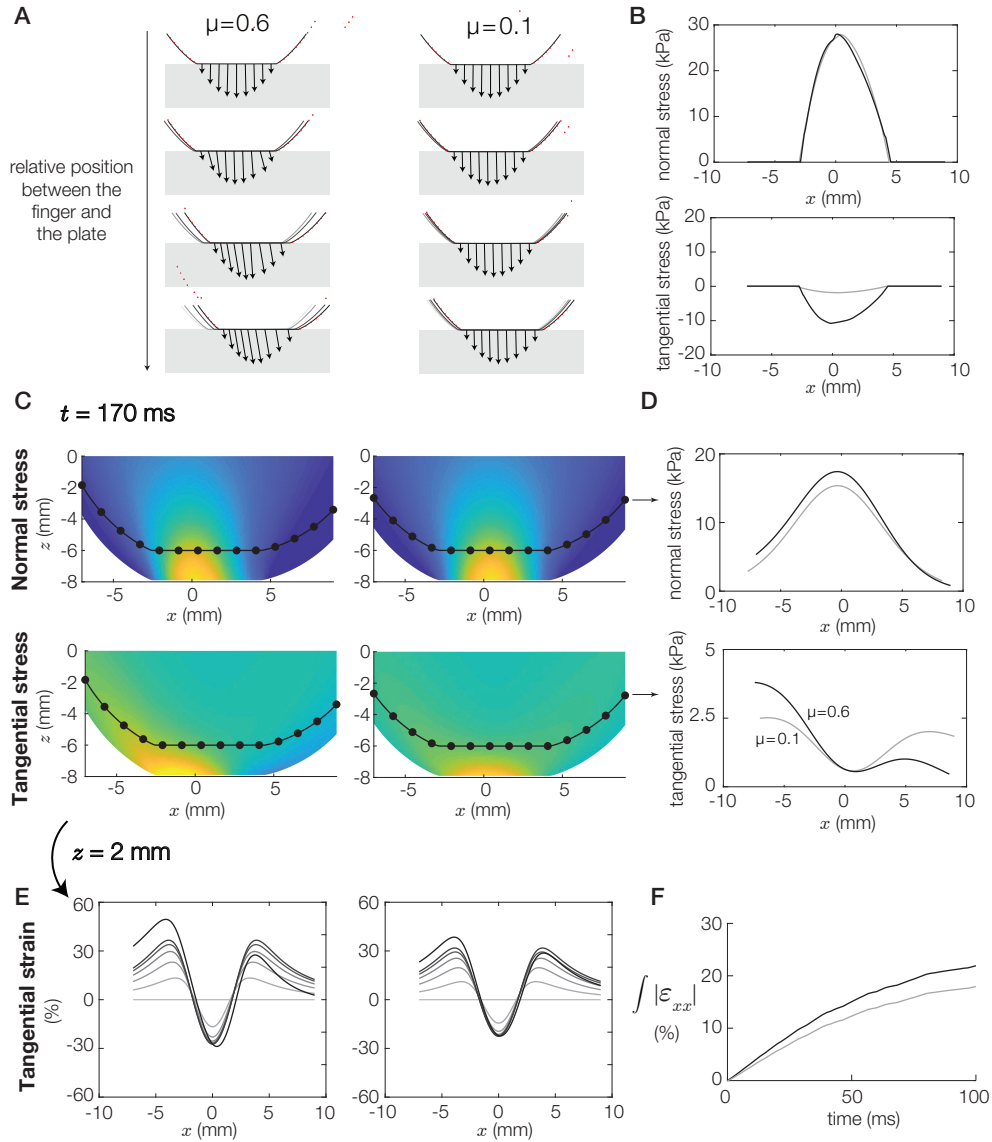


FIGURE 6.3: Influence of friction on in-depth strains during sliding. **A.** Evolution of interfacial pressure and skin deformation. **B.** Normal and tangential stresses for a high- and a low-friction condition. **C.** Spatial stress distribution inside the finger skin. The black dots correspond to the position of the mechanoreceptors, separated by 1.2 mm and 2 mm below the skin surface. **D.** Normal and tangential stresses at the mechanoreceptors' depth. **E.** Temporal attenuation of the strains 2 mm below the skin surface. We can see a dilatation of the central part and a compression aside. **F.** The internal layer of the skin is almost 20% more compressed in the high-friction case.

6.4 Tactile persistency

In the previous section, we show that partial slippages can be detected on a flat surface due to a compressive strain of 15% at the depth of the mechanoreceptors. However, it was long hypothesized that the relative motion between the skin and an object is mediated by micro-vibrations produced by dynamic events such as micro-slippage. This hypothesis was formed because it was observed that the relative motion could escape detection if the surface was atomically smooth [207]. Thus, this viscoelastic model of the skin can serve to study how a moving signal on the surface triggers the mechanoreceptors buried inside the skin layers.

6.4.1 Spatio-temporal model

The spatio-temporal model presented in 6.2, embodies two main characteristics of skin mechanics that could explain perceptual confounds. First, the spatial filtering provides a lower limit on the resolution of individual tactile stimulation, which could be the cause of the two-points threshold [208]. Second, the temporal filtering is also likely to impede discrimination between two successive impulses at the same location.

In realistic conditions, such as an object moving on the surface of the skin, the stimulus evolves spatially and temporally. If the velocity of the moving stimulus is constant then, a discontinuity will induce impulsive pressure on the surface, which are both separated in space and time. The resulting strain in the soft tissues, 2 mm deep in the skin will be a filtered version similar to Figure 6.4.

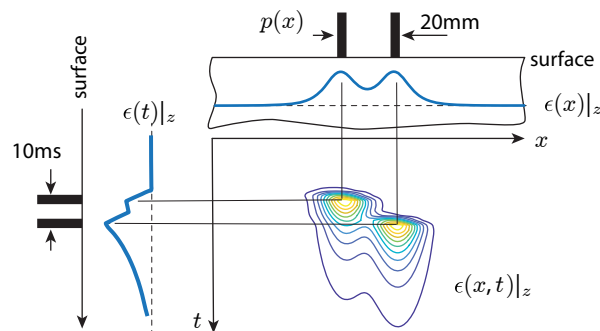


FIGURE 6.4: Spatio-temporal representation of the normal strains applied on the surface (black bars) and 2 mm deep in the skin (blue lines and contour plots)

This filtered version of the 2 impulses looks like two blurred signals in space and time, but it is not clear whether the central nervous system is able to discriminate between these two, given a spatial density of the mechanoreceptors. Indeed, they can be induced by two discrete stimuli or a larger and longer one with one missing point. Future work will focus on computing the probability of both scenarios using for example a Wiener deconvolution since the characteristics of the filter are known. Anyway, the results of the simulation would like us to think that humans have a

tactile illusion of persistency, where 2 discrete stimuli can be felt as one continuous stimulus. In the next section, this illusion will be tested experimentally on human subjects.

6.4.2 Materials and Methods

Procedure

This experiment was achieved on subjects' forearm, due to its size. Although the forearm and the finger skin have different dynamic parameters, both viscoelastic. Thus, similarly to the finger, the forearm skin is filtering a stimulus on the surface both spatially and temporally due to its viscoelasticity.

The experiment starts with the participant's spatial and temporal acuity measurements. The spatial acuity was defined as the two-points threshold, which is the smallest spacing between 2 points that can be identified as two by the subject (Figure 6.5A); and the temporal acuity was computed using a speaker which was activated twice separated by a short glance (Figure 6.5B). To estimate the thresholds of each subject, we used a MoBS (Modified Binary Search) technique, an adaptive procedure allowing a rapid convergence to the actual threshold.

Stimuli

Discrete spatio-temporal stimuli were provided via a wheel rolling without slippage on the skin (Figure 6.5C). The wheels were imprinted with a square-wave pattern which duty cycle (ratio between the size of the tooth and the spatial period) could be changed (Figure 6.5D). The wheels were driven by a servo-controlled DC-motor (Faulhaber 2657W012CXR-275) on a linear rail and maintained at a constant normal force via a low-stiffness suspension. Participants were presented with six 50 mm-diameter wheels with a fixed tooth length and variable gap. The duty cycles of these wheels vary from 50% to 90% based on preliminary investigations, which corresponds to a range of spatial periods between 11.8 mm and 22.3 mm.

A 2-Alternative Forced Choice procedure was chosen for the psychophysical experiment. A random series of paired stimuli (one patterned and one smooth wheel) was presented to the participant's forearm. In each trial, subjects had to report which wheel was the smooth one and his/her answers were saved. Three different linear speeds were tested for each wheel: 5 cm/s, 10 cm/s and 20 cm/s. The setup is shown in Figure 6.5C and the stimuli presented in Figure 6.5D.

6.4.3 Results

Spatial and temporal acuity measurements

The spatial acuity measurement varies across participants with values ranging from 5.8 ± 3.9 mm. These values are lower than the expected two-points threshold on the

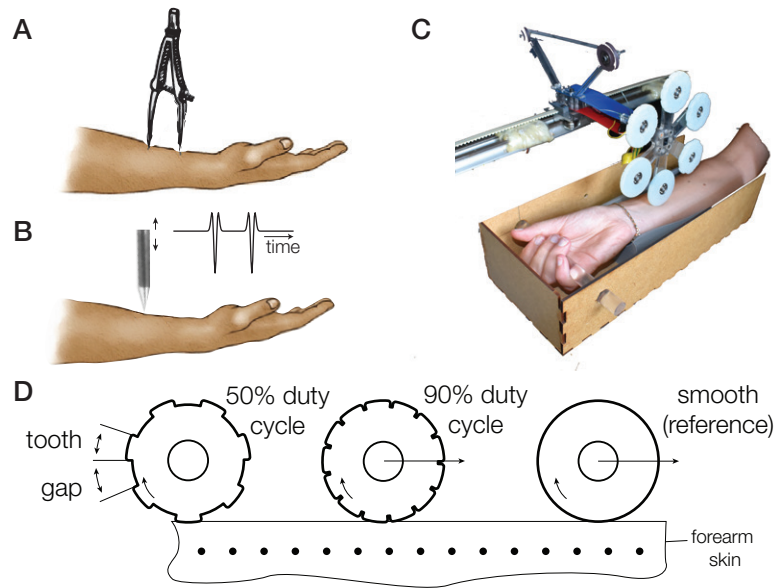


FIGURE 6.5: **A.** Spatial acuity measurement. **B.** Temporal acuity measurement with the speaker. **C.** Photography of the experimental setup with wheels. **D.** Schematics of the presented stimuli. Trajectories follow a no-slip condition.

forearm (20 mm) and this is partly due to the fact that we used our custom-made apparatus with sharp pins. The temporal acuity measurement is also variable across subjects with values ranging from 44 ± 29 ms.

Psychophysical experiment

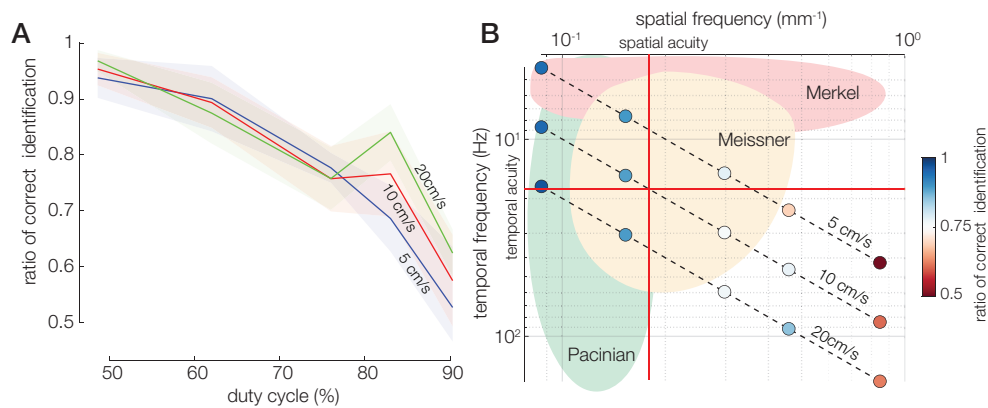


FIGURE 6.6: **A.** Psychometric curve on eight subjects for the 3 speeds. The solid lines plot the mean and the color shadings represent the standard deviation computed with a bootstrap method. **B.** Correct identification ratio in the space-time domain. The color gives the correct identification ratio, with blue corresponding to a ratio above 75%. The red lines plot the spatial and temporal acuity measurements.

The results of eight participants are presented in Figure 6.6A. The percentage of correct identification of the smooth wheel decreases with increasing duty cycles, for all three speeds. At the lowest duty cycle, the mean ratio of correct identification for

all subjects and speeds is approximately 90% and at the highest duty cycle, the subjects made correct identification in 60% of cases in average. According to the method of constant stimuli, this study suggests that the limit of the spatio-temporal acuity could be located around 75% of duty cycle, which translate to a gap of 3.3 mm. The effect of speed on the ratio of correct identification is present only for duty cycle higher than 75%. Before this threshold, the proportion of correct answer is slightly higher for the lowest speed. However, above this threshold, participants have a better chance to identify the smooth wheel correctly when the highest speed is presented, shining light to a contribution to the mechanoreceptors sensitive to higher temporal frequency. Figure 6.6B maps the ratio of correct identification in the spatio-temporal space (with logarithmic scales). Red dots code for low percentage when blue dots code for higher score. The spatio-temporal sensitivity of skin mechanoreceptors are highlighted by the 3 colored zones. On this figure, we can see that the zone when the spatial frequency is lower than the mean of the spatial acuity and the temporal frequency lower than the mean of the temporal acuity elicits more than 75% of correct identification. Furthermore, there is one point outside this zone where the ratio of correct identification is higher than 75%, but the temporal frequency is higher than the temporal acuity limit. Our hypothesis is that the frequency of this stimulus might turn on the Pacinian Corpuscles, which might help to distinguish the discontinuity.

6.5 Conclusion

The study conducted extends the notion of two points threshold to discontinuous mechanical events that evolve both in time and space. All in all, the results are consistent with the hypothesis that the viscoelastic behavior of the skin acts as a filter that blurs the mechanical stimulation on the surface. While this study focused on square-wave signals displayed on the forearm, the approach can be extended to richer spatio-temporal signals and to different body parts.

Chapter 7

Conclusion

Contents

7.1 Summary of the contributions	99
7.2 Applications to robotics	100
7.3 Future directions	100

IN this thesis, I strived to understand how the skin deforms when interacting with objects to extract tactile invariants as friction. This chapter first summarizes the main contributions and discuss in a second time the implications of the results and potential research leads.

7.1 Summary of the contributions

Everyday tasks involve a fine manipulation driven by the friction between the fingertip and the object in contact. The applied grip force should be strong enough to avoid a catastrophic loss of grip, yet gentle enough so that the object is not squeezed in our hands. For example, when removing the stem of a cherry, the tangential force is increasing gradually at the interface. However, we are able to control our grip force in real time so that the cherry does not slip away, yet it is not getting squeezed. This grip adjustment is as much swift as precise since the safety margin is maintained between 10 and 20% in less than 200 ms.

The first contribution of this thesis is the development of a mechanical model of the finger skin (see chapter 3). This model is able to predict the frictional dynamics of the interaction with an object and, thus, can be used as a strong predictor of the stress experienced by our mechanoreceptors buried deep inside the skin layers.

In chapter 4, I showed that humans are able to gauge the slipperiness of a surface at the very beginning of the contact, before any tangential force is observed so before any shear deformation of the skin occurs. This astonishing ability emerges from a specific pattern of deformation, appearing as an outward skin expansion. I found that the amplitude of this pattern is correlated with friction at the interface.

The regulation of grip forces starts at the very beginning of contact, and continues during the transport and release of the object. During the subsequent phases, the deformation of the skin following partial slips contains important cues that are used to quickly react to potential slippage by adjusting the grip force in real time. But the pattern of deformation depends dramatically on the coefficient of friction of the surface. Given the widely different signals, how can the nervous system decode slippage? In chapter 5, I present a novel method to quantify the margin from total slippage from the skin deformation during incipient slippage. This method, based on dimensionality reduction, has been proven to correctly estimate the safety margin with an 85% accuracy, regardless of the level of friction.

Finally, in chapter 6, we looked at the sensitivity of the mechanoreceptors to these skin strain patterns. Since they are located deep in the skin layers, the mechanical stress they are subjected to is less important due to the skin acting as a high-frequency filter. With the help of a parsimonious model, we discovered a tactile illusion of persistency, producing a perception of continuous motion when not.

7.2 Applications to robotics

In this thesis, I was mainly focused on human tactile perception. However, I had the chance to collaborate with roboticists to initiate the importance of studying how a soft material is deforming to distill tactile attributes (friction, edges, shapes...) when interacting with objects. The first results we obtained so far were about curvature perception with a tactile sensor developed in my lab, called ChromaTouch, based on color-mixing principle [137]. It has been demonstrated that a stable grasp depends on local curvature [97]. Indeed, when holding an object, we generally try to find the most concave part in order to lift it efficiently. With ChromaTouch, we presented a method to estimate the local curvature after a millimeter-size indentation from the sensor deformation and Hertz contact theory [138, 187] (Figure 7.1).

We can imagine robots that, in a near future, can adjust their grasping force according to the frictional strength earlier, using this divergent pattern of deformation highlighted in chapter 4. Also, the dimensionality reduction method presented in chapter 5 could help in turn to control prosthesis or robotic grippers for soft objects manipulation as fruits or biological materials, by providing *gentle touch* to robots.

7.3 Future directions

This thesis contributes largely to the neuroscience field by highlighting the mechanisms responsible for an early and precise adjustment of the grip force. The findings can improve haptic human-machine interaction and can inform the design of advanced tactile sensors for robotics or prosthetics. The multidisciplinary

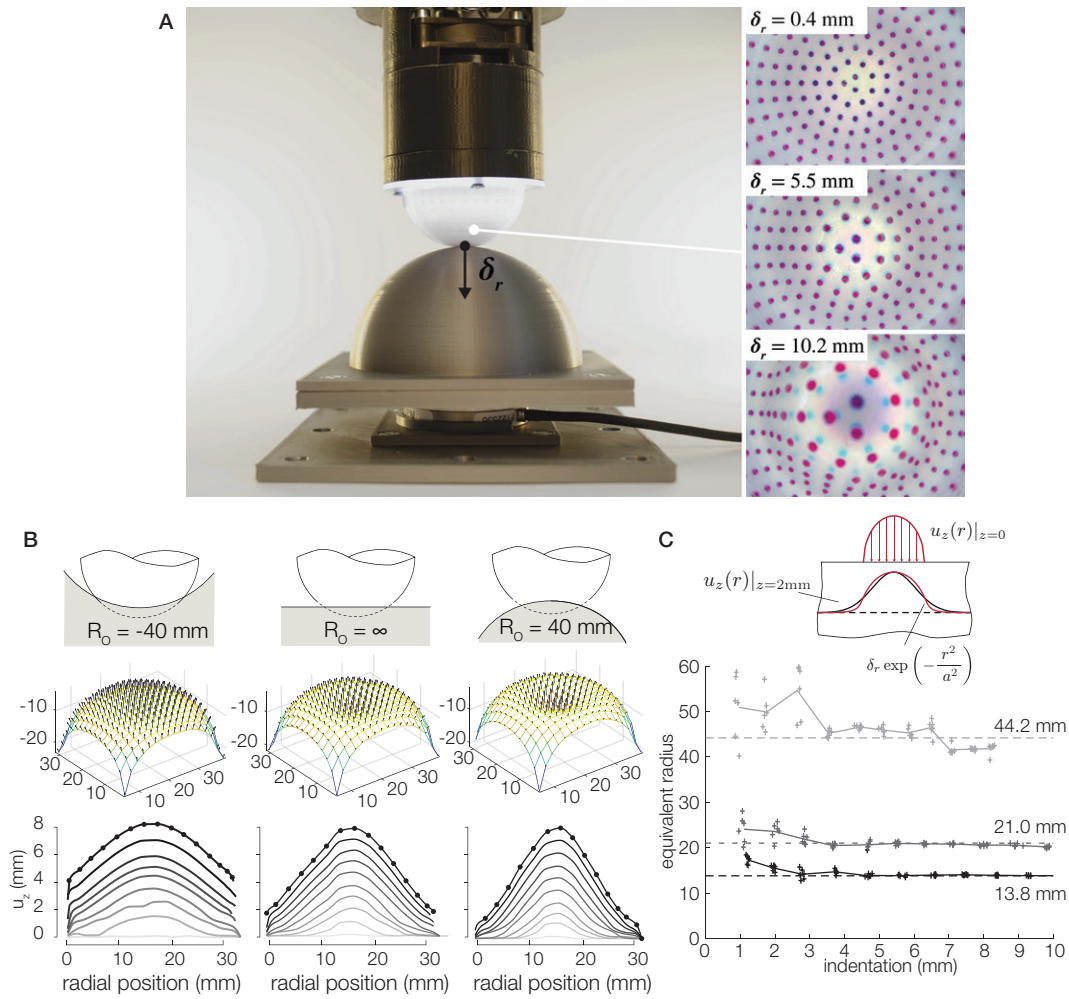


FIGURE 7.1: **A.** The 3D-printed ChromaTouch tactile sensor. Normal and lateral forces are transduced into changes in hue, centroid and apparent size of the markers. **B.** Profile of the sensor deformation (top) and displacement of the central cross-section of the sensor (bottom). **C.** Results of the curvature estimation for an increasing normal indentation.

involved in this thesis and the promising nature of the results suggests several avenues for further investigation.

How to measure the frictional strength of a contact? In Chapter 5, the dynamic friction coefficient between the skin and the glass plate was quantified by the ratio of the tangential and the normal force when the finger was steadily sliding over the plate. But even when no tangential force is exerted, the frictional strength is present, since the intimate contact holds a potential for adhesion. In Chapter 4, this frictional strength were measured by counting the number of skin asperities which are in intimate contact with plate. However, optical methods can be bulky and computationally expensive in terms of processing.

During my thesis, we developed a new method based on the principle of absorption and reflection of acoustic waves to estimate the frictional strength of a contact on glass plates [100]. When using an ultrasonic friction reduction device, a

portion of the acoustic energy is transferred to the fingertip while the number of junctions between the skin and the glass plate is reducing. Thus, the ultrasonic impedance can be used to provide a measure of the real contact area and hence, the frictional strength of the contact from a calibration value. Because of its low computational effort, this method is suited for controlling friction on the surface haptic devices or estimating friction on robotic grippers.

Nonetheless, the method has not been applied yet to others materials, especially soft ones. Therefore, more work is needed to develop a reliable method in those conditions.

How sensitive are the mechanoreceptors to the stimuli elicited by different friction coefficient presented in this thesis? This thesis quantified the strain differences of the finger skin surface when in contact with various friction surfaces. A model had been developed to approximate the strains the mechanoreceptors, 2 mm below the skin surface, are subjected to. Nonetheless, how the central nervous system is extracting the friction attribute from those deformation patterns still need to be clarified. Microneurography is a recent method, developed in the late 1960s, to visualize the impulses conducted in the peripheral nerves. The principal advantage of this method is that the subject is awake and able to cooperate and perform voluntary actions. Thus, microneurography will be a powerful tool in the near future to describe the huge quantity of sensory signals sent during a grasping task.

How friction influences the grip force regulation on initial contact and after a perturbation?

The results on tactile perception of friction and estimation of the safety margin highlighted in this thesis, have for aim a better understanding of the astonishing grip force regulation in humans. The work achieved in this thesis was based on two previous studies: On one hand, Johansson et al. [107] showed that participants might be regulating their grip force according to textures, a correlate of friction, and on the other hand, Cadoret et al. [30] shows that friction, not textures, are influencing the regulation of the grip force. However, in the latter the friction conditions were not randomized, making them predictable by the participants. To the best of our knowledge, the influence of friction on grip force regulation from the initial contact has not been studied yet.

Future work will focus on mounting ultrasonic glass plates on a manipulandum similar to the one developed by Johansson, to replicate his experiment

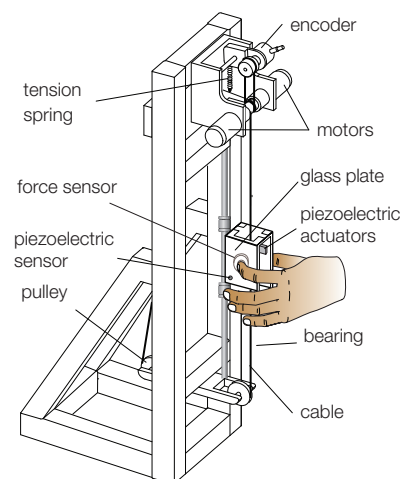


FIGURE 7.2: Manipulandum equipped with friction reduction glass plate to study grip force reactions to load force and friction perturbation

with changes of friction coefficient instead of textures. A schematic of this device is presented on Figure 7.2. This device can also be used to highlight the safety margin humans are applying. Furthermore, it will help to understand how fast and accurate is our reaction to a load force or friction perturbation.

Can we prevent a slippage before it occurs? In this thesis, we mainly focus on the grip force adaptation to sensory feedback signals relevant to object properties (as friction) or to mechanical events (as slippage). Previous study shows that when passively exploring stimuli, participants performed at chance level in a friction discrimination task [118], whereas in the chapter 4, active exploration procedure results in a more successful discrimination. In the active case, we are able to predict the dynamic of gross deformation of our own actions to isolate sensory features as the diverging deformation pattern. Whereas in the passive case, the nervous system while trying to disentangle features of the global indentation of the skin and subtle effects of friction might have to deal with too many permutations to rely on frictional cues. This early predictive behavior was also observed in the case of transient perturbations, as in catch trials [23]. In this case, the short duration of load force increase does not allow a reactive correction to ensure a stable grasp, therefore, the strategy must be predictive with a preparatory grip force prior to the perturbation and an increase of the grip force after the perturbation [233]. Those feedforward mechanisms in motor commands are responsible for this anticipatory responses to prevent a slippage.

Can a specific skin deformation drive actual tactile perception on fingertip? Bicchi et al. [19] have shown that softness perception is correlated with the rate of growth of the contact surface. In chapter 4, we also highlighted a correlation between the friction perception and the outward pattern of skin deformation. Correlation between skin deformation and perception has already been proven, but the causation still cannot be deduced. Previous study has already shown that it is possible to create a stiffness illusion with skin stretch [71]. A future experiment will focus on driving particular patterns of skin deformation and studying what the participants are feeling. For example, applying a diverging pattern of deformation to the skin can make the material in contact appear softer or more compliant to the touch.

How do we perceive the world? Perception is defined by the ability to see, hear, or become aware of something through our senses. The mechanisms underlying our senses have triggered our curiosity for thousands of years. However, research on touch is still in its infancy compared to visual and auditory perception. In 1944, Joseph Erlanger and Herbert Gasser put their hands on the mechanisms of tactile perception, and received the Nobel Prize of Physiology or Medicine for their discovery of different types of sensory nerve fibers that react to painful and non-painful touch. But yet, 77 years after, how the nervous system senses and interprets our environment is still containing unsolved questions. One month ago, David Julius and Ardem Patapoutian have been rewarded by the Nobel Prize again

for their work on the mechanisms converting temperature and mechanical stimuli into electrical impulses in the nervous system.

Nonetheless, it was for long hypothesized that the brain extracted knowledge from sensations. The 21st century witnessed an inversion with the theory of *predictive coding* [180]. According to this theory, the brain is actively constructing explanations for each external sensation. Hence, perception is a process of inference in which the brain interprets noisy sensory signals with respect to some *prior beliefs* or *expectations*. Predictive coding speculates that the brain is processing the

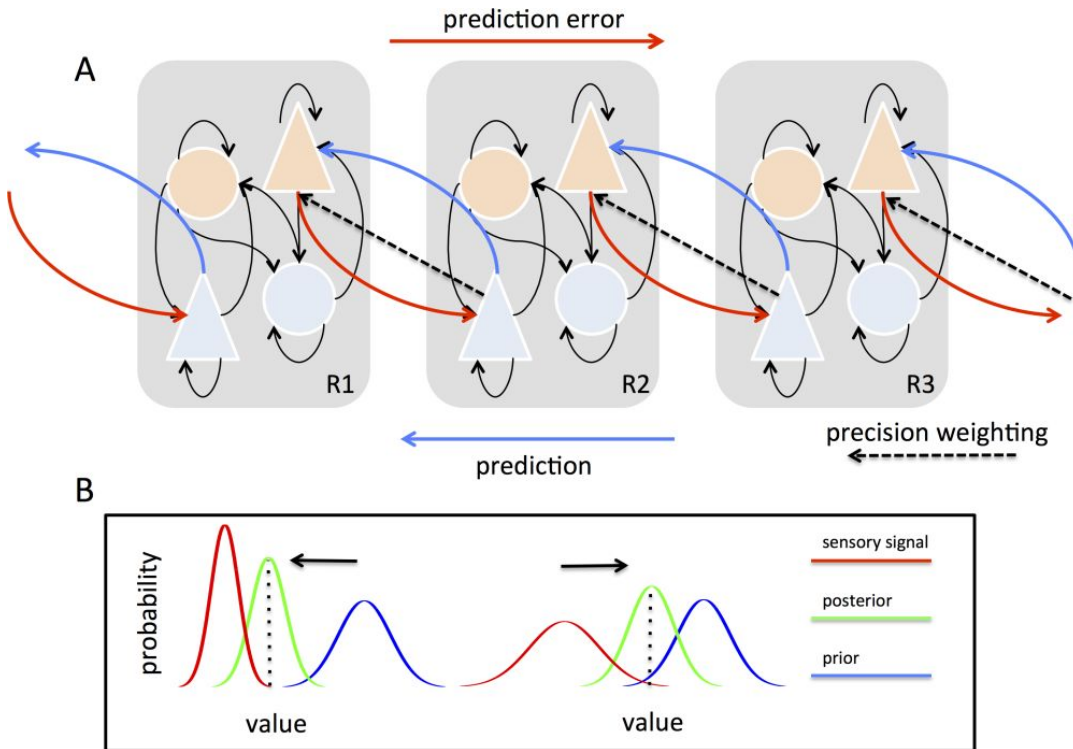


FIGURE 7.3: **A.** Hierarchical predictive coding. R1, R2 and R3 are three cortical regions from the lowest to the highest. Bottom-up projections (red) originate from “error units” (orange) in superficial cortical layers and terminate on “state units” (light blue) in the deep layers; while top-down projections (dark blue) convey predictions originating in deep layers and project to the superficial layers. Prediction errors are associated with precisions, which determine the relative influence of bottom-up and top-down signal flow via precision weighting (dashed lines). **B.** Probability distributions over the value of a sensory signal (x-axis). On the left, high precision-weighting of sensory signals (red) enhances their influence on the posterior (green) as compared to the prior (blue). On the right, low sensory precision weighting has the opposite effect. (from [195])

information using top-down or inside-out connections that convey predictions from high to lower levels of the brain, back out to the sensory surfaces. In Figure 7.3A, blue arrows convey the brain’s predictions about the causes of sensory signals. The prediction error (i.e. the difference between what the brain expects and what it gets at each level of description) should be minimized at each levels of the

hierarchy. Perception is becoming a form of best guessing: sensory signals and prior belief can be represented as probability distributions (Figure 7.3B), and perception is the optimal combination of both. Predictive coding offers a new way of thinking to understand how the central nervous system is interpreting the environment.

Are we in touch with the reality? Touch, as all senses, is subjected to illusions, and we can experience a discrepancy between perception and reality (see Figure 2.12 in chapter 2). In chapter 6, a new illusion of tactile persistency was highlighted, whereby a discontinuous stimulus can be felt as continuous when the spatio-temporal frequency is high. All of these illusions question about whether we can trust our feelings. Illusions aren't necessarily a bad thing, but a sign that your brain can handle confusing situations well. But be aware, "touching *is not* believing" and your sense are not always telling you the truth!

Appendix **A**

Additional results of the friction perception experiment

A.1 Motivations

This appendix presents some additional results about the friction perception experiment. Notably, the first section shows how the other components of skin strain and the strain energy evolve along the trial and according to the friction condition. The second section pictures the individual performance against the friction discrimination task and highlight two groups of skin properties.

A.2 Strain components

We found a strong linear correlation between the median longitudinal strains and the divergence (Pearson's coefficient = 0.77) (Fig.A.1G).

Strain energy densities are shown for a typical trial in Fig. A.2A. The median strain energy rates for each vibration amplitude are plotted in Fig. A.2C. These rates peak at 1.2 ± 0.2 mJ/s when the normal force reaches 0.4 ± 0.1 N. The linear correlation between total strain energy and divergence is plotted in Fig. A.2D. Its slope varies from one participant to another (slope = 3.6 ± 2.3 mJ) because the Young's modulus we chose for this calculation does not fit for every participant of the study.

A.3 Individual performance

The median of all divergence difference between reference and comparison was computed for each participant. Since the distribution is bimodal (see Fig.A.3A) we divided the population of subjects into two groups. The first group contains the participants with small medians of divergences and therefore stiffer skins. The second group shows higher divergences, physically meaning larger deformations.

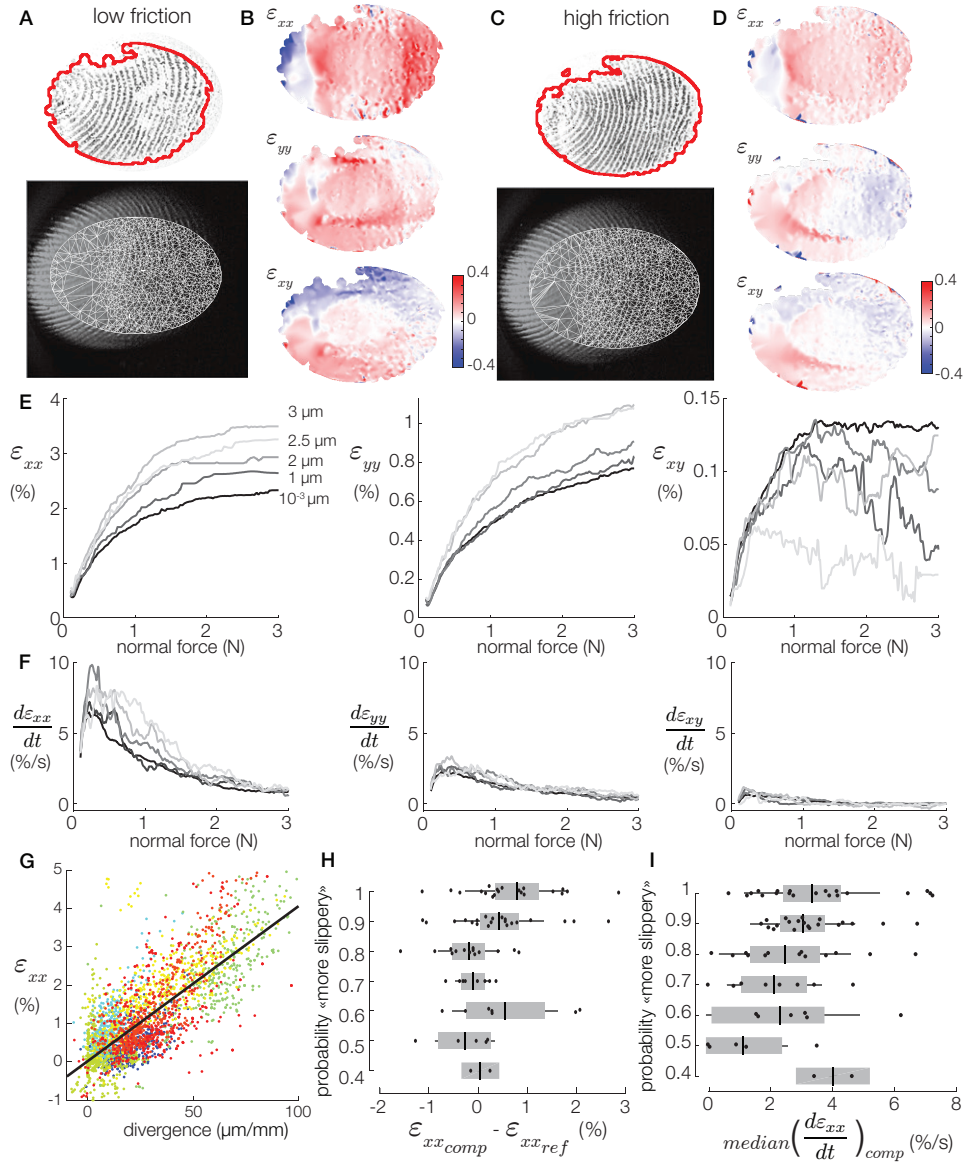


FIGURE A.1: Raw contact image and fingerprint image with the Delaunay triangulation built from the tracked points in a low friction condition (A) and in a high friction condition (C). Three strain components (ϵ_{xx} , ϵ_{yy} and ϵ_{xy}) represented as heatmaps for a low friction condition (B) and a high friction condition (D). E. Median strain components (ϵ_{xx} , ϵ_{yy} and ϵ_{xy}) for each vibration amplitude as a function of the normal force. F. Median strain components rate in %/s for each vibration amplitude. G. Correlation between longitudinal strain and the divergence metric ($y = 0.040x - 0.225$, $R^2 = 0.61$). Each color stands for one participant. The probability to answer comparison is "more slippery" is plotted against the median of longitudinal strain difference (H) and the median strain rate of the comparison stimulus (I).

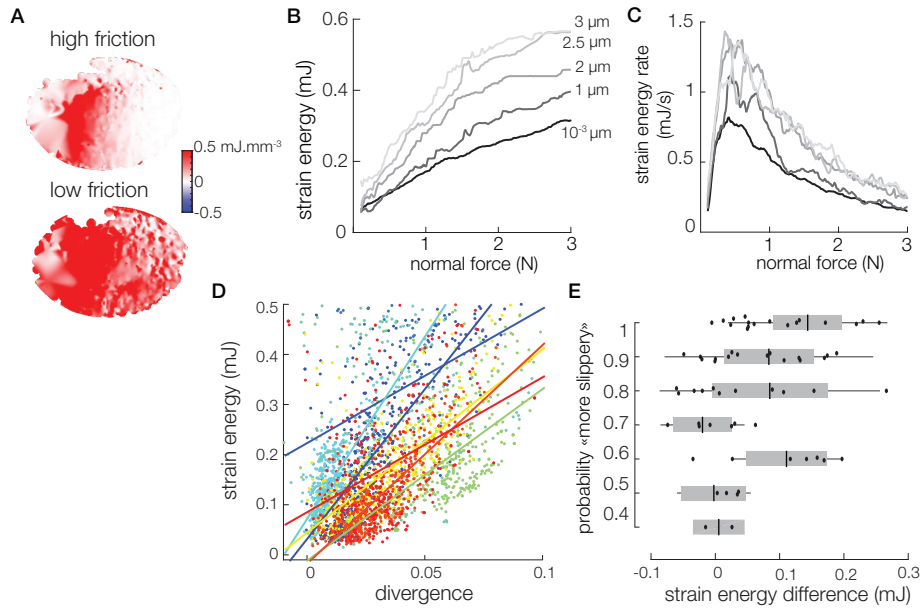


FIGURE A.2: **A.** Strain energy density in $\text{mJ}\cdot\text{mm}^{-3}$ for a high and a low friction conditions. Total strain energy (**B**) and strain energy rate (**C**) against normal force for each vibration amplitude. **D.** The correlation between total strain energy and the divergence metric depends on the mechanical properties of participant's skin. Each color stands for one participant. **E.** The probability to answer comparison is "more slippery" are plotted against the median of strain energy difference.

We believe that the main contributor of the difference between the two groups is a difference in skin stiffness, as softer skin deform more under similar loading.

In both cases, the divergence difference increases with the probabilities of answering comparison is "more slippery" (Fig.A.3B). Nevertheless, we observed that the group with softer skin has higher probabilities for the small vibration amplitude $\alpha \leq 1\ \mu\text{m}$ than the group with stiffer skin (Fig.A.3C).

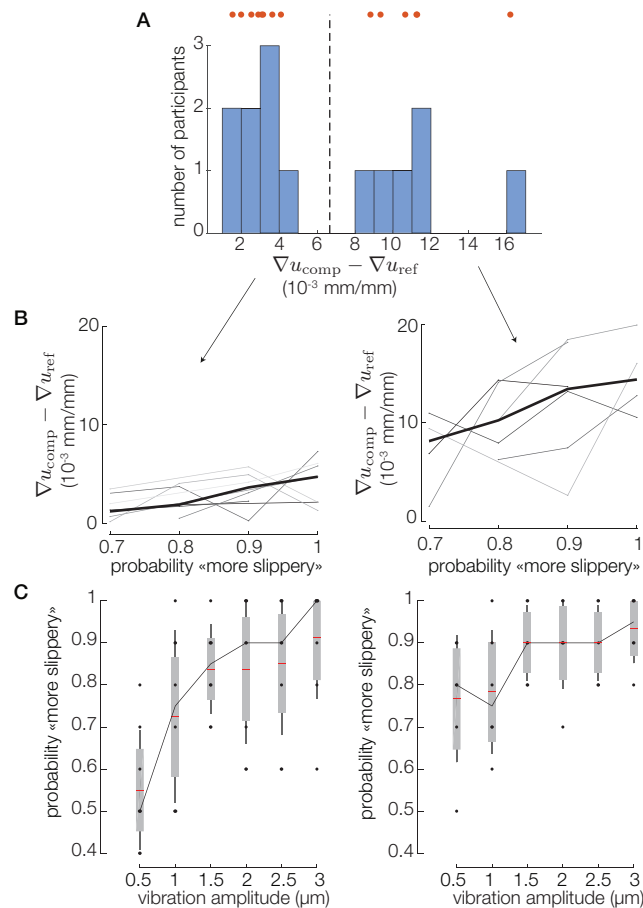


FIGURE A.3: Individual performance in friction discrimination. **A**. The histogram shows the median difference of divergences of each subject, and the dotted line divides the population of participants into 2 groups. **B**. The one on the left has a stiffer skin and experiences small deformations. The group on the right has a softer skin, experiencing more deformation. **C**. The group with softer skin has higher probability to detect the more slippery stimulus for the small vibration amplitudes, lower than $1\mu\text{m}$.

Appendix **B**

Appendix B: Skin strains during incipient slippage

This appendix aims at showing the individual skin strains acquired during the experiment of chapter 5. Four skin strain data for each friction condition (high, medium, low) and each subject are presented in Figure B.1. For subject 11, the ultrasonic vibrations cause a limited friction reduction, leading to no low friction strain data. The inter-subject variability is high, whereas the data for a same subject is repeatable. The magnitude of the tensile and compressive longitudinal strains are shown for all friction conditions in figure B.2.

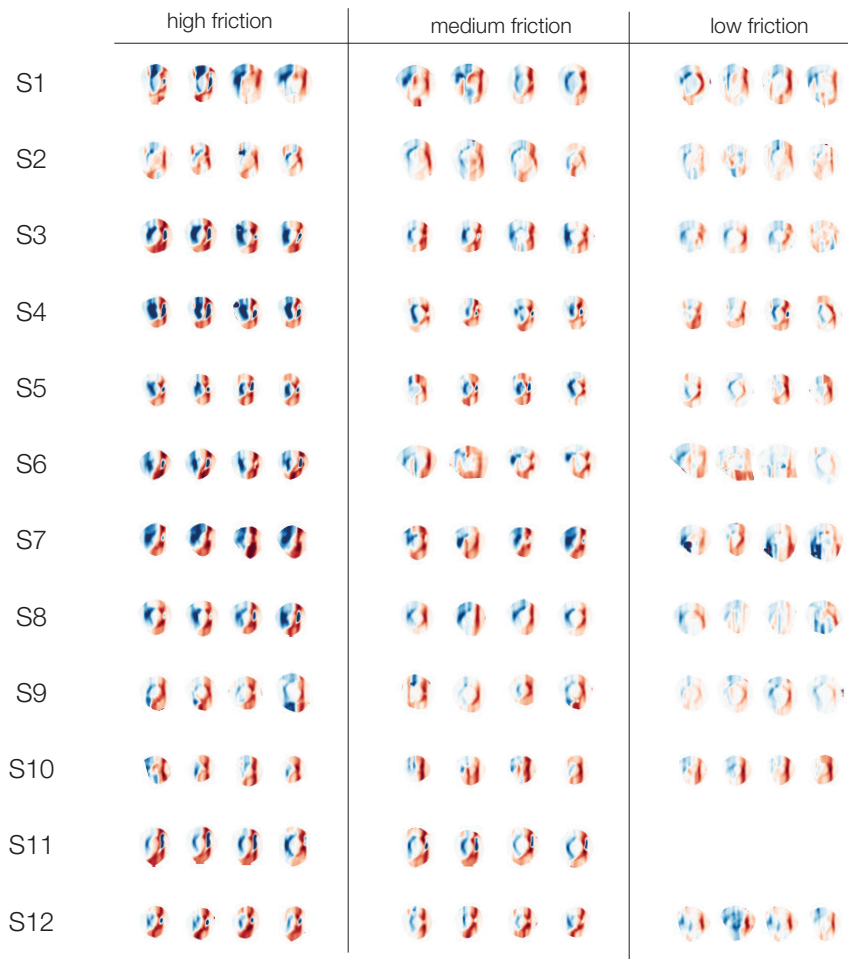


FIGURE B.1: Strains for all subjects (S1 to S12) when the relative displacements between the finger and the plate is 6 mm.

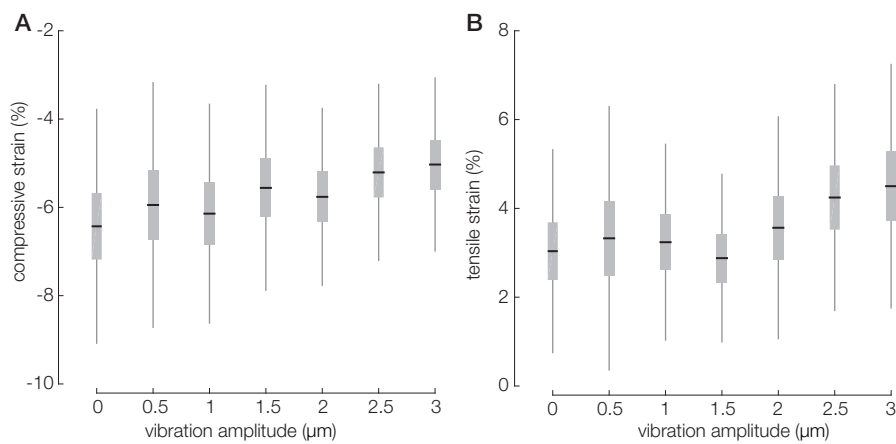


FIGURE B.2: Median compressive strains (A) and tensile strains (B) as a function of the vibration amplitude when the relative displacement is 6 mm.

Appendix C

Appendix C: Dimensionality reduction technique

An overview of the existing dimensionality reduction techniques are presented in Figure C.1. In our case we are looking for a linear method that projects the original data on a smaller space by extracting some components-based features. Amongst the linear method, Factor Analysis assumes that the latent factors exist in the observed data. Independent Component Analysis (ICA) is seeking for statistically independent directions which might be not orthogonal. The main drawback of ICA is that it is not able to rank each component. The Non-negative Matrix Factorization decomposed the input in a non-negative linear combination. This method is often used by the neuroscientists because it is biologically-inspired, since our neurons are more likely to sum inputs. However, it has been found recently that we have some inhibitory neurons by opposition to the excitatory ones, that would be able to subtract the information [211]. Finally, the Principal Components Analysis (PCA) can explain the maximal variance of a dataset and give the direction of the greatest variability. The Singular Value Decomposition (SVD) is a computationally-efficient PCA since the factorization is done on the data matrix rather on the covariance matrix which is large.

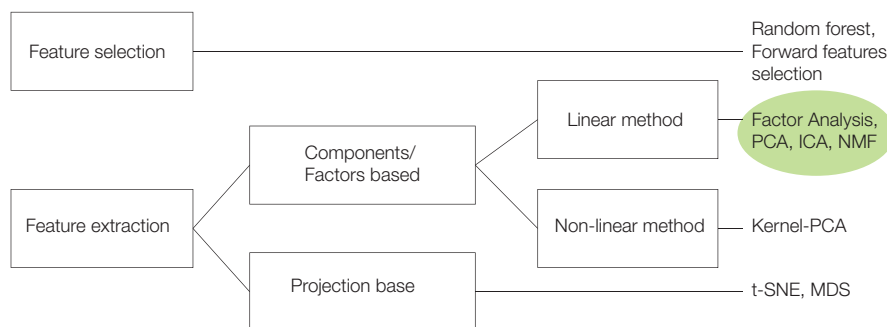


FIGURE C.1: Overview of the dimensionality reduction methods.

How to choose the best dimensionality reduction technique?

The dimensionality reduction method was chosen based on a time-efficiency criterion. The technique must maximize the distance between classes while running in a reasonable amount of time. The distance was estimated with the Generalized Discrimination Value (GDV) Δ computed from the mean intra-class distances \bar{d} and the mean inter-class distance d , Euclidean speaking:

$$\Delta = \frac{1}{\sqrt{2}} \left(\frac{\bar{d}(C_{Sm<0.5}) + \bar{d}(C_{Sm>0.5})}{2} - d(C_{Sm<0.5}, C_{Sm>0.5}) \right) \quad (C.1)$$

where the classes $C_{Sm<0.5}$ and $C_{Sm>0.5}$ correspond to a safety margin respectively lower and higher than 0.5. The GDV is always between 0 and -1, and a GDV close to 1 refers to a high discriminability between the classes.

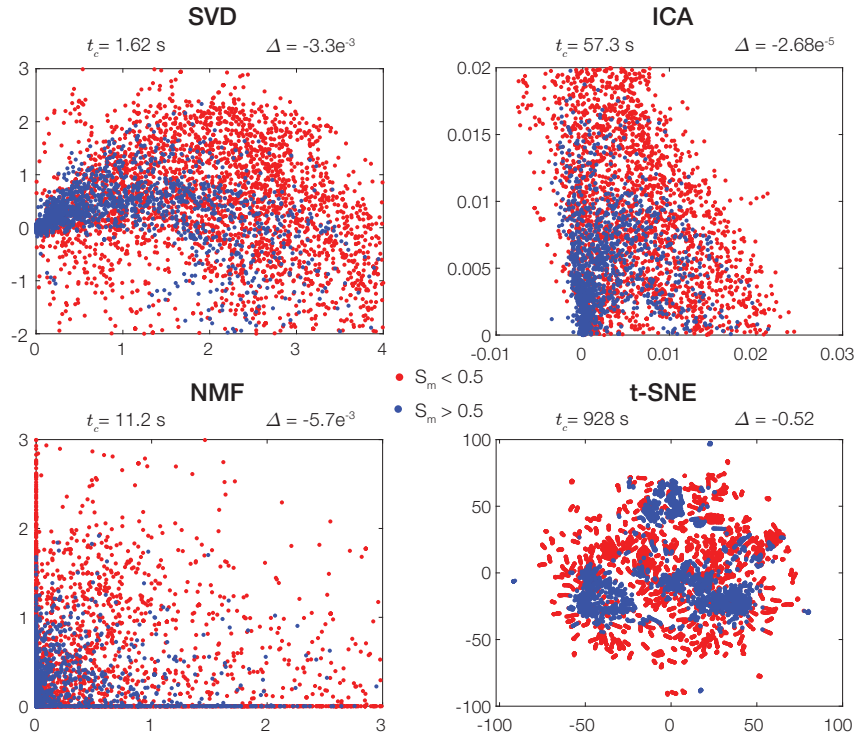


FIGURE C.2: Comparison between dimensionality reduction methods.

Fig. C.2 shows the 2D-points in the space determined by the first 2 bases. The red and the blue color represent the safety margin lower and higher than 0.5 respectively. The GDV and the total time are shown above each plot. The singular value decomposition is the fastest method, keeping an acceptable Generalized Discrimination Value. It is interesting to note that even if the t-SNE algorithm has the lowest GDV, the mapping of the classification is not meaningful in terms of principal components.

Moreover, we found that the set of primitives extracted with the singular value decomposition is invariant to friction, consistent with the human reflexive behavior

with surfaces of various frictional strength. For those reasons, we decided to use the singular value decomposition to reduce the dimensionality.

Bibliography

- [1] Michael J Adams et al. "Finger pad friction and its role in grip and touch". In: *Journal of The Royal Society Interface* 10.80 (2013), p. 20120467.
- [2] Rick A Adams, Stewart Shipp, and Karl J Friston. "Predictions not commands: active inference in the motor system". In: *Brain Structure and Function* 218.3 (2013), pp. 611–643.
- [3] Edward H Adelson and James R Bergen. "Spatiotemporal energy models for the perception of motion". In: *Josa a* 2.2 (1985), pp. 284–299.
- [4] Wisesty UN Adiwijaya et al. "Dimensionality reduction using principal component analysis for cancer detection based on microarray data classification". In: *Journal of Computer Science* 14.11 (2018), pp. 1521–1530.
- [5] Pierre G Agache et al. "Mechanical properties and Young's modulus of human skin in vivo". In: *Archives of dermatological research* 269.3 (1980), pp. 221–232.
- [6] Thibaut André, Philippe Lefèvre, and Jean-Louis Thonnard. "A continuous measure of fingertip friction during precision grip". In: *Journal of neuroscience methods* 179.2 (2009), pp. 224–229.
- [7] Thibaut André et al. "Effect of skin hydration on the dynamics of fingertip gripping contact". In: *Journal of The Royal Society Interface* 8.64 (2011), pp. 1574–1583.
- [8] Anne-Sophie Augurelle et al. "Importance of cutaneous feedback in maintaining a secure grip during manipulation of hand-held objects". In: *Journal of neurophysiology* 89.2 (2003), pp. 665–671.
- [9] DL Bader and P Bowker. "Mechanical characteristics of skin and underlying tissues in vivo". In: *Biomaterials* 4.4 (1983), pp. 305–308.
- [10] AO Barel. "Suction method for measurement of skin mechanical properties: the cutometer". In: *Handbook of non-invasive methods and the skin* (1995).
- [11] Horace B Barlow et al. "Possible principles underlying the transformation of sensory messages". In: *Sensory communication* 1.01 (1961).

- [12] M Barquins and AD Roberts. "Rubber friction variation with rate and temperature: some new observations". In: *Journal of Physics D: Applied Physics* 19.4 (1986), p. 547.
- [13] Allan Barrea et al. "Perception of partial slips under tangential loading of the fingertip". In: *Scientific reports* 8.1 (2018), pp. 1–8.
- [14] Allan Barrea et al. "Simple and reliable method to estimate the fingertip static coefficient of friction in precision grip". In: *IEEE transactions on haptics* 9.4 (2016), pp. 492–498.
- [15] Anthony J Bell and Terrence J Sejnowski. "The "independent components" of natural scenes are edge filters". In: *Vision research* 37.23 (1997), pp. 3327–3338.
- [16] Jonathan Bell, Stanley Bolanowski, and Mark H Holmes. "The structure and function of Pacinian corpuscles: a review". In: *Progress in neurobiology* 42.1 (1994), pp. 79–128.
- [17] Oded Ben-David, Shmuel M Rubinstein, and Jay Fineberg. "Slip-stick and the evolution of frictional strength". In: *Nature* 463.7277 (2010), pp. 76–79.
- [18] Corentin Bernard et al. "Detection of friction-modulated textures is limited by vibrotactile sensitivity". In: *IEEE Transactions on Haptics* (2020).
- [19] Antonio Bicchi, Enzo Pasquale Scilingo, and Danilo De Rossi. "Haptic discrimination of softness in teleoperation: the role of the contact area spread rate". In: *IEEE Transactions on Robotics and Automation* 16.5 (2000), pp. 496–504.
- [20] Antonio Bicchi et al. "10 Tactile Flow and Haptic Discrimination of Softness". In: *Multi-point interaction with real and virtual objects*. Springer, 2005, pp. 165–176.
- [21] Antonio Bicchi et al. "Tactile flow explains haptic counterparts of common visual illusions". In: *Brain research bulletin* 75.6 (2008), pp. 737–741.
- [22] Ingvars Birznieks et al. "Encoding of direction of fingertip forces by human tactile afferents". In: *Journal of Neuroscience* 21.20 (2001), pp. 8222–8237.
- [23] Yannick Bleyenheuft, Philippe Lefevre, and Jean-Louis Thonnard. "Predictive mechanisms control grip force after impact in self-triggered perturbations". In: *Journal of motor behavior* 41.5 (2009), pp. 411–417.
- [24] Serena Bochereau et al. "Characterizing and imaging gross and real finger contacts under dynamic loading". In: *IEEE transactions on haptics* 10.4 (2017), pp. 456–465.
- [25] Stanley J Bolanowski Jr et al. "Four channels mediate the mechanical aspects of touch". In: *The Journal of the Acoustical society of America* 84.5 (1988), pp. 1680–1694.

- [26] Joseph Boussinesq. *Application des potentiels à l'étude de l'équilibre et du mouvement des solides élastiques: principalement au calcul des déformations et des pressions que produisent, dans ces solides, des efforts quelconques exercés sur une petite partie de leur surface ou de leur intérieur: mémoire suivi de notes étendues sur divers points de physique, mathématique et d'analyse*. Vol. 4. Gauthier-Villars, 1885.
- [27] Frank Philip Bowden and David Tabor. "The area of contact between stationary and moving surfaces". In: *Proceedings of the Royal Society of London. Series A. Mathematical and Physical Sciences* 169.938 (1939), pp. 391–413.
- [28] BJ Briscoe and D Tabor. "Shear properties of thin polymeric films". In: *The Journal of Adhesion* 9.2 (1978), pp. 145–155.
- [29] Christopher L Buckley and Taro Toyozumi. "A theory of how active behavior stabilises neural activity: Neural gain modulation by closed-loop environmental feedback". In: *PLoS computational biology* 14.1 (2018), e1005926.
- [30] Geneviève Cadoret and Allan M Smith. "Friction, not texture, dictates grip forces used during object manipulation". In: *Journal of neurophysiology* 75.5 (1996), pp. 1963–1969.
- [31] Olivia Carter et al. "Tactile rivalry demonstrated with an ambiguous apparent-motion quartet". In: *Current Biology* 18.14 (2008), pp. 1050–1054.
- [32] Cs Cattaneo. "Sul contatto de due corpi elastici: Distribuzione locale degli sforzi". In: *Rendiconti dell'Accademia nazionale dei Lincei* 6 (1938), pp. 342–349.
- [33] Nikolajs Cauna. "Nature and functions of the papillary ridges of the digital skin". In: *The Anatomical Record* 119.4 (1954), pp. 449–468.
- [34] V Cerruti. "Acc. Lincei., Mem. Fis. Mat". In: *Roma* 3 (1882), p. 81.
- [35] Matthew Chalk, Olivier Marre, and Gašper Tkačik. "Toward a unified theory of efficient, predictive, and sparse coding". In: *Proceedings of the National Academy of Sciences* 115.1 (2018), pp. 186–191.
- [36] C Elaine Chapman. "Active versus passive touch: factors influencing the transmission of somatosensory signals to primary somatosensory cortex". In: *Canadian journal of physiology and pharmacology* 72.5 (1994), pp. 558–570.
- [37] Wei Chen et al. "An eight-legged tactile sensor to estimate coefficient of static friction". In: *2015 37th Annual International Conference of the IEEE Engineering in Medicine and Biology Society (EMBC)*. IEEE. 2015, pp. 4407–4410.
- [38] GP Chimata and Christian J Schwartz. "Investigation of friction mechanisms in finger pad sliding against surfaces of varying roughness". In: *Biotribology* 3 (2015), pp. 11–19.

- [39] Roger W Cholewiak and Amy A Collins. "The generation of vibrotactile patterns on a linear array: Influences of body site, time, and presentation mode". In: *Perception & Psychophysics* 62.6 (2000), pp. 1220–1235.
- [40] KELLY J Cole and JAMES H Abbs. "Grip force adjustments evoked by load force perturbations of a grasped object". In: *Journal of neurophysiology* 60.4 (1988), pp. 1513–1522.
- [41] J Edward Colgate and Gerd G Schenkel. "Passivity of a class of sampled-data systems: Application to haptic interfaces". In: *Journal of robotic systems* 14.1 (1997), pp. 37–47.
- [42] P Corcuff, C Bertrand, and JL Leveque. "Morphometry of human epidermis in vivo by real-time confocal microscopy". In: *Archives of dermatological research* 285.8 (1993), pp. 475–481.
- [43] Pierre Corcuff et al. "In vivo confocal microscopy of human skin: a new design for cosmetology and dermatology". In: *Scanning: The Journal of Scanning Microscopies* 18.5 (1996), pp. 351–355.
- [44] James C Craig and XU Baihua. "Temporal order and tactile patterns". In: *Perception & psychophysics* 47.1 (1990), pp. 22–34.
- [45] James C Craig and Kenneth O Johnson. "The two-point threshold: Not a measure of tactile spatial resolution". In: *Current Directions in Psychological Science* 9.1 (2000), pp. 29–32.
- [46] Michael L Crichton et al. "The viscoelastic, hyperelastic and scale dependent behaviour of freshly excised individual skin layers". In: *Biomaterials* 32.20 (2011), pp. 4670–4681.
- [47] Phil R Dahl. *A solid friction model*. Tech. rep. Aerospace Corp El Segundo Ca, 1968.
- [48] Philip R Dahl. "Solid friction damping of mechanical vibrations". In: *AIAA journal* 14.12 (1976), pp. 1675–1682.
- [49] Colin H Daly. "Biomechanical properties of dermis". In: *Journal of Investigative Dermatology* 79.1 (1982), pp. 17–20.
- [50] Kiran Dandekar, Balasundar I Raju, and Mandayam A Srinivasan. "3-D finite-element models of human and monkey fingertips to investigate the mechanics of tactile sense". In: *J. Biomech. Eng.* 125.5 (2003), pp. 682–691.
- [51] Ian Darian-Smith. "The sense of touch: performance and peripheral neural processes". In: *Comprehensive Physiology* (2011), pp. 739–788.
- [52] J De Rigal and J-L Leveque. "In vivo measurement of the stratum corneum elasticity". In: *Bioengineering and the Skin* 1.1 (1985), pp. 13–23.
- [53] C Canudas De Wit et al. "A new model for control of systems with friction". In: *IEEE Transactions on automatic control* 40.3 (1995), pp. 419–425.

- [54] Alexandre Delalleau et al. "A nonlinear elastic behavior to identify the mechanical parameters of human skin in vivo". In: *Skin research and Technology* 14.2 (2008), pp. 152–164.
- [55] Benoit Delhayé, Philippe Lefevre, and Jean-Louis Thonnard. "Dynamics of fingertip contact during the onset of tangential slip". In: *Journal of The Royal Society Interface* 11.100 (2014), p. 20140698.
- [56] Benoit Delhayé et al. "Surface strain measurements of fingertip skin under shearing". In: *Journal of The Royal Society Interface* 13.115 (2016), p. 20150874.
- [57] Benoit P Delhayé et al. "High-resolution imaging of skin deformation shows that afferents from human fingertips signal slip onset". In: *Elife* 10 (2021), e64679.
- [58] Patrick Delmas, Jizhe Hao, and Lise Rodat-Despoix. "Molecular mechanisms of mechanotransduction in mammalian sensory neurons". In: *Nature Reviews Neuroscience* 12.3 (2011), pp. 139–153.
- [59] Alexandra Dépeault, El-Mehdi Meftah, and C Elaine Chapman. "Tactile speed scaling: contributions of time and space". In: *Journal of neurophysiology* 99.3 (2008), pp. 1422–1434.
- [60] S Diridollou et al. "An in vivo method for measuring the mechanical properties of the skin using ultrasound". In: *Ultrasound in medicine & biology* 24.2 (1998), pp. 215–224.
- [61] S Diridollou et al. "In vivo model of the mechanical properties of the human skin under suction". In: *Skin Research and technology* 6.4 (2000), pp. 214–221.
- [62] Basil Duvernoy et al. "Numerosity Identification Used to Assess Tactile Stimulation Methods for Communication". In: *IEEE Transactions on Haptics* (2020).
- [63] Brygida Dzidek et al. "Why pens have rubbery grips". In: *Proceedings of the National Academy of Sciences* 114.41 (2017), pp. 10864–10869.
- [64] Brygida M Dzidek et al. "Contact mechanics of the human finger pad under compressive loads". In: *Journal of The Royal Society Interface* 14.127 (2017).
- [65] Benoni B Edin. "Quantitative analyses of dynamic strain sensitivity in human skin mechanoreceptors". In: *Journal of neurophysiology* 92.6 (2004), pp. 3233–3243.
- [66] Benoni B Edin. "Quantitative analysis of static strain sensitivity in human mechanoreceptors from hairy skin". In: *Journal of neurophysiology* 67.5 (1992), pp. 1105–1113.
- [67] Benoni B Edin, Göran Westling, and Roland S Johansson. "Independent control of human finger-tip forces at individual digits during precision lifting." In: *The Journal of physiology* 450.1 (1992), pp. 547–564.

- [68] Marc O Ernst. "Learning to integrate arbitrary signals from vision and touch". In: *Journal of vision* 7.5 (2007), pp. 7–7.
- [69] Catherine Escoffier et al. "Age-related mechanical properties of human skin: an in vivo study". In: *Journal of Investigative Dermatology* 93.3 (1989), pp. 353–357.
- [70] GK Essick, O Franzen, and BL Whitsel. "Discrimination and scaling of velocity of stimulus motion across the skin". In: *Somatosensory & motor research* 6.1 (1988), pp. 21–40.
- [71] Mor Farajian et al. "Stretching the skin immediately enhances perceived stiffness and gradually enhances the predictive control of grip force". In: *Elife* 9 (2020), e52653.
- [72] L Farran et al. "Tensile and shear properties of fingernails as a function of a changing humidity environment". In: *Journal of biomechanics* 42.9 (2009), pp. 1230–1235.
- [73] David J Field. "What is the goal of sensory coding?" In: *Neural computation* 6.4 (1994), pp. 559–601.
- [74] AY Finlay. "The physical properties and function of nails". In: *The Physical Nature of the Skin*. Springer, 1988, pp. 143–154.
- [75] J Randall Flanagan and Michael A Beltzner. "Independence of perceptual and sensorimotor predictions in the size–weight illusion". In: *Nature neuroscience* 3.7 (2000), pp. 737–741.
- [76] Cormac Flynn et al. "Simulating the three-dimensional deformation of in vivo facial skin". In: *Journal of the mechanical behavior of biomedical materials* 28 (2013), pp. 484–494.
- [77] Yuan-cheng Fung. *Biomechanics: mechanical properties of living tissues*. Springer Science & Business Media, 2013.
- [78] Esther P Gardner and Bradley F Sklar. "Discrimination of the direction of motion on the human hand: a psychophysical study of stimulation parameters". In: *Journal of Neurophysiology* 71.6 (1994), pp. 2414–2429.
- [79] Marion Geerligts et al. "In vitro indentation to determine the mechanical properties of epidermis". In: *Journal of biomechanics* 44.6 (2011), pp. 1176–1181.
- [80] Frank A Geldard and Carl E Sherrick. "The cutaneous" rabbit": a perceptual illusion". In: *Science* 178.4057 (1972), pp. 178–179.
- [81] George A Gescheider, Stanley J Bolanowski, and Sarah K Chatterton. "Temporal gap detection in tactile channels". In: *Somatosensory & motor research* 20.3-4 (2003), pp. 239–247.
- [82] James J Gibson. "Observations on active touch." In: *Psychological review* 69.6 (1962), p. 477.

- [83] AW Goodwin, VG Macefield, and JW Bisley. "Encoding of object curvature by tactile afferents from human fingers". In: *Journal of neurophysiology* 78.6 (1997), pp. 2881–2888.
- [84] John Gosline et al. "Elastic proteins: biological roles and mechanical properties". In: *Philosophical Transactions of the Royal Society of London. Series B: Biological Sciences* 357.1418 (2002), pp. 121–132.
- [85] David Gueorguiev et al. "Touch uses frictional cues to discriminate flat materials". In: *Scientific reports* 6 (2016), p. 25553.
- [86] Ahsan Habib et al. "SkinSim: A simulation environment for multimodal robot skin". In: *2014 IEEE International Conference on Automation Science and Engineering (CASE)*. IEEE. 2014, pp. 1226–1231.
- [87] Alkis M Hadjiosif and Maurice A Smith. "Flexible control of safety margins for action based on environmental variability". In: *Journal of Neuroscience* 35.24 (2015), pp. 9106–9121.
- [88] Charlotte Häger-Ross and Roland S Johansson. "Nondigital afferent input in reactive control of fingertip forces during precision grip". In: *Experimental brain research* 110.1 (1996), pp. 131–141.
- [89] Zdenek Halata, Milos Grim, and Klaus I Bauman. "Friedrich Sigmund Merkel and his "Merkel cell", morphology, development, and physiology: review and new results". In: *The Anatomical Record Part A: Discoveries in Molecular, Cellular, and Evolutionary Biology: An Official Publication of the American Association of Anatomists* 271.1 (2003), pp. 225–239.
- [90] NJ Harrick. "Fingerprinting via total internal reflection". In: *Philips Tech Rev* 1963.24 (1962), p. 271.
- [91] Vincent Hayward and M Cruz-Hernandez. "Tactile display device using distributed lateral skin stretch". In: *Proceedings of the haptic interfaces for virtual environment and teleoperator systems symposium*. Vol. 69. 2. Citeseer. 2000, pp. 1309–1314.
- [92] Harry Helson and Samuel M King. "The tau effect: an example of psychological relativity." In: *Journal of Experimental Psychology* 14.3 (1931), p. 202.
- [93] Yuichi Hiramatsu et al. "Control of precision grip force in lifting and holding of low-mass objects". In: *PloS one* 10.9 (2015), e0138506.
- [94] Ira J Hirsh and Carl E Sherrick Jr. "Perceived order in different sense modalities." In: *Journal of experimental psychology* 62.5 (1961), p. 423.
- [95] A. V. Ho and S. Hirai. "Toward a Platform of Human-Like Fingertip Model in Haptic Environment for Studying Sliding Tactile Mechanism". In: *Robotics: Science and Systems*. 2013.
- [96] GA Holzapfel. *Biomechanics of soft tissues: handbook of material behaviour*. 2000.

- [97] W Stamps Howard and Vijay Kumar. "On the stability of grasped objects". In: *IEEE transactions on robotics and automation* 12.6 (1996), pp. 904–917.
- [98] Kathryn M Hudson et al. "Effects of changing skin mechanics on the differential sensitivity to surface compliance by tactile afferents in the human finger pad". In: *Journal of neurophysiology* 114.4 (2015), pp. 2249–2257.
- [99] Nicolas Huloux, Corentin Bernard, and Michael Wiertlewski. "Estimation of the Modulation of Friction from the Mechanical Impedance Variations." In: *IEEE Transactions on Haptics* (2020).
- [100] Nicolas Huloux, Laurence Willemet, and Michael Wiertlewski. "How to measure the area of real contact of skin on glass". In: *IEEE Transactions on Haptics* (2021).
- [101] Emmanuelle Jacquet et al. "A new experimental method for measuring skin's natural tension". In: *Skin Research and technology* 14.1 (2008), pp. 1–7.
- [102] Roland S Johansson and Ingvars Birznieks. "First spikes in ensembles of human tactile afferents code complex spatial fingertip events". In: *Nature neuroscience* 7.2 (2004), pp. 170–177.
- [103] Roland S Johansson and J Randall Flanagan. "Coding and use of tactile signals from the fingertips in object manipulation tasks". In: *Nature Reviews Neuroscience* 10.5 (2009), pp. 345–359.
- [104] Roland S Johansson, Ulf Landstro, Ronnie Lundstro, et al. "Responses of mechanoreceptive afferent units in the glabrous skin of the human hand to sinusoidal skin displacements". In: *Brain research* 244.1 (1982), pp. 17–25.
- [105] Roland S Johansson and AB Vallbo. "Tactile sensibility in the human hand: relative and absolute densities of four types of mechanoreceptive units in glabrous skin." In: *The Journal of physiology* 286.1 (1979), pp. 283–300.
- [106] Roland S Johansson and G Westling. "Signals in tactile afferents from the fingers eliciting adaptive motor responses during precision grip". In: *Experimental brain research* 66.1 (1987), pp. 141–154.
- [107] Roland S Johansson and Goran Westling. "Roles of glabrous skin receptors and sensorimotor memory in automatic control of precision grip when lifting rougher or more slippery objects". In: *Experimental brain research* 56.3 (1984), pp. 550–564.
- [108] Kenneth Langstreth Johnson and Kenneth Langstreth Johnson. *Contact mechanics*. Cambridge university press, 1987.
- [109] Kenneth O Johnson. "The roles and functions of cutaneous mechanoreceptors". In: *Current opinion in neurobiology* 11.4 (2001), pp. 455–461.
- [110] Kenneth O Johnson and Steven S Hsiao. "Neural mechanisms of tactual form and texture perception". In: *Annual review of neuroscience* 15.1 (1992), pp. 227–250.

- [111] Kenneth O Johnson and John R Phillips. "Tactile spatial resolution. I. Two-point discrimination, gap detection, grating resolution, and letter recognition". In: *Journal of neurophysiology* 46.6 (1981), pp. 1177–1192.
- [112] Lynette A Jones and Susan J Lederman. *Human hand function*. Oxford University Press, 2006.
- [113] Seitaro Kaneko, Hiroyuki Kajimoto, and Vincent Hayward. "A case of perceptual completion in spatio-temporal tactile space". In: *International Conference on Human Haptic Sensing and Touch Enabled Computer Applications*. Springer. 2018, pp. 49–57.
- [114] Alireza Karimi et al. "Measurement of the viscoelastic mechanical properties of the skin tissue under uniaxial loading". In: *Proceedings of the Institution of Mechanical Engineers, Part L: Journal of Materials: Design and Applications* 230.2 (2016), pp. 418–425.
- [115] David Katz and Lester E Krueger. *The world of touch*. Psychology press, 2013.
- [116] Mitsuo Kawato. "Internal models for motor control and trajectory planning". In: *Current opinion in neurobiology* 9.6 (1999), pp. 718–727.
- [117] Heba Khamis et al. "Classification of texture and frictional condition at initial contact by tactile afferent responses". In: *International Conference on Human Haptic Sensing and Touch Enabled Computer Applications*. Springer. 2014, pp. 460–468.
- [118] Heba Khamis et al. "Friction sensing mechanisms for perception and motor control: Passive touch without sliding may not provide perceivable frictional information". In: *Journal of Neurophysiology* 125.3 (2021).
- [119] Heba A Khamis et al. "Tactile afferents encode grip safety before slip for different frictions". In: *2014 36th Annual International Conference of the IEEE Engineering in Medicine and Biology Society*. IEEE. 2014, pp. 4123–4126.
- [120] Jacob H Kirman. "Tactile apparent movement: The effects of interstimulus onset interval and stimulus duration". In: *Perception & Psychophysics* 15.1 (1974), pp. 1–6.
- [121] Norimichi Kitagawa, Yuka Igarashi, and Makio Kashino. "The tactile continuity illusion." In: *Journal of Experimental Psychology: Human Perception and Performance* 35.6 (2009), p. 1784.
- [122] Roberta L Klatzky and Susan J Lederman. "Identifying objects from a haptic glance". In: *Perception & Psychophysics* 57.8 (1995), pp. 1111–1123.
- [123] Brandon A Krick et al. "Optical in situ micro tribometer for analysis of real contact area for contact mechanics, adhesion, and sliding experiments". In: *Tribology letters* 45.1 (2012), pp. 185–194.

- [124] Siddarth Kumar et al. "Viscoelastic characterization of the primate finger pad in vivo by microstep indentation and three-dimensional finite element models for tactile sensation studies". In: *Journal of biomechanical engineering* 137.6 (2015).
- [125] Scinob Kuroki and Shin'ya Nishida. "Motion Direction Discrimination with Tactile Random-Dot Kinematograms". In: *i-Perception* 12.2 (2021), p. 20416695211004620.
- [126] ROBERT H LaMotte and MANDAYAM A Srinivasan. "Neural encoding of shape: responses of cutaneous mechanoreceptors to a wavy surface stroked across the monkey fingerpad". In: *Journal of neurophysiology* 76.6 (1996), pp. 3787–3797.
- [127] Robert H LaMotte and James Whitehouse. "Tactile detection of a dot on a smooth surface: peripheral neural events". In: *Journal of neurophysiology* 56.4 (1986), pp. 1109–1128.
- [128] Anatole Lécuyer, Jean-Marie Burkhardt, and Laurent Etienne. "Feeling bumps and holes without a haptic interface: the perception of pseudo-haptic textures". In: *Proceedings of the SIGCHI conference on Human factors in computing systems*. 2004, pp. 239–246.
- [129] Susan J Lederman and Lynette A Jones. "Tactile and haptic illusions". In: *IEEE Transactions on Haptics* 4.4 (2011), pp. 273–294.
- [130] Susan J Lederman and Roberta L Klatzky. "Hand movements: A window into haptic object recognition". In: *Cognitive psychology* 19.3 (1987), pp. 342–368.
- [131] Daniel D Lee and H Sebastian Seung. "Learning the parts of objects by non-negative matrix factorization". In: *Nature* 401.6755 (1999), pp. 788–791.
- [132] Caroline Lees, Julian FV Vincent, and J Eric Hillerton. "Poisson's ratio in skin". In: *Bio-medical materials and engineering* 1.1 (1991), pp. 19–23.
- [133] Raz Leib, Amir Karniel, and Ilana Nisky. "The effect of force feedback delay on stiffness perception and grip force modulation during tool-mediated interaction with elastic force fields". In: *Journal of neurophysiology* 113.9 (2015), pp. 3076–3089.
- [134] Vincent Levesque and Vincent Hayward. "Experimental evidence of lateral skin strain during tactile exploration". In: *Proceedings of EUROHAPTICS*. Vol. 2003. Citeseer. 2003.
- [135] Michael S Lewicki. "Efficient coding of natural sounds". In: *Nature neuroscience* 5.4 (2002), pp. 356–363.
- [136] Xing Liang and Stephen A Boppart. "Biomechanical properties of in vivo human skin from dynamic optical coherence elastography". In: *IEEE Transactions on Biomedical Engineering* 57.4 (2009), pp. 953–959.

- [137] Xi Lin and Michaël Wiertlewski. "Sensing the frictional state of a robotic skin via subtractive color mixing". In: *IEEE Robotics and Automation Letters* 4.3 (2019), pp. 2386–2392.
- [138] Xi Lin et al. "Curvature sensing with a spherical tactile sensor using the color-interference of a marker array". In: *2020 IEEE International Conference on Robotics and Automation (ICRA)*. IEEE. 2020, pp. 603–609.
- [139] Jack M Loomis and Susan J Lederman. "Tactual perception". In: *Handbook of perception and human performances* 2.2 (1986), p. 2.
- [140] Bruce D Lucas and Takeo Kanade. "An iterative image registration technique with an application to stereo vision". In: *1981 Proceedings 7th IJCAI*. Vancouver, British Columbia, 1981, pp. 121–130.
- [141] Takashi Maeno, Shinichi Hiromitsu, and Takashi Kawai. "Control of grasping force by detecting stick/slip distribution at the curved surface of an elastic finger". In: *IEEE International Conference on Robotics and Automation* 4 (2000), pp. 3895–3900.
- [142] Takashi Maeno, Tomoyuki Kawamura, and Sen-Chieh Cheng. "Friction estimation by pressing an elastic finger-shaped sensor against a surface". In: *IEEE Transactions on Robotics and Automation* 20.2 (2004), pp. 222–228.
- [143] Takashi Maeno, Kazumi Kobayashi, and Nobutoshi Yamazaki. "Relationship between the structure of human finger tissue and the location of tactile receptors". In: *JSME International Journal Series C Mechanical Systems, Machine Elements and Manufacturing* 41.1 (1998), pp. 94–100.
- [144] Flavia Mancini et al. "Whole-body mapping of spatial acuity for pain and touch". In: *Annals of neurology* 75.6 (2014), pp. 917–924.
- [145] Benoit Mandelbrot. "How long is the coast of Britain? Statistical self-similarity and fractional dimension". In: *science* 156.3775 (1967), pp. 636–638.
- [146] JFM Manschot and AJM Brakkee. "The measurement and modelling of the mechanical properties of human skin in vivo". In: *Journal of Biomechanics* 19.7 (1986), pp. 517–521.
- [147] Michele Marino. "Molecular and intermolecular effects in collagen fibril mechanics: a multiscale analytical model compared with atomistic and experimental studies". In: *Biomechanics and modeling in mechanobiology* 15.1 (2016), pp. 133–154.
- [148] Stephen A Mascaró and H Harry Asada. "Understanding of fingernail-bone interaction and fingertip hemodynamics for fingernail sensor design". In: *Haptic Interfaces for Virtual Environment and Teleoperator Systems, International Symposium on*. 2002, pp. 113–113.

- [149] PB Matthews. "The contrasting stretch reflex responses of the long and short flexor muscles of the human thumb." In: *The Journal of physiology* 348.1 (1984), pp. 545–558.
- [150] Walter Maurel et al. *Biomechanical models for soft tissue simulation*. Vol. 48. Springer, 1998.
- [151] Anna Metzger and Matteo Toscani. "Unsupervised learning of haptic material properties". In: *bioRxiv* (2021).
- [152] Raymond David Mindlin. "Compliance of elastic bodies in contact". In: (1949).
- [153] RJ Minns, PD Soden, and DS Jackson. "The role of the fibrous components and ground substance in the mechanical properties of biological tissues: a preliminary investigation". In: *Journal of biomechanics* 6.2 (1973), pp. 153–165.
- [154] Jocelyn Monnoyer et al. "Perception of ultrasonic switches involves large discontinuity of the mechanical impedance". In: *IEEE transactions on haptics* 11.4 (2018), pp. 579–589.
- [155] Joël Monzée, Yves Lamarre, and Allan M Smith. "The effects of digital anesthesia on force control using a precision grip". In: *Journal of neurophysiology* 89.2 (2003), pp. 672–683.
- [156] Carl Ed Murchison. "A handbook of general experimental psychology." In: (1934).
- [157] David J Murray et al. "Charpentier (1891) on the size—weight illusion". In: *Perception & Psychophysics* 61.8 (1999), pp. 1681–1685.
- [158] Nobuaki Nakazawa, Ryojun Ikeura, and Hikaru Inooka. "Characteristics of human fingertips in shearing direction". In: *The Japanese Journal of Ergonomics* 34.Supplement (1998), pp. 520–521.
- [159] Nobuaki Nakazawa, Ryojun Ikeura, and Hikaru Inooka. "Characteristics of human fingertips in the shearing direction". In: *Biological cybernetics* 82.3 (2000), pp. 207–214.
- [160] Saekwang Nam et al. "Physical Variables Underlying Tactile Stickiness During Fingerpad Detachment". In: *Frontiers in Neuroscience* 14 (2020), p. 235.
- [161] Wilhelm Neuhaus. "Experimentelle Untersuchung der Scheinbewegung." In: *Archiv für die gesamte Psychologie* (1930).
- [162] Dennis A Nowak and Joachim Hermsdörfer. "Digit cooling influences grasp efficiency during manipulative tasks". In: *European journal of applied physiology* 89.2 (2003), pp. 127–133.
- [163] Bruno A Olshausen and David J Field. "Emergence of simple-cell receptive field properties by learning a sparse code for natural images". In: *Nature* 381.6583 (1996), pp. 607–609.

- [164] Hans Oxlund, Jan Manschot, and A Viidik. "The role of elastin in the mechanical properties of skin". In: *Journal of biomechanics* 21.3 (1988), pp. 213–218.
- [165] C Pailler-Mattei, S Bec, and H Zahouani. "In vivo measurements of the elastic mechanical properties of human skin by indentation tests". In: *Medical engineering & physics* 30.5 (2008), pp. 599–606.
- [166] Rich Pang, Benjamin J Lansdell, and Adrienne L Fairhall. "Dimensionality reduction in neuroscience". In: *Current Biology* 26.14 (2016), R656–R660.
- [167] Michel Pare, Catherine Behets, and Olivier Cornu. "Paucity of presumptive ruffini corpuscles in the index finger pad of humans". In: *Journal of Comparative Neurology* 456.3 (2003), pp. 260–266.
- [168] Michel Pare et al. "The Meissner corpuscle revised: a multiafferented mechanoreceptor with nociceptor immunochemical properties". In: *Journal of Neuroscience* 21.18 (2001), pp. 7236–7246.
- [169] Maria A Pastor et al. "The functional neuroanatomy of temporal discrimination". In: *Journal of Neuroscience* 24.10 (2004), pp. 2585–2591.
- [170] Subrahmanyam M Pasumarty et al. "Friction of the human finger pad: influence of moisture, occlusion and velocity". In: *Tribology Letters* 44.2 (2011), p. 117.
- [171] Todd C Pataky, Mark L Latash, and Vladimir M Zatsiorsky. "Viscoelastic response of the finger pad to incremental tangential displacements". In: *Journal of biomechanics* 38.7 (2005), pp. 1441–1449.
- [172] Dianne TV Pawluk and Robert D Howe. "Dynamic lumped element response of the human fingerpad". In: (1999).
- [173] Peter A Payne. "Measurement of properties and function of skin". In: *Clinical Physics and Physiological Measurement* 12.2 (1991), p. 105.
- [174] BNJ Persson et al. "Contact area between a viscoelastic solid and a hard, randomly rough, substrate". In: *The Journal of chemical physics* 120.18 (2004), pp. 8779–8793.
- [175] John R Phillips and Kenneth O Johnson. "Tactile spatial resolution. III. A continuum mechanics model of skin predicting mechanoreceptor responses to bars, edges, and gratings". In: *Journal of neurophysiology* 46.6 (1981), pp. 1204–1225.
- [176] T Piatkowski. "Dahl and LuGre dynamic friction models—the analysis of selected properties". In: *Mechanism and Machine Theory* 73 (2014), pp. 91–100.
- [177] J Andrew Pruszynski, J Randall Flanagan, and Roland S Johansson. "Fast and accurate edge orientation processing during object manipulation". In: *Elife* 7 (2018), e31200.

- [178] Milind Rajadhyaksha et al. "In vivo confocal scanning laser microscopy of human skin II: advances in instrumentation and comparison with histology". In: *Journal of Investigative Dermatology* 113.3 (1999), pp. 293–303.
- [179] Christophe Ramstein and Vincent Hayward. "The pantograph: a large workspace haptic device for multimodal human computer interaction". In: *Conference companion on Human factors in computing systems*. 1994, pp. 57–58.
- [180] Rajesh PN Rao and Dana H Ballard. "Predictive coding in the visual cortex: a functional interpretation of some extra-classical receptive-field effects". In: *Nature neuroscience* 2.1 (1999), pp. 79–87.
- [181] Dan Reznik and Christian Laugier. "Dynamic simulation and virtual control of a deformable fingertip". In: *Proceedings of IEEE International Conference on Robotics and Automation*. Vol. 2. IEEE. 1996, pp. 1669–1674.
- [182] Gabriel Robles-De-La-Torre and Vincent Hayward. "Force can overcome object geometry in the perception of shape through active touch". In: *Nature* 412.6845 (2001), pp. 445–448.
- [183] R Sahli et al. "Evolution of real contact area under shear and the value of static friction of soft materials". In: *Proceedings of the National Academy of Sciences* 115.3 (2018), pp. 471–476.
- [184] Evren Samur, J Edward Colgate, and Michael A Peshkin. "Psychophysical evaluation of a variable friction tactile interface". In: *Human vision and electronic imaging XIV*. Vol. 7240. International Society for Optics and Photonics. 2009, 72400J.
- [185] R Sanders. "Torsional elasticity of human skin in vivo". In: *Pflügers Archiv* 342.3 (1973), pp. 255–260.
- [186] Krishnankutty Sathian et al. "Perceived roughness of a grating: correlation with responses of mechanoreceptive afferents innervating the monkey's fingerpad". In: *Journal of Neuroscience* 9.4 (1989), pp. 1273–1279.
- [187] Rob Scharff et al. "Rapid manufacturing of color-based hemispherical soft tactile fingertips". In: *submitted to IEEE Robotics and Automation Letters* (2021).
- [188] Julien Scheibert et al. "The role of fingerprints in the coding of tactile information probed with a biomimetic sensor". In: *Science* 323.5920 (2009), pp. 1503–1506.
- [189] Erich Schröger, Anna Marzecová, and Iria SanMiguel. "Attention and prediction in human audition: a lesson from cognitive psychophysiology". In: *European Journal of Neuroscience* 41.5 (2015), pp. 641–664.
- [190] Cornelius Schwarz. "The slip hypothesis: tactile perception and its neuronal bases". In: *Trends in neurosciences* 39.7 (2016), pp. 449–462.
- [191] Carl E Seashore et al. "Some psychological statistics II. The material weight illusion". In: *University of Iowa Studies in Psychology* 2 (1899), pp. 36–46.

- [192] Thomas Sednaoui et al. "Experimental evaluation of friction reduction in ultrasonic devices". In: *2015 IEEE World Haptics Conference (WHC)*. IEEE. 2015, pp. 37–42.
- [193] Tatjana Seizova-Cajic and Janet L Taylor. "Somatosensory space abridged: rapid change in tactile localization using a motion stimulus". In: *PLoS One* 9.3 (2014), e90892.
- [194] Elaine R Serina et al. "A structural model of the forced compression of the fingertip pulp". In: *Journal of biomechanics* 31.7 (1998), pp. 639–646.
- [195] Anil K Seth. "Interoceptive inference, emotion, and the embodied self". In: *Trends in cognitive sciences* 17.11 (2013), pp. 565–573.
- [196] Yitian Shao, Vincent Hayward, and Yon Visell. "Compression of dynamic tactile information in the human hand". In: *Science Advances* 6.16 (2020), eaaz1158.
- [197] Carl E Sherrick and Ronald Rogers. "Apparent haptic movement". In: *Perception & Psychophysics* 1.3 (1966), pp. 175–180.
- [198] Jianbo Shi et al. "Good features to track". In: *1994 Proceedings of IEEE conference on computer vision and pattern recognition*. IEEE. 1994, pp. 593–600.
- [199] David Shooter. "Use of two-point discrimination as a nerve repair assessment tool: preliminary report". In: *ANZ journal of surgery* 75.10 (2005), pp. 866–868.
- [200] Frederick H Silver, Joseph W Freeman, and Dale DeVore. "Viscoelastic properties of human skin and processed dermis". In: *Skin research and technology* 7.1 (2001), pp. 18–23.
- [201] Frederick H Silver, Lorraine M Siperko, and Gurinder P Seehra. "Mechanobiology of force transduction in dermal tissue". In: *Skin Research and Technology* 9.1 (2003), pp. 3–23.
- [202] Cristina Simões-Franklin, Teresa Aisling Whitaker, and Fiona N Newell. "Active and passive touch differentially activate somatosensory cortex in texture perception". In: *Human brain mapping* 32.7 (2011), pp. 1067–1080.
- [203] Omer Sirin et al. "Fingerpad contact evolution under electrovibration". In: *Journal of the Royal Society Interface* 16.156 (2019), p. 20190166.
- [204] Allan M Smith and Stephen H Scott. "Subjective scaling of smooth surface friction". In: *Journal of neurophysiology* 75.5 (1996), pp. 1957–1962.
- [205] Allan M Smith et al. "Role of friction and tangential force variation in the subjective scaling of tactile roughness". In: *Experimental brain research* 144.2 (2002), pp. 211–223.
- [206] Mandayam A Srinivasan. "Surface deflection of primate fingertip under line load". In: *Journal of biomechanics* 22.4 (1989), pp. 343–349.

- [207] Mandayam A Srinivasan, JM Whitehouse, and Robert H LaMotte. "Tactile detection of slip: surface microgeometry and peripheral neural codes". In: *Journal of neurophysiology* 63.6 (1990), pp. 1323–1332.
- [208] Arun P Sripathi, Sliman J Bensmaia, and Kenneth O Johnson. "A continuum mechanical model of mechanoreceptive afferent responses to indented spatial patterns". In: *Journal of neurophysiology* 95.6 (2006), pp. 3852–3864.
- [209] Joseph C Stevens and Kenneth K Choo. "Spatial acuity of the body surface over the life span". In: *Somatosensory & motor research* 13.2 (1996), pp. 153–166.
- [210] Yoji Suto. "The Effect of Space on Time Estimation (S-ffect) in Tactual Space (I)". In: *Japanese journal of Psychology* 22 (1951), pp. 189–204.
- [211] Olivia K Swanson and Arianna Maffei. "From hiring to firing: activation of inhibitory neurons and their recruitment in behavior". In: *Frontiers in molecular neuroscience* 12 (2019), p. 168.
- [212] M Tada. "How does a fingertip slip?-visualizing partial slippage for modeling of contact mechanics". In: *2006 Proceedings of Eurohaptics*. 2006, pp. 415–420.
- [213] M Tada and T Kanade. "An imaging system of incipient slip for modelling how human perceives slip of a fingertip". In: *The 26th Annual International Conference of the IEEE Engineering in Medicine and Biology Society*. Vol. 1. IEEE. 2004, pp. 2045–2048.
- [214] Mitsunori Tada and Dinesh K Pai. "Finger shell: predicting finger pad deformation under line loading". In: *2008 Symposium on Haptic Interfaces for Virtual Environment and Teleoperator Systems*. IEEE. 2008, pp. 107–112.
- [215] A Talarico, M Malvezzi, and Domenico Prattichizzo. "Modeling the human touch: a FEM model of the human hand fingertips for Haptic application". In: *Proc. of the COMSOL Conf*. 2014.
- [216] Alexander V Terekhov and Vincent Hayward. "Minimal adhesion surface area in tangentially loaded digital contacts". In: *Journal of biomechanics* 44.13 (2011), pp. 2508–2510.
- [217] Alexander V Terekhov and Vincent Hayward. "The brain uses extrasomatic information to estimate limb displacement". In: *Proceedings of the Royal Society B: Biological Sciences* 282.1814 (2015), p. 20151661.
- [218] Edward Bradford Titchener. "On ethnological tests of sensation and perception with special reference to tests of color vision and tactile discrimination described in the reports of the Cambridge anthropological expedition to Torres Straits". In: *Proceedings of the American Philosophical Society* 55.3 (1916), pp. 204–236.
- [219] Ake B Vallbo, Roland S Johansson, et al. "Properties of cutaneous mechanoreceptors in the human hand related to touch sensation". In: *Hum neurobiol* 3.1 (1984), pp. 3–14.

- [220] Robert W Van Boven and Kenneth O Johnson. "The limit of tactile spatial resolution in humans: grating orientation discrimination at the lip, tongue, and finger". In: *Neurology* 44.12 (1994), pp. 2361–2361.
- [221] Clayton L Van Doren, George A Gescheider, and Ronald T Verrillo. "Vibrotactile temporal gap detection as a function of age". In: *The Journal of the Acoustical Society of America* 87.5 (1990), pp. 2201–2206.
- [222] F Vega-Bermudez and KO Johnson. "Surround suppression in the responses of primate SA1 and RA mechanoreceptive afferents mapped with a probe array". In: *Journal of neurophysiology* 81.6 (1999), pp. 2711–2719.
- [223] Ronald T Verrillo. "Effect of contactor area on the vibrotactile threshold". In: *The Journal of the Acoustical Society of America* 35.12 (1963), pp. 1962–1966.
- [224] Ronald T Verrillo. "Investigation of some parameters of the cutaneous threshold for vibration". In: *The Journal of the Acoustical Society of America* 34.11 (1962), pp. 1768–1773.
- [225] Qi Wang and Vincent Hayward. "In vivo biomechanics of the fingerpad skin under local tangential traction". In: *Journal of biomechanics* 40.4 (2007), pp. 851–860.
- [226] Qi Wang and Vincent Hayward. "Tactile synthesis and perceptual inverse problems seen from the viewpoint of contact mechanics". In: *ACM Transactions on Applied Perception (TAP)* 5.2 (2008), pp. 1–19.
- [227] Zhongkui Wang et al. "A 3-D nonhomogeneous FE model of human fingertip based on MRI measurements". In: *IEEE Transactions on Instrumentation and Measurement* 61.12 (2012), pp. 3147–3157.
- [228] Peter H Warman and A Roland Ennos. "Fingerprints are unlikely to increase the friction of primate fingerpads". In: *Journal of Experimental Biology* 212.13 (2009), pp. 2016–2022.
- [229] Helena Backlund Wasling et al. "Tactile directional sensitivity and postural control". In: *Experimental brain research* 166.2 (2005), pp. 147–156.
- [230] Sidney Weinstein. "Intensive and extensive aspects of tactile sensitivity as a function of body part, sex and laterality". In: *The skin senses* (1968).
- [231] G Westling and Roland S Johansson. "Responses in glabrous skin mechanoreceptors during precision grip in humans". In: *Experimental brain research* 66.1 (1987), pp. 128–140.
- [232] G Westling and RS Johansson. "Factors influencing the force control during precision grip". In: *Experimental brain research* 53.2 (1984), pp. 277–284.
- [233] Olivier White et al. "Switching in feedforward control of grip force during Tool-Mediated interaction with elastic force fields". In: *Frontiers in neurorobotics* 12 (2018), p. 31.

- [234] Michaël Wiertlewski, Rebecca Fenton Friesen, and J Edward Colgate. "Partial squeeze film levitation modulates fingertip friction". In: *Proceedings of the national academy of sciences* 113.33 (2016), pp. 9210–9215.
- [235] Michael Wiertlewski and Vincent Hayward. "Mechanical behavior of the fingertip in the range of frequencies and displacements relevant to touch". In: *Journal of biomechanics* 45.11 (2012), pp. 1869–1874.
- [236] GL Wilkes, IA Brown, and RH Wildnauer. "The biomechanical properties of skin." In: *CRC critical reviews in bioengineering* 1.4 (1973), pp. 453–495.
- [237] Laura Winfield et al. "T-pad: Tactile pattern display through variable friction reduction". In: *World Haptics Conference*. IEEE. 2007, pp. 421–426.
- [238] Alice G Witney et al. "The cutaneous contribution to adaptive precision grip". In: *Trends in neurosciences* 27.10 (2004), pp. 637–643.
- [239] Edward J Wood and Philip T Bladon. *The human skin*. Arnold, 1985.
- [240] John Z Wu et al. "Finite element analysis of the penetrations of shear and normal vibrations into the soft tissues in a fingertip". In: *Medical engineering & physics* 29.6 (2007), pp. 718–727.
- [241] Kenneth S Wu, William W van Osdol, and Reinhold H Dauskardt. "Mechanical properties of human stratum corneum: effects of temperature, hydration, and chemical treatment". In: *Biomaterials* 27.5 (2006), pp. 785–795.
- [242] Li Zhaoping. "Theoretical understanding of the early visual processes by data compression and data selection". In: *Network: computation in neural systems* 17.4 (2006), pp. 301–334.